Mode group diversity multiplexing in multimode fiber transmission systems

Mode group diversity multiplexing in multimode fiber transmission systems

Christos P. Tsekrekos

Mode group diversity multiplexing in multimode fiber transmission systems

PROEFSCHRIFT

ter verkrijging van de graad van doctor aan de
Technische Universiteit Eindhoven, op gezag van de
Rector Magnificus, prof.dr.ir. C.J. van Duijn, voor een
commissie aangewezen door het College voor
Promoties in het openbaar te verdedigen
op maandag 14 januari 2008 om 16.00 uur

door

Christos Panagiotis Tsekrekos

geboren te Cholargos, Griekenland

Dit proefschrift is goedgekeurd door de promotoren:

prof.ir. A.M.J. Koonen
en
prof.dr.ir. J.W.M. Bergmans

Copromotor:
dr.ir. B.P. de Hon

The work described in this thesis was performed in the Faculty of Electrical Engineering of the Eindhoven University of Technology and was financially supported by the Freeband Impulse Program of the Ministry of Economic Affairs of the Netherlands.

CIP-DATA LIBRARY TECHNISCHE UNIVERSITEIT EINDHOVEN

Tsekrekos, Christos P.

Mode group diversity multiplexing in multimode fiber transmission systems / by Christos Panagiotis Tsekrekos. - Eindhoven : Technische Universiteit Eindhoven, 2008.
Proefschrift. - ISBN 978-90-386-1724-4
NUR 959
Trefw.: optische telecommunicatie / breedbandcommunicatie / vezeloptica / lokale computernetwerken.
Subject headings: optical fibre communication / MIMO systems / polymer fibres / local area networks.

Typeset using LaTeX, printed in the Netherlands.

to my parents Panagiotis and Zoe
and my sisters Maria and Eleni

Summary

Mode group diversity multiplexing in multimode fiber transmission systems

Multimode fibers (MMFs) and particularly graded-index (GI) MMFs are widely employed in campus and in-building networks. MMF is also considered to be an interesting option for future optical in-house networks. Next to silica-based MMF, polymer optical fiber (POF) may be an interesting option due to its large core and the flexibility of the polymer material that facilitate handling and installation in ducts. MMF connections can offer a larger bandwidth compared to electrical wireless and copper-based ones. Light in an MMF propagates in several spatial modes. The bandwidth of MMF links is limited by modal dispersion, which originates in the differential propagation delay of the modes. At the same time, these spatial modes offer extra degrees of freedom that can be exploited in transmission.

Most MMF systems use light intensity modulation and direct detection (IM-DD). IM-DD is the simplest way of building an optical communication link. An orthogonality relation exists for the fields of the propagating modes of an MMF. Nothing similar, though, holds for the intensity profiles of the modes. Any effort to exploit the spatial modes should be simple and pragmatic, since MMFs are used in short-range applications where simplicity and low cost are key issues. The development of multiple-input multiple-output techniques in wireless communications has triggered similar research in transmission over MMFs. Several schemes have been so far proposed, mode group diversity multiplexing (MGDM) being one of them. MGDM creates parallel, independent communication channels, transparent to the transmission format, using groups of the propagating modes. MGDM uses IM-DD, but it does not require orthogonality among the intensity profiles of the detected mode groups, since it mitigates cross-talk — due to the lack of orthogonality — with electronic signal processing.

To the author's knowledge, this is the first doctoral thesis to present a theoretical and experimental investigation of the MGDM technique. This thesis primarily deals with the optical aspects of MGDM transmission over GI-MMFs. A mathematical model is developed and the conditions under which a broadband MGDM system can be described by a real-valued transmission matrix are identified. This matrix relates the electrical output to the electrical input signals of the system. In the most general case, irrespective of the amount of spatial overlap among the fields of the detected mode groups, these fields should be mutually incoherent. The

real-valued transmission matrix expresses the spatial overlap among the intensity profiles of the detected mode groups and cannot compensate for differential delays. Therefore, the MGDM system should operate below the dispersion limit. Further, the effect of noise is studied, considering matrix inversion as the demultiplexing algorithm in line with the requirement of signal format transparency.

A major objective of this thesis is to show that it is possible to build a simple, stable and robust MGDM system. Guidelines for the design of such a system are drawn and concrete conclusions are obtained that can be used for the design and manufacture of an MGDM multi/demultiplexer. Numerical simulations support the experimental observation that propagation in silica-based GI-MMFs does not affect the design of the multi/demultiplexer for at least 1 km of propagation. The case of GI-POFs differs in that mode mixing is stronger and therefore the transmission matrix of a GI-POF-based MGDM system depends strongly on the GI-POF length. Further, GI-POF is more sensitive to bending and stressing. A stable two-input, two-output MGDM link with silica-based GI-MMF is demonstrated, using components originally made for other applications.

The proposed design approach for an MGDM system benefits from the all-electronic mitigation of cross-talk. However, it lacks scalability with the number of channels. More specifically, although it would be possible to build a robust system with two or three channels, for a larger number of channels, the performance of the system would become very sensitive to changes in the transmission matrix. The robustness of the system depends on the condition number of the transmission matrix. The ideal case is a system without cross-talk, i.e. a system characterized by the identity matrix. To increase the robustness of an MGDM system and allow for a larger number of channels, mode-selective spatial filtering (MSSF) is introduced and demonstrated.

MSSF is a new optical technique, first proposed in the framework of the research presented in this thesis. It only requires an imaging system, e.g. a lens, to project the near-field intensity pattern at the GI-MMF output facet onto the detectors of the MGDM system. The numerical aperture (NA) of the imaging system at the side of the output facet of the GI-MMF should be smaller than the central NA of the GI-MMF. MSSF provides an optical way to mitigate cross-talk. For a system with up to three channels, MSSF could eliminate the need for electronic demultiplexing. Further, a robust five-channel MGDM system can be realized with MSSF and partial electronic cross-talk mitigation. MSSF greatly relaxes the requirement of mutual incoherence among the fields of the mode groups at the output end of the GI-MMF and hence it facilitates the combination of MGDM with wavelength division multiplexing.

The results presented in this thesis offer insight into light propagation in GI-MMFs and give a new perspective in the use of the propagating modes of GI-MMFs for transmission applications. So far, a stable, robust and transparent five-channel modal multiplexing system would only have seemed fanciful. However, this thesis shows the way of turning such a scenario into a practical reality.

Contents

Chapter 1

Introduction

This dissertation presents an investigation of the mode group diversity multiplexing (MGDM) technique. MGDM is an intensity-modulation, direct-detection, multiple-input, multiple-output transmission method. It creates parallel, independent communication channels over a multimode fiber (MMF). This chapter provides an introduction to the area of interest in which MGDM falls. In particular, it is the purpose of this chapter to introduce MMFs, to describe applications where MMFs are used, to present multiplexing techniques that can be used in MMF transmission and to give the main characteristics of MGDM.

1.1 Multimode fiber telecommunication systems

Telecommunications is one of the major fields of technology where human activities have focused. The need to communicate is vital in human activities. For example, in the case of research and development, it would seem impossible to achieve any progress whatsoever, without sufficiently communicating the already known results. In this case, communications facilitate the transfer of knowledge and experience. In our information-based societies, advanced telecommunication technologies are a prerequisite for economic growth.

Telecommunication systems are characterized by their geographical range. They span from very short interconnections between chips or equipment to long-haul transoceanic links. Optical fiber communications offer a very attractive solution for a telecommunication infrastructure. Optical systems enable high-speed and reliable communications. They can be very diverse and can be found in many different applications. The international undersea network uses fiber optics systems [1]. The same can hold for intercity, metropolitan, campus, in-building or automobile systems and networks. In access networks, fiber to the home/fiber to the premises (FTTH/FTTP) appears as a very promising solution to meet the requirements of broadband communications [2].

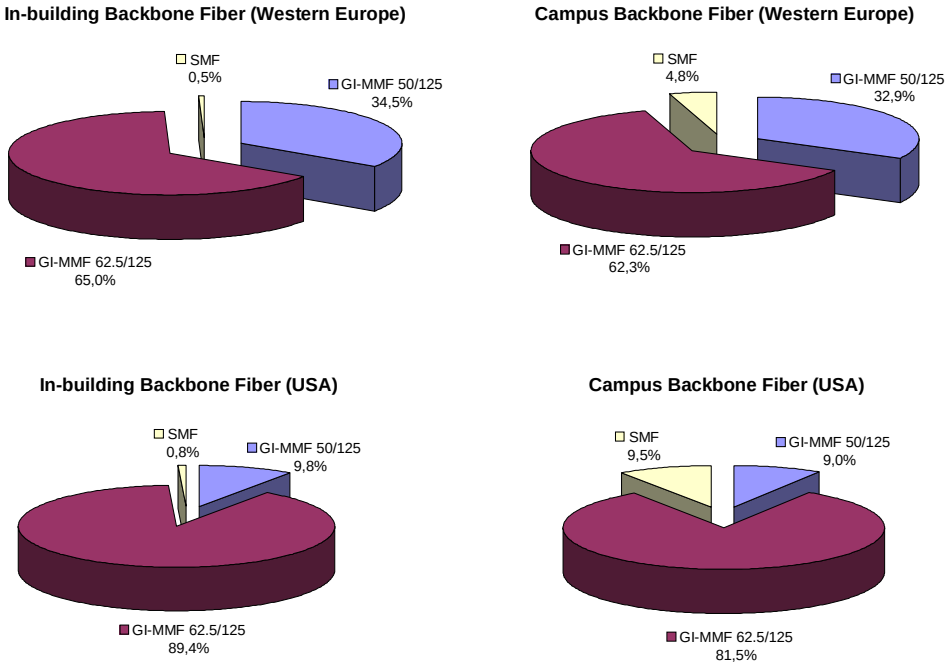

Figure 1.1: Statistics showing the types of silica-based optical fiber links in in-building and campus networks. The statistics represent the cases of Western Europe and the Unites States of America in 1999. SMF: single-mode fiber. GI-MMF 62.5/125 (50/125): graded-index multimode fiber with a core/cladding diameter of 62.5/125 (50/125) μm.

In short range optical networks, where the length of the optical fibers does not exceed a few kilometers, multimode fibers (MMFs) have been primarily used. A good reason for this is that the size of their core is much larger than the size of the core of single-mode fibers (SMFs). Therefore handling of MMFs is easier than of SMFs, since there is more tolerance in the required alignment for the coupling of light in and out of the MMF as well as for splicing MMFs.

1.1.1 Campus and in-building networks

In campus and in-building networks, MMF has been the transmission medium of choice. Figure 1.1 shows the statistics of the types of silica-based optical fibers used in these local area networks (LANs). These statistics represent the cases of Western Europe and the United States of America in 1999 [3, 4]. The wider use of SMFs can be found in campus networks in the USA. Even in this case, however, the use of SMFs does not exceed the 10% of the links in these networks. From

Table 1.1: Fiber length in in-building and campus backbone in Western Europe and the Unites States of America (1999).

Area	In-building backbone	Campus backbone
Western Europe	< 300 m, 88%	< 1 km, 90%
USA	< 300 m, 84%	< 1 km, 85%

Figure 1.1, it is clear that the transmission medium of choice in these LANs is the graded-index (GI) MMF with a core/cladding diameter of 62.5/125 μm. Since 1999, the use of the 62.5/125 μm GI-MMF has been decreased in favor of the use of the 50/125 μm GI-MMF as well as of SMF that support higher transmission bandwidth [4].

The length of the fiber links in the LANs of Figure 1.1 is usually up to a few hundreds of meters. Table 1.1 shows the percentage of the fiber links in these networks with a length shorter than 300 m and 1 km. In Western Europe and the USA, the length of 90% and 85% of these fiber links, respectively, does not exceed 1 km.

1.1.2 Transparent in-house networks

The residential user has access to different services, such as internet, telephony and cable digital or analog television (CATV). Currently, several telecommunication

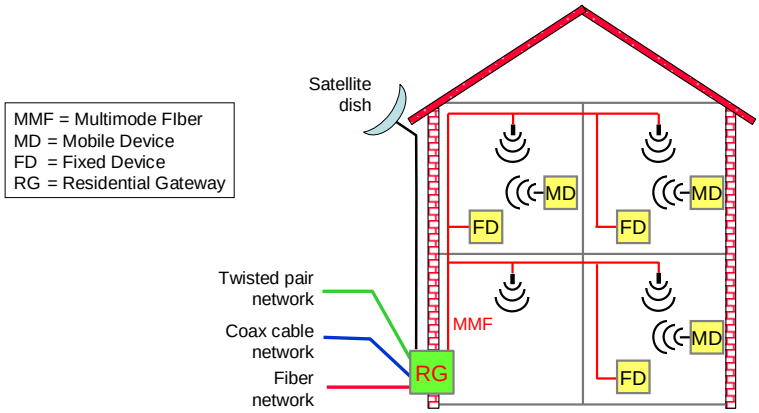

Figure 1.2: A transparent MMF in-house network, integrating many different services. (By courtesy of prof. A. M. J. Koonen)

operators offer these three services, which is commonly called "triple play". Traditionally, for each of these services a different telecommunication infrastructure is used for its distribution to and inside the house. Having a common broadband infrastructure allows for more flexible access, with dynamic bandwidth allocation and service provision based on the users' demands.

An MMF infrastructure can meet both the requirements of broadband access and flexibility of future residential networks. Figure 1.2 shows an example of an MMF-based in-house network where several services are integrated. Different access connections reach a residential gateway, via which the various services are distributed in the house over the MMF infrastructure.

1.1.3 Optical interconnects

Optical systems are considered a viable option for high speed optical interconnects [5, 6]. Current electrical interconnects are reaching their performance limits. This is due to power dissipation and other engineering challenges that need to be met for the continuous reduction of the dimensions of transistor devices. Optics can potentially offer solutions featuring large bandwidth, electrical isolation and low power consumption. MMFs can be used in optical interconnects and have already been employed in proposed interconnection systems [7–9].

1.2 Multimode fibers

1.2.1 Basic properties

An optical fiber is a dielectric cylindrical waveguide. Light propagates in the core of the optical fiber. The core is surrounded by the cladding, which has a smaller refractive index. Therefore the mechanism of light propagation in optical fibers is total internal reflection. It is possible to create optical waveguides using photonic band-gap effects and not total internal reflection [10, 11]. However, in this doctoral thesis we are not dealing with photonic band-gap fibers.

The diameters of the core and the cladding, the profile of the refractive index, as well as the material of the fiber define the type of the optical fiber and give its particular characteristics. An optical fiber is multimode when light propagates in more than one spatial guided mode. A spatial guided mode, or simply a mode, can be viewed as a solution to the electromagnetic wave propagation problem of monochromatic light in an optical fiber [12–17]. It is common not to refer to the two orthogonal polarizations of the electromagnetic field as two different modes, but rather as the two polarizations of a mode. Alternatively, a distinct ray-trace of light propagation in the optical fiber corresponds to a certain mode. An SMF supports only one mode in its specified wavelength operation range. Besides the optical power that propagates along the fiber, some of the power is not bound and it is radiated. This is usually described by the radiation modes [13, 15, 16]. There

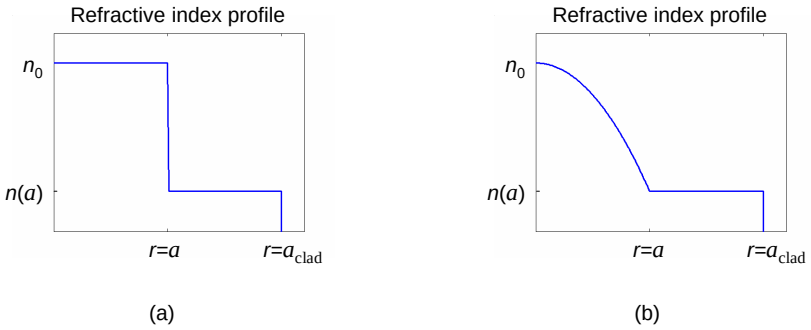

Figure 1.3: Refractive index profile $n(r)$ of (a) an SI-MMF ($\alpha = \infty$) and (b) a parabolic GI-MMF ($\alpha = 2$).

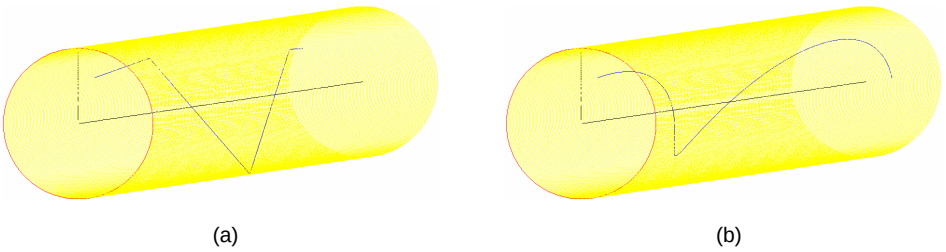

Figure 1.4: Ray trace in (a) an SI-MMF ($\alpha = \infty$) and (b) a parabolic GI-MMF ($\alpha = 2$). The launch conditions of the ray on the input facet of the MMF are the same in both cases. The cylindrical area represents the core of the MMF.

is also a third category of modes which are not guided ones, neither radiation ones. Some part of the optical power can propagate only over a certain distance along the fiber. This type of light propagation is described by the leaky or tunneling modes [13, 15, 16]. Light described by the leaky modes is not totally bound in the fiber and along propagation it steadily escapes in the cladding and then it is radiated.

The refractive index profile $n(r, \lambda)$ of multimode fibers is usually given by the following power-law expression,

$$n(r,\lambda) = \begin{cases} n_0(\lambda)\sqrt{1 - 2\Delta(\lambda)\left(\frac{r}{a}\right)^{\alpha}}, & 0 \le r \le a, \\ n_0(\lambda)\sqrt{1 - 2\Delta(\lambda)}, & a \le r \le a_{\text{clad}}, \end{cases} \tag{1.1}$$

where $n_0(\lambda) = n(0, \lambda)$, a is the core radius of the MMF, a_{clad} is the outer radius of the cladding, $\Delta(\lambda) = [n_0^2(\lambda) - n^2(a, \lambda)]/[2n_0^2(\lambda)]$ and α is the parameter that determines the shape of the profile in the MMF core. Here, r is the radial distance

from the MMF axis and λ is the wavelength of light in vacuum. It is usual to refer to this profile as the α-profile. If $\alpha = \infty$, the optical fiber is a step-index (SI) one, while in any other case it is a GI one. For $\alpha = 2$, the profile is called parabolic and it is of great interest in practical GI-MMFs. In GI-MMFs, modal dispersion, due to the differential propagation delays of the modes, is much reduced compared to SI-MMFs. The parabolic index profile is very close to the optimal profile where differential mode delays are minimized. Figures 1.3(a) and 1.3(b) show the refractive index profile of an SI-MMF and a parabolic GI-MMF, respectively. In an SI-MMF, any propagating ray which is not parallel to the fiber axis always reflects on the core-cladding interface and its trace consists of straight segments. In contrast, in GI-MMFs, the curve of the trace a non-parallel ray has no critical points where the derivative does not exist and need not reach the core-cladding interface. Figure 1.4 shows the trace of a ray in an SI-MMF and a parabolic GI-MMF. The launch conditions of the ray are the same in both cases.

The range of angles under which an optical system can accept or emit a ray is expressed by the numerical aperture (NA). The NA is a dimensionless number and it is defined by

$$\mathrm{NA} = n \sin\theta, \tag{1.2}$$

where n is the refractive index of the medium where rays propagate and θ denotes half the value of the angle that defines the cone of light acceptance or emission of the optical system in the same medium. For a GI-MMF, θ is the maximum angle between a ray that can enter the GI-MMF and the fiber axis. The local NA of a GI-MMF for guided rays is given by

$$\mathrm{NA}_{\text{GI-MMF}}(r, \lambda) = \sqrt{n^2(r, \lambda) - n^2(a, \lambda)}. \tag{1.3}$$

The value $\mathrm{NA}_{\text{GI-MMF}}(0, \lambda)$ is commonly referred to as the central NA of a GI-MMF.

The number of guided modes N_m of an optical fiber can be approximated by [16]

$$N_m(\lambda) = \frac{\alpha}{\alpha + 2} \left(\frac{\pi a}{\lambda}\right)^2 \mathrm{NA}^2_{\text{GI-MMF}}(0, \lambda), \tag{1.4}$$

The number N_m is a property of the fiber and it depends on the wavelength. When light propagates in an MMF, it is not always the case that all modes are excited. It may be that the optical power is distributed only among a few of these modes. This is commonly referred as to selective or restricted excitation. Excitation of all the modes is described as overfilled launch. The distribution of the optical propagating power among the modes depends on the excitation conditions and mode mixing. Mode mixing is the gradual redistribution of the optical power among the modes as light propagates along the MMF. Mode mixing is due to irregularities in the refractive index profile, either macroscopic or microscopic. These irregularities may change in time, e.g. due to temperature variations. Ideally, light propagates in a straight, cylindrical waveguide, with a refractive index that depends only on

the radial coordinate. Any deviation from this ideal case, for example due to bending or impurities of the material, can induce mode mixing.

1.2.2 Silica- and polymer-based MMFs

As mentioned in the previous section, an MMF is characterized by the diameters of the core and the cladding, as well as the refractive index profile. Another important feature is the material of which an MMF is made. MMFs are manufactured from glass or polymer materials. There can also be fibers made of a combination of materials, such as plastic-clad silica (PCS) fibers. PCS fibers have a silica-based core and a plastic cladding, and are mostly used in automotive and sensor applications [19–21]. Glass optical fibers (GOFs) are based on silica. Polymer optical fibers (POFs) are mostly made of polymethylmethacrylate (PMMA) or perfluorinated (PF) polymer. Dopant elements are used to form the refractive index profile. POFs are mostly used in short range connections, such as in automotive applications, and are considered good candidates for high speed LAN and in-house connections [22, 23].

GOFs and POFs do not have the same characteristics on absorption and scattering. Therefore, loss and mode mixing are different in GOFs and POFs. Figure 1.5 shows typical attenuation spectra for GOFs and POFs [18]. PF-POFs have significantly lower attenuation than PMMA-POFs, however still higher than GOFs. The attenuation spectra of GOFs and PF-POFs allow for a much broader wavelength range to be used in transmission applications compared to the case of PMMA-POFs. It should be noted that the refractive index profile influences the

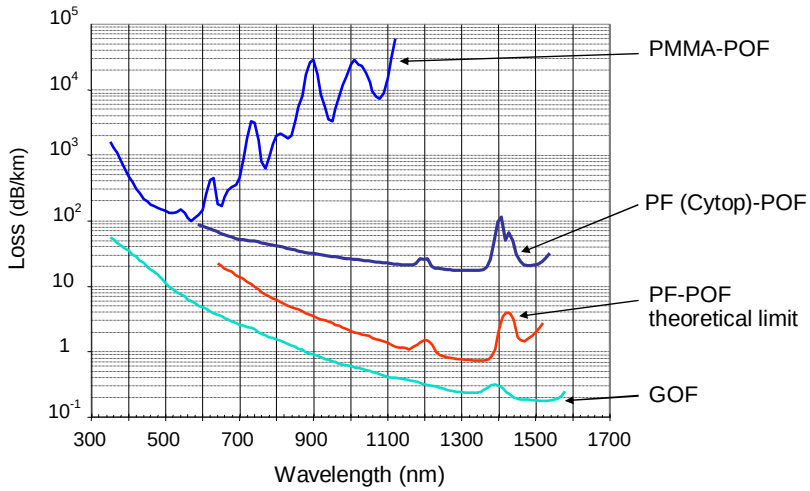

Figure 1.5: Attenuation spectrum of different types of optical fibers [18]. (By courtesy of ir. H. P. A. van den Boom)

Table 1.2: Typical characteristics of GI-MMFs.

material	core/cladding diameter (μm)	NA
silica	62.5/125	0.275
silica	50/125	0.200
PMMA	500/750	0.290
PF	120/500	0.171

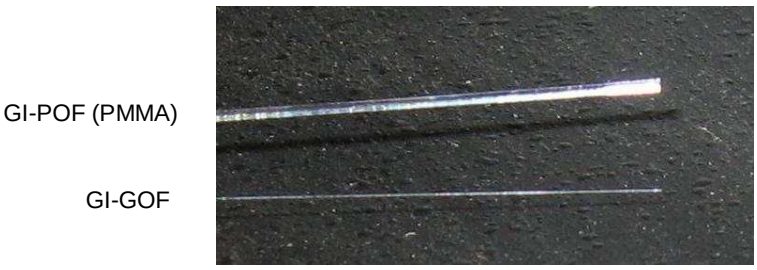

Figure 1.6: Photograph of two bare GI-MMFs; one GOF and one PMMA-POF.

attenuation spectrum of a fiber. This is due to the different dopant concentration required to form the index profile [24].

In this dissertation, GI-MMFs will be considered. Silica-based GI-MMFs are commonly used in existing optical system, while much research is still being put into GI-POFs. Table 1.2 shows typical values of core/cladding diameter and the NA of the most common GI-MMFs, either silica- or polymer-based. Typically, POFs have a larger core/cladding diameter than GOFs, as can be also seen in Figure 1.6.

1.3 Multiplexing techniques

Multiplexing techniques are widely used in telecommunication systems. They allow several users to access the same transmission medium. In principle, in multiplexing, the transmission resources are shared among the users. The type of multiplexing depends on the shared resource. In the following subsections, we discuss several known multiplexing techniques.

1.3.1 WDM, SCM, TDM, PDM and CDM

Wavelength division multiplexing

A powerful technique in optical communications is wavelength division multiplexing (WDM). WDM creates several channels over the same fiber, either SMF or MMF, using a different wavelength for each channel. At the receiving side of a WDM system, optical filters are required in order to demultiplex the transmitted signals. The format of the transmitted signals can be arbitrary since the demultiplexing is based on wavelength differentiation. There are two WDM variants, namely dense WDM (DWDM) and coarse WDM (CWDM). CWDM, sometimes referred to as wideband WDM, uses a much wider spacing in the wavelengths of the optical sources and therefore it has increased tolerance with respect to wavelength drifting and consequently to temperature fluctuations. CWDM is a lower cost technique than DWDM due to the more relaxed requirements in the system design and related components. Therefore CWDM seems more suitable for application in MMF systems. Both CWDM [25–27] and DWDM [28, 29] have been considered and demonstrated in MMF transmission.

Subcarrier multiplexing

Similarly to WDM, in radio communications, frequency division multiplexing (FDM) is applied. In a sense, WDM is an optical form of FDM. It is possible to use a radio FDM signal to modulate the laser intensity of an optical link. At the end of such a link, the electrical received signal can be processed with an FDM demultiplexer. Therefore several radio channels can be multiplexed over the same fiber, either SMF or MMF. This technique is known as subcarrier multiplexing (SCM) and it is mainly used in radio-over-fiber systems, such as the cable television (CATV) distribution systems [30]. In SCM, the transmission channels are transparent to the transmission format and their bandwidth is limited by the subcarrier spacing. SCM transmission has been considered over MMF [31–35], and combined with DWDM has yielded a very high aggregate bit rate of 204 Gbit/s over 3 km of 50/125 μm silica-based GI-MMF [28].

Time division multiplexing

In digital communications, it is possible to divide the transmission time in slots and transmit each digital channel periodically. This technique is called time division multiplexing (TDM). Similarly to WDM and FDM, TDM can apply directly in the optical domain or electrical TDM can apply over the intensity of the transmitted optical carrier [36–38]. TDM requires a digital signal format. Optical TDM aims at achieving a very high capacity per transmission wavelength in long-haul SMF transmission systems. Electrical TDM can be a cost-effective approach in LANs and optical access systems.

Polarization division multiplexing

In SMFs, the optical field propagates in one mode with two orthogonal polarizations. Therefore, polarization division multiplexing (PDM) can be achieved and two channels can be transmitted over an SMF [39]. The two polarizations should be separated at the receiving end to demultiplex the two channels, which can transport signals of any format. PDM requires that polarization is maintained along propagation and it is an example of spatial multiplexing. It is usually employed in transmission experiments where record capacities are pursued. In principle, PDM can also apply in MMF transmission to create two independent channels, as long as polarization maintenance can be achieved [40, 41].

Code division multiplexing

In all multiplexing techniques, a minimum level of orthogonality is needed in a certain domain among the received signals in order to demultiplex the channels. The previously mentioned techniques achieve the necessary orthogonality in the wavelength, frequency, time and polarization (space) domains. It is possible to create several communication channels by using a unique code at each channel to transmit a digital data stream. The necessary orthogonality can then be achieved with the use of mutually orthogonal codes. This technique is called code division multiplexing (CDM) or code division multiple access (CDMA), depending on the application and whether it uses synchronous or asynchronous transmission. CDMA has been originally introduced in radio communications but optical CDMA has been investigated as well [42–45]. In CDM/CDMA, the communication channels can use the same wavelength, frequency, time or polarization (in general, spatial mode).

1.3.2 Wireless MIMO techniques

In electrical wireless systems, multiple-input multiple-output (MIMO) techniques using multiple antennas at both the transmitting and receiving sides have recently attracted a lot of attention. They can improve the spectral efficiency and the robustness of wireless communication systems [46–49]. The huge capacity growth that these MIMO techniques promise is due to the exploitation of the spatial dimensions of the system. A rich scattering environment is required and the capacity scales linearly with the number of antennas, while keeping the total transmitted power and channel bandwidth constant.

Figure 1.7 illustrates a wireless MIMO link. The impulse response of the link has a matrix form $\mathbf{H}$ to reflect the spatial dimensions of the system. The received signals $\mathbf{s}_R$ are related to the transmitted signals $\mathbf{s}_T$ via $\mathbf{H}$. Techniques for the estimation of $\mathbf{H}$ are required in a MIMO system. It should be noted that with too much scattering, the elements of $\mathbf{H}$ will be almost identical, rendering impossible to recover $\mathbf{s}_R$ at the receiving side of the link.

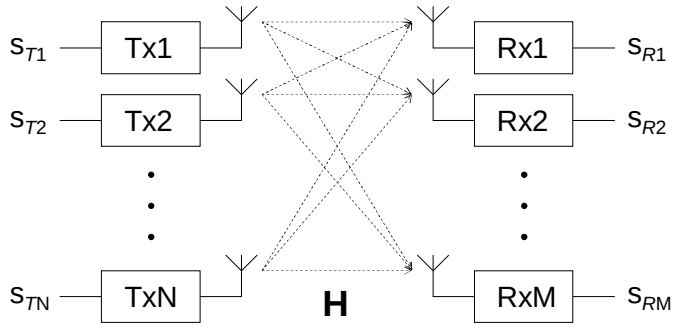

Figure 1.7: A wireless MIMO link.

1.3.3 Modal multiplexing techniques

The guided modes of an MMF offer spatial degrees of freedom that can be used in transmission and multiplexing systems. However, the way of implementing such a system is not trivial. Several approaches can be found in the literature, each of them exploiting a different characteristic of light propagation in MMFs. A different term was used to describe each of these modal approaches, in relevance to its principle of operation. In this subsection, a short overview of these approaches is presented.

The fields of the propagating modes form an orthogonal function set [13]. If it were possible to excite each mode separately and design a receiver that exploits the orthogonality of the modal fields to detect each mode, modal multiplexing would be achieved. This would be similar to PDM and it would require that power propagating in one mode is not transferred to another mode during propagation. In other words, mode mixing should be negligible. Although mode mixing is limited in GOFs, the components that such a scheme requires for exciting and detecting each modal channel are not trivial. A method that transmits several channels in mutually orthogonal field patterns and uses holographic demultiplexing to separate the channels approximates the principle described above [50–52].

Intensity-modulation direct-detection (IM-DD) is the simplest way of building an optical communication link. In short range applications, where MMFs are used, simplicity and low cost are key issues. Besides modal multiplexing with holography, IM-DD approaches have been also proposed [53, 54]. Mode division multiplexing [53] and angular multiplexing [54–57] are based on the excitation of modes or mode groups, the intensity profiles of which are orthogonal on a certain plane. Mode division multiplexing is applied over GI-MMFs and it is based on the excitation of individual tubular modes with nearly orthogonal near-field (intensity) patterns [58]. To launch these modes a mask is required at the front side of the MMF link [58]. Computer-generated holograms can be used to produce such masks [59]. Angular multiplexing is applied over SI-MMFs and exploits the fact

that the far-field (intensity) pattern of principal mode groups (PMGs), i.e. a group of modes with very similar propagation coefficients, forms a ring, the radius of which depends on the order of the PMG. Each PMG propagates with a different angle with respect to the propagation axis. Excitation of a PMG can be achieved by launching light with a proper angle on the input facet of the SI-MMF.

The developments in wireless MIMO systems have triggered research in optical MIMO transmission over MMFs. The first reported optical MIMO technique is dispersive multiplexing [60, 61]. In dispersive multiplexing, phase modulated electrical subcarriers are used to intensity-modulate the lasers and a complex-valued matrix relates the electrical input and output signals of the system. The technique requires that there is a significant phase difference among the propagation paths. This is achieved with an MMF which is highly dispersive and/or a high frequency electrical subcarrier. To allow for short MMFs to be used, coherent optical MIMO has been introduced [62, 63]. Coherent optical MIMO is the optical analogy of radio MIMO [64], but it comes at the expense of complexity due to the optical coherent demodulation. IM-DD MIMO can be also applied with other digital signal formats, such as on-off keying [9, 65]. Mode group diversity multiplexing (MGDM) [66–69] is a MIMO technique that uses IM-DD and creates parallel, independent communication channels, transparent to the signal format, as is further explained in the next section.

1.4 Mode group diversity multiplexing

MGDM is a modal multiplexing technique that creates parallel, independent communication channels over an MMF. MGDM has been proposed as a way to integrate various services over an MMF network, such as a POF-based in-house network [66, 67]. Similarly to dispersive multiplexing [61], MGDM is an IM-DD MIMO technique that uses a matrix to relate the electrical input and output signals. This matrix description requires that the system is linear with respect to the optical intensity. It differs, though, from dispersive multiplexing in that it supports transparency to the signal format. This means that the signal processing algorithms in MGDM should ideally be independent of the transmission format.

The principle of MGDM is shown in Figure 1.8. At the transmitting side, N sources are used to launch a different group of modes each. At the output of the MMF, each of M photodetectors responds to a different combination of the optical power carried by the N mode groups. It should be noted that these mode groups are not the principal mode groups, which consist of modes with very similar propagation coefficient [15]. As will be explained in Chapter 2, in a transparent, broadband MGDM system that operates below the dispersion limit, a real-valued matrix can be used to relate the electrical output to the electrical input signals. Electrical processing of the signals after the photodetectors is used to demultiplex the channels. Therefore, no signal orthogonality is required in the optical intensity domain. An algorithm for the signal processing that satisfies the requirement of

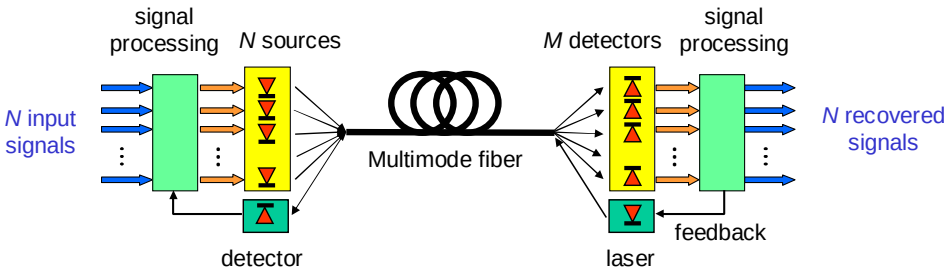

Figure 1.8: Mode group diversity multiplexing principle. (By courtesy of prof. A. M. J. Koonen)

signal-format transparency is matrix inversion. Matrix inversion is a zero-forcing algorithm that cancels cross-talk among the channels [49]. In the work presented in this thesis, matrix inversion is considered.

In the following chapters, when referring to an $M \times N$ MGDM system, we assume the following characteristics:

- An $M \times N$ real-valued transmission matrix $\mathbf{H}$ relates the M electrical output signals to the N electrical input ones.
- The MGDM system is transparent to the transmission format.
- Electronic matrix inversion is used to demultiplex the MGDM channels.

The IM-DD transmission bandwidth over each optical path from transmitter j to detector i depends on dispersion within this path. In principle, when the bandwidth of an MGDM channel is compared to the bandwidth of a single channel that comprises all modes and the whole power at the output end of the MMF is detected, any option is likely, i.e. larger, smaller or similar. Dispersion in an optical MMF link that uses selective excitation and detection is not determined by the number of excited and detected modes, as long as they are more than one, but by the differential mode delays and attenuation of the optical path, as well as mode mixing along propagation [70].

In Figure 1.8, a feedback loop from the transmitter to the receiver is shown. The necessity of this loop depends on the time variations of the MGDM link, i.e. the time fluctuations of the elements $h_{i,j}$ of $\mathbf{H}$. Such a feedback loop, although it can provide stability and reliability to an MGDM system, will increase the complexity of the system and as such may restrain the implementation of MGDM. Therefore the design of a system with a feedback loop can be justified only when it offers substantial advantages, such as increasing the scalability of the system. Further, this loop could be used to inform the transmitter of the value of $h_{i,j}$. That would allow for electronic pre-compensation of the signal mixing. In this thesis, the simple case of an MGDM system without a feedback loop is considered,

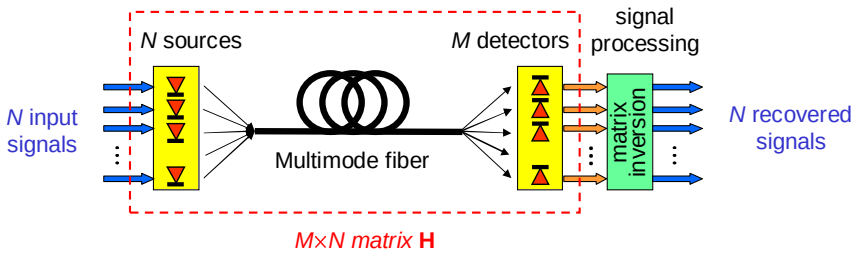

Figure 1.9: A mode group diversity multiplexing system without a feedback loop. The electronic processing is based on matrix inversion.

as shown in Figure 1.9. A major track of the presented work is the design and implementation of a stable system that can perform reliably without feedback from the receiver to the transmitter. However, adaptive estimation of $\mathbf{H}$ at the receiving side of the system is still required to account for moderate changes in the value of $h_{i,j}$.

1.5 Outline of the thesis

In this thesis, several aspects of the MGDM technique are considered and analyzed. The work is primarily devoted to the optical aspects of the system. Given that this thesis presents some of the first results on MGDM, some effort has been put to reveal the aspects of MGDM that deserve special attention and research. The main goal is to reach practical conclusions that enable the efficient design and applicability of an MGDM system. As mentioned in Section 1.3.3, conceptually, it is well-known that the modes offer spatial degrees of freedom that could be used for transmission purposes. However, the orthogonality of the modes is with respect to their fields, while MGDM uses *intensity-modulation* and *direct-detection*. In Chapters 2 to 6, silica-based GI-MMFs are used to obtain experimental results, since they are widely employed in other transmission systems and have very low mode mixing. In Chapter 7, the use of GI-POFs is investigated.

More specifically, Chapter 2 presents an MGDM model. This model tries to show under which conditions the MGDM link is linear with the optical intensity and can be described by a simple $M \times N$ matrix. It is shown that the matrix elements are real-valued in a transparent, broadband system. Given the linearity of the MGDM system, the effect of noise is examined and the power penalty due to additive thermal and shot noise is calculated. Further, the factors that limit the bandwidth of an MGDM system are identified and it is shown that, although in principle $M \geq N$, $M = N$ may improve the signal-to-noise ratio (SNR).

MGDM uses selective excitation and selective detection. Design considerations for an $N \times N$ MGDM system with GI-MMF are given in Chapter 3. On the input facet of the GI-MMF, N radially offset Gaussian-like beams are launched and

at the receiving end a multisegment detector geometry is proposed for spatially selective detection of the near-field pattern (NFP). This detector consists of N concentric annular segments. The power budget and the robustness of the proposed scheme are evaluated in terms of the power penalty due to the electronic matrix inversion, calculated in Chapter 2. The radial offsets of the input beams and the areas of the detector segments are chosen so as to minimize the power penalty due to the electronic matrix inversion. It is shown that the geometric parameters of an MGDM system, i.e. the radial offsets of the input beams and the areas of the detector segments, do not depend on the GI-MMF length for at least up to 1 km long silica-based GI-MMF. Other issues are also addressed, such as introducing an angular offset into the input beams and the use of standard GI-MMF passive optical components in MGDM transmission over network topologies beyond the basic point-to-point scenario.

One of the strongest aspects of the MGDM link proposed in Chapter 3 is that the geometric parameters of the system design hold independently of the GI-MMF length for at least 1 km long silica-based GI-MMF. In Chapter 4, the impact of the propagation effects on the NFP on the output facet of GI-MMFs is examined. These effects include differential mode delay and attenuation as well as mode mixing. Selective excitation with a radially offset SMF is considered. Given the launch conditions, the NFP depends on these propagation effects and the refractive index profile of the GI-MMF. It is shown that although light propagation affects the speckle pattern, the overall NFP does not change due to differential mode delay and attenuation, small deviations in the refractive index profile of the GI-MMF, or full intra-group mode mixing. The latter refers to mixing among the modes of a principal mode group. Finally, it is shown that when the refractive index profile exhibits a central dip, the overall NFP under central excitation can significantly expand, while in the case of a central peak, the overall NFP remains practically intact.

Factors such as temperature changes, wavelength drifting, or mechanical vibrations may change the distribution of the optical power among the modes, the launch conditions on the MMF input facet, and the coupling of the optical power to the photodetectors. Any such change will cause temporal variations in the transmission matrix of an MGDM system and will therefore affect its performance. Chapter 5 describes an experimental 2×2 MGDM link and it shows that such a link can be stable over time. In principle, to achieve reliable and high quality transmission, the MGDM system should be adaptive. Based on measurements of the transmission matrix over 12.7 h, cross-talk between the two channels is calculated as a function of the period of estimation of the transmission matrix.

The research presented in this thesis was carried out in the frame of the project "High capacity multi-service in-house networks, using mode group diversity multiplexing". This was a part of the Freeband Impulse Program of the Ministry of Economic Affairs of the Netherlands. Within this project, the Signal Processing Systems group of the Faculty of Electrical Engineering of the Eindhoven University of Technology led the investigation of the electrical signal processing aspects

of MGDM, both theoretically and experimentally. The last part of Chapter 5 gives a short description of the expansion of the 2×2 experimental setup, in order to include the electronic unit that performs the signal demultiplexing based on matrix inversion. A non-adaptive as well as an adaptive circuit was implemented and two analog, low-bandwidth signals were transmitted, showing the feasibility of the MGDM technique.

The linearity of an MGDM link as discussed in Chapter 2 requires that the fields of the mode groups at the output end of the GI-MMF are mutually incoherent. Further, when the number of channels increases, the power penalty due to the electronic matrix inversion also increases and the system becomes less robust to changes in the transmission matrix. An optical method to reduce cross-talk would allow for a more robust system, a larger number of channels and it would relax the requirement of mutual incoherence among the fields of the mode groups. Further, if cross-talk is sufficiently low, the need for electronic demultiplexing can be eliminated and a single source can be used with external modulators. This is a very important feature in order to combine MGDM with WDM, using a single source for each wavelength, and it would allow the use of MGDM in applications where maximization of the aggregate bandwidth per wavelength would be desired. In Chapter 6, mode-selective spatial filtering (MSSF), a new optical method to reduce cross-talk, is introduced and demonstrated. MSSF is shown to be very effective, while still keeping the MGDM system simple, since it can be achieved with only a single lens between the GI-MMF output end and the detectors.

In Chapter 7, the possibility of using POF in MGDM systems is examined. Literature results on POF are explored and some experimental results are presented. In principle, GI-POFs can be used in MGDM systems in a similar fashion as GI-GOFs. However, mode mixing in GI-POFs is very strong and this is detrimental to the use of GI-POF in MGDM systems, since the transmission matrix would strongly depend on the fiber length. Further, it is indicated that the flexibility of GI-POF, although advantageous for in-building installation, can pose practical difficulties in achieving a reliable system, since the NFP at its output end can be strongly affected by bending the GI-POF close to its output end or by applying stress to the GI-POF.

The final chapter of this thesis, Chapter 8, highlights the main conclusions from the research results presented in the preceding chapters. Further, MGDM is compared with other multiplexing techniques and suggestions for further research are given.

Chapter 2

Model of an $M \times N$ MGDM system

A mathematical model that describes an N-input, M-output MGDM system is presented. The model shows under which conditions the MGDM system is linear with respect to the optical intensity. For a broadband system, transparent to the signal format, the elements of the transmission matrix are positive, real numbers. The effect of noise sources that may influence an MGDM system is examined and the power penalty due to the additive thermal and shot noise is calculated. Furthermore, limitations in the bandwidth of the transmitted signals are explored. Finally, the relation between M and N is investigated, showing that preferably $M = N$.

2.1 Introduction

In Chapter 1, the principle of MGDM was briefly introduced. A simple relation was claimed to hold between the electrical input and output signals of an MGDM system. In particular, the $N \times 1$ vector $\mathbf{s}_T(t)$ of the N electrical signals that modulate the intensity of the N optical sources is related to the $M \times 1$ vector $\mathbf{s}_R(t)$ of the M output electrical signals after photodetection and electrical amplification via an $M \times N$ transmission matrix $\mathbf{H}(t)$ with real-valued elements $h_{i,j}(t)$, i.e.,

$$\mathbf{s}_R(t) = \mathbf{H}(t)\mathbf{s}_T(t) + \mathbf{n}(t), \tag{2.1}$$

where $\mathbf{n}(t)$ is an $M \times 1$ additive noise vector. Electronic matrix inversion can then recover the input signals, irrespective of their format. A real-valued matrix only expresses the spatial diversity and cannot compensate for differential delays in the system. Therefore, Eq. (2.1) assumes that dispersion does not pose a limitation,

Parts of this chapter are published in Ref. [4] of Appendix B.

i.e. the reciprocals of the differential delays are much larger than the bandwidth of the transmitter signals. The relative delay between the transmitted and received signals is not included in Eq. (2.1) to keep the notation simple. The time dependence of $\mathbf{H}(t)$ is due to several reasons such as temperature changes and mechanical vibrations, as will be further explained in Chapter 5. For Eq. (2.1) to hold, the value of $h_{i,j}(t)$ must vary slowly with time and more specifically, much slower than the signal vector $\mathbf{s}_T(t)$. The element $h_{i,j}(t)$ expresses the portion of the total received power from the jth mode group that is seen by the ith segment of the MGDM detector. Therefore, the sum of the elements of each column of $\mathbf{H}$ is equal to one, i.e.,

$$\sum_{i=1}^{M} h_{i,j} = 1. \tag{2.2}$$

A matrix for which Eq. (2.2) holds is commonly called column stochastic or left stochastic matrix.

In this chapter, we address the following questions:

- *Under which conditions does Eq. (2.1) hold?*
- *How does noise affect an MGDM system?*
- *Which are the factors that limit the bandwidth of the transmitted signals?*
- *What should be the relation between M and N?*

The analysis presented in this chapter uses the wave description of light, as well as some elements from communication and matrix theories. To provide better insight, a simple experimental result is included.

2.2 Linearity of an MGDM link

2.2.1 Propagation in MMFs

Propagation in MMFs introduces dispersion, attenuation and mode mixing. Let us assume that light from the jth source (T_j) is launched into the MMF. The propagating electric ($\mathbf{e}^j$) and magnetic ($\mathbf{h}^j$) complex fields are

$$\begin{bmatrix} \mathbf{e}^j(r,\phi,z,t) \\ \mathbf{h}^j(r,\phi,z,t) \end{bmatrix} = \sum_m c_m^j(z) \begin{bmatrix} \mathbf{e}_m(r,\phi) \\ \mathbf{h}_m(r,\phi) \end{bmatrix} e^{\mathrm{j}\omega_j t} \tag{2.3}$$

where $\mathbf{e}_m$, $\mathbf{h}_m$ are the modal electric and magnetic complex fields of the mth guided normal mode ($m = 1 \ldots N_m$), normalized to unit power, c_m^j is the complex modal amplitude, ω_j is the optical frequency of T_j and j is the imaginary unit [13]. Here, r, ϕ, z are cylindrical coordinates with the z-axis coinciding with the MMF axis. At the MMF input end $z = 0$ and at the MMF output end $z = L$. It

should be noted that for simplicity of notation, the dependence of $\mathbf{e}_m$ and $\mathbf{h}_m$ on ω_j is suppressed, given that this dependence is low in an MGDM system for which the N sources have the same or very similar ω_j. Further, when the optical sources are modulated with electrical signals, c_m^j is time-dependent. Therefore, strictly speaking, Eq. (2.3) holds for continuous wave sources. However, since the bandwidth of the modulating electrical signals is typically much lower than ω_j, again for reasons of simplicity of notation, the dependence of c_m^j on time is suppressed.

Propagation affects the propagating fields as far as the value of $c_m^j(z)$ is concerned, as can be seen in Eq. (2.3). In general,

$$\mathbf{c}^j(z+\Delta z) = \mathbf{D}(\Delta z)\,\mathbf{c}^j(z), \tag{2.4}$$

where $\mathbf{c}^j$ is the $N_m \times 1$ vector of the modal amplitudes. Here, $\mathbf{D} = \mathbf{BA}$, and $\mathbf{D}$, $\mathbf{B}$, $\mathbf{A}$ are complex-valued $N_m \times N_m$ matrices describing the effect of propagation. In particular, $\mathbf{A}$ and $\mathbf{B}$ express the loss and phase shift due to propagation, respectively. It is assumed that loss is limited, so that it can be treated as a perturbation of the lossless case [13]. In the case of a lossless MMF, $\mathbf{A}$ is equal to the $N_m \times N_m$ identity matrix and $\mathbf{D} = \mathbf{B}$. $\mathbf{B}$ is always a unitary matrix expressing energy conservation in the absence of losses. If mode mixing is neglected, matrices $\mathbf{B}$ and $\mathbf{A}$ are diagonal with elements

$$b_{m,m}(\Delta z) = e^{-\mathrm{j}\beta_m \Delta z} \quad \text{and} \quad a_{m,m}(\Delta z) = e^{-\gamma_m \Delta z}, \tag{2.5}$$

where β_m, γ_m are the propagation and attenuation coefficients of the normal mode m. Therefore,

$$c_m^j(z) = c_m^j(0) e^{-\mathrm{j}\beta_m z} e^{-\gamma_m z}. \tag{2.6}$$

The complex value of $c_m^j(0)$ depends on the excitation condition at the MMF input end and it can be calculated by the overlap integral method at $z = 0$. Particularly, the orthogonality of the modal fields at $z = 0$ reads

$$c_m(0) = \int_0^{2\pi}\int_0^{\infty} \mathbf{e}_{in}(r,\phi) \times \mathbf{h}_m^*(r,\phi) \cdot \hat{u}_z r \mathrm{d}r\mathrm{d}\phi \tag{2.7}$$

where $\mathbf{e}_{in}(r,\phi)$ is the excitation electric field at $z = 0$ and $\hat{u}_z$ is the unit vector in the direction of propagation.

In an MGDM link comprising N optical sources, the total propagating electric ($\mathbf{e}$) and magnetic ($\mathbf{h}$) fields are given as the superposition of the fields due to source T_j ($j = 1 \ldots N$), i.e.,

$$\begin{bmatrix} \mathbf{e}(r,\phi,z,t) \\ \mathbf{h}(r,\phi,z,t) \end{bmatrix} = \sum_j \begin{bmatrix} \mathbf{e}^j(r,\phi,z,t) \\ \mathbf{h}^j(r,\phi,z,t) \end{bmatrix} \tag{2.8}$$

and the corresponding intensity distribution at $z = L$ is given by

$$I(r,\phi,L,t) = \frac{1}{2}\mathrm{Re}\big[\mathbf{e}(r,\phi,L,t) \times \mathbf{h}^*(r,\phi,L,t) \cdot \hat{u}_z\big]. \tag{2.9}$$

Substituting (2.8) to (2.9) gives

$$I(r,\phi,L,t) = \frac{1}{2}\mathrm{Re}\left[\sum_j \mathbf{e}^j(r,\phi,L)\times\mathbf{h}^{j*}(r,\phi,L)\cdot\hat{u}_z + \sum_{j\neq k}\mathbf{e}^j(r,\phi,L)\times\mathbf{h}^{k*}(r,\phi,L)e^{\mathrm{j}(\omega_j-\omega_k)t}\cdot\hat{u}_z\right]. \quad (2.10)$$

The second term on the right-hand side (RHS) of Eq. (2.10) shows that non-linear interference among the channels may occur.

2.2.2 Spatially selective detection

The power detected over an area A_s at $z = L$ is

$$P_{A_s}(t) = \int_{A_s} I(r,\phi,L,t)\,\mathrm{d}A. \quad (2.11)$$

Substituting (2.10) to (2.11) gives

$$P_{A_s}(t) = \frac{1}{2}\mathrm{Re}\left[\sum_j \int_{A_s}\mathbf{e}^j(r,\phi,L)\times\mathbf{h}^{j*}(r,\phi,L)\cdot\hat{u}_z\mathrm{d}A + \sum_{j\neq k}\int_{A_s}\mathbf{e}^j(r,\phi,L)\times\mathbf{h}^{k*}(r,\phi,L)e^{\mathrm{j}(\omega_j-\omega_k)t}\cdot\hat{u}_z\mathrm{d}A\right]. \quad (2.12)$$

MGDM uses spatially selective detection and A_s is the area of one of the M detectors. The first term on the RHS of Eq. (2.12) is the summation of the optical powers due to each T_j alone and the second term expresses the interference of the N field distributions. Each field distribution carries different information. Equation (2.12) shows that, in principle, due to this interference term, the MGDM link is not linear with the optical power and signal distortion can be caused. Even in the case where each mode group comprises a completely different set of modes, the term expressing interference will not be zero since the modes are not orthogonal over the finite cross section A_s [13].

For a single-channel case with spatially selective detection, Eqs. (2.10) and (2.12) can still give the intensity and power, respectively, at $z = L$, with $\omega_j = \omega_k$ and j, k referring to different modes. Integration over the finite A_s yields a non-zero interference term. When dispersion cannot be neglected, the signal will be distorted, since at $z = L$ each modal field carries the signal with a different delay. This sort of distortion is different from the distortion caused by modal dispersion alone and it is the combined effect of modal dispersion and spatially selective detection. Modal dispersion is included in the phase of the fields in Eqs. (2.10) and (2.12).

Furthermore, Eq. (2.12) shows that optical heterodyning can occur when the optical frequencies ω_j are not the same. In a system with N different sources, such a possibility exists. If the intermediate frequency $\omega_j - \omega_k$ falls within the transmission bandwidth, the system performance degrades. Heterodyning, though, could be used as a way to filter out the non-linear system response, since it can set the interference term of Eq. (2.12) out of the transmission band. However, this would require some control over ω_j and thus the system would not be entirely wavelength-blind. Indeed, in Ref. [61], it is suggested that the wavelengths should not overlap exactly, in order to avoid coherent optical beat noise in the receiver. In order (2.1) to hold always, the interference term of Eq. (2.12) should be equal to zero independent of A_s, $\mathbf{c}^j(L)$, ω_j and the amount of spatial overlap among the fields of the mode groups at $z = L$. This could be achieved on average when the N field distributions at $z = L$ are mutually incoherent. In practice, optical sources with a relatively wide linewidth can fulfill this requirement within a certain bandwidth. Although on average the interference term of Eq. (2.12) can be zero, its standard deviation will not be zero, hence inducing beat noise. The larger the transmission bandwidth, the stronger the impact of this beat noise.

2.3 An experimental example of non-linear system response

A straightforward way to observe experimentally the non-linear system response expressed by the second term on the RHS of Eq. (2.12) is to launch two highly coherent, continuous wave signals with slightly different wavelengths at the MMF input end. The interference term is then demonstrated as heterodyning.

The experimental setup is shown in Figure 2.1. We used two external cavity type, tunable, semiconductor, continuous wave lasers with a linewidth of 85 kHz and a 100 m long 50/125 μm silica-based GI-MMF with a numerical aperture of 0.2. The lasers were pigtailed with standard single-mode fibers and a 50/50 single-mode directional coupler was used to launch the two signals in the GI-MMF. The wavelengths were tuned to 1350 nm. In particular, the wavelength of one laser was kept constant while the other laser was slightly de-tuned so as to observe heterodyning. At the GI-MMF output end a photodiode detected the whole area of the GI-MMF core. The photodiode was followed by a wideband amplifier (100 kHz to 20 GHz) with 20 dB gain.

Figure 2.2 shows the beat tone in the electrical spectrum at the amplifier output. This tone corresponds to the difference in the optical frequencies of the two lasers. In Figures 2.2(a) and 2.2(b), light at the output of the coupler was launched into the GI-MMF with 0 μm and 15 μm radial offset from the GI-MMF axis, correspondingly, by means of translational stages. In both cases, the lasers emitted equal power and the total optical power at the GI-MMF output end was approximately -3 dBm. For the 15 μm offset launch, the power emitted by the lasers was higher than for central launch to compensate for coupling and propagation losses.

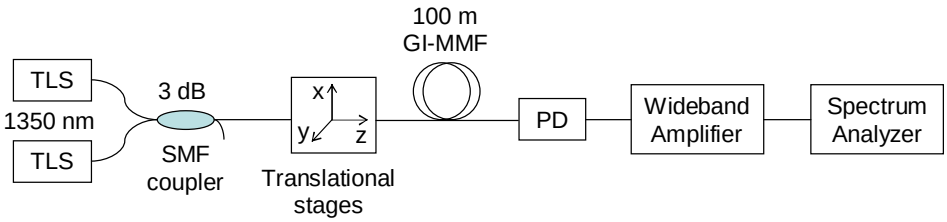

Figure 2.1: Experimental setup for the observation of heterodyning as an example of non-linear system response. TLS: tunable laser source. PD: photodiode.

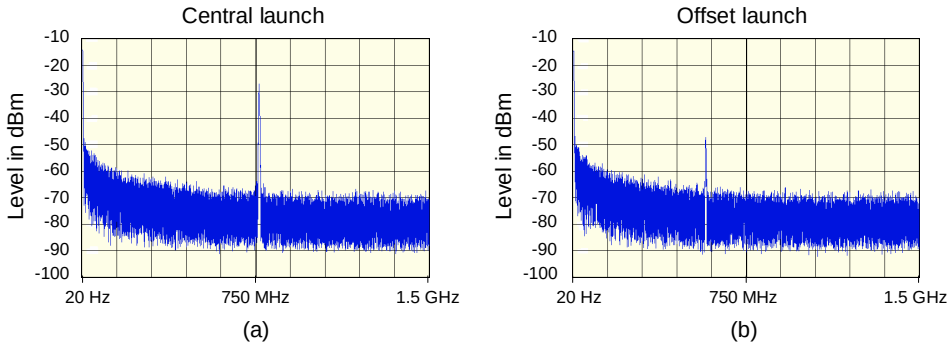

Figure 2.2: Heterodyning at the output end of a 100 m 50/125 μm GI-MMF, when two beams are launched on the GI-MMF input facet with (a) 0 μm (b) 15 μm radial offset from the GI-MMF axis.

This change in power caused some de-tuning of the lasers that appeared as a shift in the beat tone, as can be seen in Figure 2.2. The level of the beat tone is higher for central launch. This should be attributed to the two modal distributions at $z = L$, i.e., $\mathbf{c}^j(L)$. The more similar $\mathbf{c}^j(L)$, the higher the level of the beat tone. Two orthogonal field distributions would not yield a beat term. Although the radial offset is the same for both input fields, in principle, their polarization is not the same. Mode mixing conditions are also not identical, since the effect of fiber irregularities depends also on the field distribution. Consequently, the two $\mathbf{c}^j(L)$ are not identical as well. There is clearly better matching between the two $\mathbf{c}^j(L)$ in the case of central launch.

2.4 The effect of noise on an MGDM system

An MMF link is usually based on the IM-DD transmission approach. MGDM is in line with this approach. Each channel comprises an intensity modulated optical source and a photodiode combined with an electrical receiver circuit. Additionally,

the received electrical signals are fed into the electrical circuit that performs matrix inversion in order to demultiplex the transmitted signals. Each transmitted signal propagates over a different group of modes and the link requires selective excitation and detection.

Following these system characteristics, the performance of an MGDM link can be affected by thermal noise, shot noise, modal noise, as well as relative intensity noise and phase (or frequency) noise from the optical sources. The phase noise of the optical sources will manifest itself as modal noise. In the following subsections, we investigate the effect of each noise source in the system.

2.4.1 Power penalty due to additive thermal and shot noise

In Section 2.2, we investigated under which conditions an MGDM link can be described by Eq. (2.1). Assuming these conditions hold, electronic matrix inversion can recover the transmitted signals. The estimated transmitted signals $\hat{\mathbf{s}}_T(t)$ are

$$\begin{aligned} \hat{\mathbf{s}}_T(t) &= \mathbf{H}^{\dagger}(t)\mathbf{s}_R(t) + \mathbf{n}_{\mathrm{de}}(t) \\ &= \mathbf{s}_T(t) + \mathbf{H}^{\dagger}(t)\mathbf{n}(t) + \mathbf{n}_{\mathrm{de}}(t), \end{aligned} \tag{2.13}$$

where $\mathbf{n}_{\mathrm{de}}(t)$ is an $M \times 1$ vector that represents noise from the demultiplexing circuit and $\mathbf{H}^{\dagger}(t) = \{h^{\dagger}_{i,j}(t)\}$ is a $N \times M$ matrix such that $\mathbf{H}^{\dagger}(t)\mathbf{H}(t) = \mathbf{I}_{N\times N}$, where $\mathbf{I}_{N\times N}$ denotes the $N \times N$ identity matrix. For an invertible $N \times N$ system, $\mathbf{H}^{\dagger}(t)$ is the inverse of $\mathbf{H}(t)$, while for an $M \times N$ system $\mathbf{H}^{\dagger}(t)$ can be the Moore-Penrose pseudoinverse [71–73]. It is assumed that the estimation of $\mathbf{H}^{\dagger}(t)$ is ideal, so that $\mathbf{H}^{\dagger}(t)\mathbf{H}(t) = \mathbf{I}_{N\times N}$. If the latter does not hold, residual cross-talk will degrade the performance of the system. The system has to adapt to changes in the value of the elements $h_{i,j}(t)$. The temporal behavior of the system will be investigated in Chapter 5.

Equation (2.13) shows that the noise term $\mathbf{n}(t)$ changes to a new value $\mathbf{H}^{\dagger}(t)\mathbf{n}(t)$. This induces a power penalty to maintain the desired value of signal-to-noise ratio (SNR). In the following, this power penalty is calculated[1]. In the calculation that follows, the term $\mathbf{n}_{\mathrm{de}}(t)$ is neglected, in order to isolate the influence of matrix inversion. We distinguish two cases where either shot or thermal noise is the prevalent noise source. Shot noise is due to the discreteness of photons and electrons as well as due to the stochastic electron-hole recombination in semiconductor materials [17]. It poses a fundamental limit to the sensitivity of the receiver of an optical link. Thermal noise is due to the random thermal motion of electrons inside electrical conductors and it is proportional to the absolute temperature [16, 17]. Both shot and thermal noise are assumed to be added to the received signals.

Let SNR_j denote the SNR at the jth electrical output of the MGDM system, i.e. at the jth output port of the electrical circuit that performs the demultiplexing based on matrix inversion. The number of the electrical output ports of the

[1]This calculation was first introduced for on-off keying modulation by Alfonso Martinez (Signal Processing Systems group, Eindhoven University of Technology, the Netherlands).

demultiplexer is N. At the jth output port, the signal that propagates over the jth mode group should appear. SNR_j is given by

$$\mathrm{SNR}_j = \frac{(R\bar{P}_j)^2}{\sigma_j^2}, \tag{2.14}$$

where R is the responsivity of the detectors, $\bar{P}_j$ is the average received optical power from the jth mode group and σ_j^2 the noise variance. It is assumed that all M detectors have the same responsivity. The variance of the noise at the jth electrical output of the system is

$$\sigma_j^2 = \mathrm{E}\left[\left(\sum_{k=1}^{M} h_{j,k}^{\dagger} n_k\right)^2\right] = \sum_{k=1}^{M} (h_{j,k}^{\dagger})^2 \,\mathrm{Var}\left(n_k\right), \tag{2.15}$$

where n_k are the statistically independent elements of the noise vector $\mathbf{n}$ with zero mean value, and E, Var denote the expected value and the variance of a random variable, respectively. Vector $\mathbf{n}$ expresses noise at the M input ports of the electronic demultiplexer. When shot noise prevails, $\mathrm{Var}\left(n_k\right)$ is proportional to the optical power [16, 17], i.e.,

$$\mathrm{Var}\left(n_k\right)\big|_{\mathrm{shot}} \propto \sum_{l=1}^{N} h_{k,l}\bar{P}_l, \tag{2.16}$$

while when noise is dominated by thermal noise, $\mathrm{Var}\left(n_k\right)$ is independent of the optical power [16, 17], i.e.,

$$\mathrm{Var}\left(n_k\right)\big|_{\mathrm{thermal}} = \sigma^2_{\mathrm{thermal}}. \tag{2.17}$$

The SNR of the single-channel case is $\mathrm{SNR}_0 = (R\bar{P}_0)^2 / \mathrm{Var}\left(n_k\right)$, where $\bar{P}_0$ is the average received optical power, $\mathrm{Var}(n_k)\big|_{\mathrm{shot}} \propto \bar{P}_0$ and $\mathrm{Var}(n_k)\big|_{\mathrm{thermal}} = \sigma^2_{\mathrm{thermal}}$. To ensure that $\mathrm{SNR}_j = \mathrm{SNR}_0$, the value of $\bar{P}_j$ will differ from the value of $\bar{P}_0$, and therefore the following optical power penalty will be induced at the thermal noise limit:

$$\left.\frac{\bar{P}_j}{\bar{P}_0}\right|_{\mathrm{thermal}} = \sqrt{\sum_{k=1}^{M} (h_{j,k}^{\dagger})^2}. \tag{2.18}$$

At the shot noise limit, assuming equal value of $\bar{P}_j$ for $j = 1 \ldots N$, the optical power penalty is

$$\left.\frac{\bar{P}_j}{\bar{P}_0}\right|_{\mathrm{shot}} = \sum_{k=1}^{M}\sum_{l=1}^{N} (h_{j,k}^{\dagger})^2 h_{k,l}. \tag{2.19}$$

In order $\mathrm{SNR}_j \geq \mathrm{SNR}_0, \forall j$, at the shot noise limit, the actual power penalty at every channel will equal the maximum of the power penalties calculated with (2.19). The above power penalty is with regard to the SNR. Other metrics, such as the bit-error rate could be used. The SNR was chosen as a suitable metric for a transmission system transparent to the signal format.

2.4.2 Modal noise

In MMF links, the SNR can be degraded by modal noise [16, 17, 74, 75]. At the output end of the MMF, light distribution exhibits a speckle pattern. Temporal variations of this speckle pattern that is detected by the photodiode, in combination with spatial filtering are translated into intensity variations. Spatial filtering is often due to connector misalignments and splices. Additionally, in MGDM the optical power at the GI-MMF output end is split among M detectors. Further, MGDM uses restricted excitation of the MMF and this may increase the variance of modal noise compared to the case of overfilled launch [76]. However, at the same time, an MGDM system uses adaptive estimation of the transmission matrix. Therefore only changes in the optical intensity seen by each detector that occur faster than the adaptation rate will be manifest as modal noise.

Modal noise does not pose a fundamental limit to the system performance and it can be combatted with a proper system design. The speckle pattern is due to interference among the modes. It depends on the optical spectrum of the sources as well as on the length of the MMF [74, 75]. Mechanical disturbances and deformation of the MMF, e.g. due to temperature variations, will affect the speckle pattern. The same holds for variations of the optical spectrum of the sources. The narrower the spectrum of the optical source, the larger its coherence time and the larger the contrast in the speckle pattern. Phase (or frequency) noise of the optical source tends to widen the optical spectrum. Employing light emitting diodes (LEDs) can eliminate modal noise. Of course, this limits the bandwidth of the transmitted signals and it is not a good choice for a system that uses selective excitation of GI-MMFs, due to the large angular divergence of light emitted by LEDs.

The use of relative wide-spectrum optical sources is beneficial for both the linearity of an MGDM link, as discussed in Section 2.2, and the reduction of modal noise. This is in line with the use of MMFs in short reach networks, where the low cost of the related components is a key parameter.

2.4.3 Relative intensity noise

The output optical power from semiconductor lasers can fluctuate, even when the laser is driven by a constant current. This is due to spontaneous emission and electron-hole recombination. In semiconductor lasers, the power fluctuations are attributed primarily to spontaneous emission [17]. This effect is referred to as relative intensity noise (RIN) and it can degrade the SNR of the transmitted signals. In an optical communication system, RIN can increase due to reflections. If $\mathbf{n}_{RIN}(t)$ is the $N \times 1$ RIN signal vector in an MGDM system, the vector of the received electrical signals will be

$$\mathbf{s}_R(t) = \mathbf{H}(t)[\mathbf{s}_T(t) + \mathbf{n}_{RIN}(t)] + \mathbf{n}(t), \tag{2.20}$$

and therefore ideal matrix inversion will not change the variance of RIN, since

$$\mathbf{H}^{\dagger}(t)\mathbf{s}_R(t) = \mathbf{s}_T(t) + \mathbf{n}_{RIN}(t) + \mathbf{H}^{\dagger}(t)\mathbf{n}(t). \tag{2.21}$$

The difference between RIN and thermal or shot noise is that noise variables at each detector due to RIN, i.e. the elements of $\mathbf{H}\mathbf{n}_{RIN}$, are not statistically independent, since the noise source is at the transmitting side of the link. The same holds for any noise that is generated at the transmitting side, e.g. thermal noise from the laser drivers.

2.5 Bandwidth limitations

An attractive feature of optical communication systems is that they support broadband transmission. As discussed above, an MGDM system can be characterized by a real-valued matrix as long as the fields of the mode groups at the output end of the GI-MMF are mutually incoherent and dispersion does not pose a limitation. This is because a real-valued matrix cannot account for any differential delay. In MGDM, $\mathbf{H}$ simply expresses the spatial diversity. Further, as discussed in Section 2.2, dispersion combined with spatial filtering can further induce signal distortion, due to the non-orthogonality of the modal fields over a finite area of detection. We can then conclude that in an MGDM system the transmission bandwidth is limited by fiber dispersion. Different transmission formats have a different tolerance with respect to dispersion. How severe is the bandwidth limitation from dispersion in GI-MMFs?

To answer this last question, we should first try to identify what is meant by broadband transmission. For the residential user, where the word broadband commonly applies, any connection that offers a bit rate of a few Mbit/s is considered broadband. Such connections are widely provided by digital subscriber line (DSL) techniques. Certainly, the DSL bandwidth can be easily furnished by fiber connections and therefore an optical fiber infrastructure is a broadband one. Furthermore, estimations for the future bandwidth demands of the residential user are debated. Predictions vary from a few hundreds of MHz to a few GHz. An MMF infrastructure offers more scalability to the bandwidth of an in-house network than any solution based on copper.

Dispersion in MMFs depends on the refractive index profile, the excitation and detection conditions as well as mode mixing. GI-MMFs have much lower dispersion than SI-MMFs and this is the main reason for their preferred use. In MMF transmission, selective excitation and detection affect the dispersive properties of the communication channel. Excitation of a single mode would correspond to SMF operation and maximization of the transmission bandwidth. When more than two modes are excited and detected, which is the standard case, the total dispersion depends on the differential delays among the modes. Beyond two, the number of excited modes is not therefore the most significant factor for the bandwidth. It is common to estimate the bandwidth of an IM-DD MMF channel for overfilled

launch, i.e. when all modes are equally excited. This condition can be achieved with a mode scrambler at the input end of the MMF. A reliable technique that can enhance by up to four times the bandwidth of silica-based GI-MMFs, even of ones with a non-optimal refractive index profile, is the offset launch technique [70, 77]. This technique uses selective excitation of a large group of higher order modes with relatively comparable propagation delays. This excitation is achieved with a Gaussian-like beam launched onto the GI-MMF input facet with a radial offset from the GI-MMF axis.

In modern silica-based GI-MMFs, optimal refractive index profiles minimize both differential mode delay and mode mixing, easily allowing for a bandwidth of several GHz over a few hundred meters of GI-MMF. In a recent experiment by Yam et. al. [78], 40 Gbit/s IM-DD transmission at 1551.73 nm over 3.4 km GI-MMF of 50/125 μm core/cladding diameter was demonstrated using on-off keying, return-to-zero format and transceivers for SMF links. GI-POFs also allow for a few GHz transmission bandwidth over a few hundreds of meters long links [18]. Further, it should be noted that because MGDM supports signal format transparency, spectrally efficient modulation formats, such as quadrature amplitude modulation, can be used [79, 80].

2.6 The relation between M and N

The $M \times N$ linear system of Eq. (2.1) describes an $M \times N$ MGDM transmission system. The existence and number of solutions of an $M \times N$ linear system depend on the relation between M and N, as well as on the system matrix, which in the case of an MGDM system is the transmission matrix $\mathbf{H}$. If $N > M$, the system can have infinitely many solutions or no solutions at all. If $M > N$ any option is possible, i.e. no solutions at all, infinitely many solutions or a unique solution. If $M = N$ the system has a unique solution if $\mathbf{H}$ is non-singular. In MGDM, the transmitted signals $\mathbf{s}_T$ should be determined by the received signals $\mathbf{s}_R$ and the transmission matrix $\mathbf{H}$. When the system has infinitely many solutions, it is impossible to find $\mathbf{s}_T$ by simply knowing $\mathbf{H}$ and $\mathbf{s}_R$. Some of the elements of $\mathbf{s}_T$ should be also known. This makes such a case impractical and therefore the system must have a unique solution. This implies that, in principle,

$$M \geq N.$$

In the case of $M > N$, it is a requirement of the link design to yield a system with a unique solution.

From the noise point of view, when the system is limited by thermal noise at the receiver, it is favorable for the SNR to have $M = N$. This is because thermal noise at each of the M electrical outputs has a given variance, while as M increases the received optical power per detector decreases. Considering modal noise, it is also favorable that M has the lowest possible value, i.e. $M = N$, since the larger the detecting area is, the smaller the variance of the modal noise will

be. When shot noise is the limiting factor, the SNR value is proportional to the received optical power [17]. Therefore it is beneficial that each detector receives the maximum possible power, which prescribes $M = N$. For these reasons, in the following chapters we will consider the case of

$$M = N.$$

Our goal will be to design an $N \times N$ system for which the diagonal elements $h_{i,i}$ have a larger value than the rest of the elements. In this case, the system's matrix is said to be a diagonally dominant one. The case $\mathbf{H} = \mathbf{I}_{N\times N}$, where $\mathbf{I}_{N\times N}$ is the $N \times N$ identity matrix, represents the ideal scenario where the channels are fully separate in the optical intensity domain and no electronic separation is required.

2.7 Conclusions

An MGDM transmission system is described by the linear system of Eq. (2.1), provided that the intensity profiles of the detected mode groups can be simply added. In the most general case, without considering the amount of spatial overlap among the fields of the detected mode groups, this implies that the fields of the mode groups at the detection plane must be mutually incoherent. An experimental example of non-linear response was given, in which optical heterodyning was observed at the output end of a 100 m long 50/125 μm silica-based GI-MMF, with two tunable lasers of narrow linewidth and slightly different central wavelengths at the input end of the GI-MMF. In practice, mutual incoherence can be achieved by using optical sources with a relatively wide optical spectrum, which also benefits the reduction of modal noise. The adaptivity of the MGDM system can partially compensate for modal noise. When the effect of dispersion can be neglected, the transmission matrix elements $h_{i,j}$ are real-valued expressing the portion of the total received power from the jth ($1 \leq j \leq N$) mode group that is seen by the ith ($1 \leq i \leq M$) detector. Electronic demultiplexing based on matrix inversion can separate the channels irrespective of the signal format. The influence of shot noise and thermal noise, at the receiver, on the variance of the output signals after electronic demultiplexing based on matrix inversion has been derived. The power penalty which is then induced to maintain the SNR of the single-channel case has been calculated. Electronic matrix inversion does not affect the variance of relative intensity noise, compared to the single-channel case. SNR considerations imply that $M = N$ is the preferred choice, which means that $\mathbf{H}$ should be a square matrix.

Chapter 3

Design of an $N \times N$ MGDM link

Geometric considerations for a mode group diversity multi/demultiplexer are given. N radially offset Gaussian-like beams are assumed on the GI-MMF input facet, together with an N-segment detector that responds to the NFP on the GI-MMF output facet. The proposed scheme is consistent with high coupling efficiency and when it is applied over silica-based GI-MMFs, the choice of the radial offsets and the detector segments does not depend on the length of the GI-MMF for at least up to 1 km. For $N = 2 \dots 5$, the scheme is evaluated in terms of the optical cross-talk and the optical power penalty due to the electronic matrix inversion. Further, the sensitivity of the link to misalignments, both at the transmitting side and the receiving side, is examined. The link becomes less robust as the number of channels increases. Finally, the use of passive optical components, such as optical splitters, is investigated. Such components are needed in network topologies beyond the basic point-to-point scenario. The results of this chapter are important for the design and manufacture of MGDM-specific components.

3.1 Selective excitation of GI-MMFs

One way to excite selectively a GI-MMF is by launching a Gaussian beam at its input end. Compared to other techniques, such as using a mask at the input of the GI-MMF [53] or side launch through a prism [81], excitation with a Gaussian beam is simple and provides high coupling efficiency. The set of excited modes depends on the launch conditions, i.e. the beam waist radius w_0, the radial ρ_0, the angular θ_0 and ψ, as well as the axial offsets. These offsets refer to the radial displacement of the beam with respect to the GI-MMF axis, its direction of propagation and

Parts of this chapter are published in Refs. [4,9,12,14,15] of Appendix B.

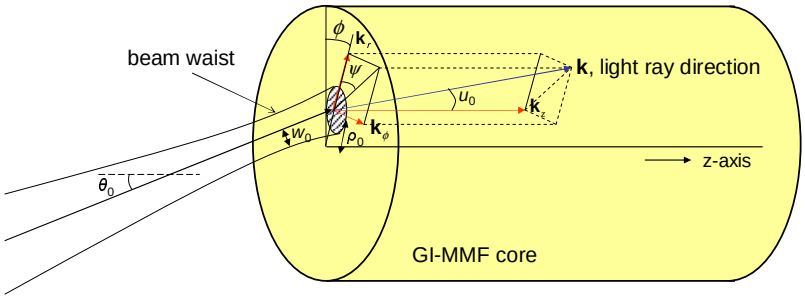

Figure 3.1: Selective excitation of a GI-MMF using a Gaussian beam on its input facet. The launch conditions depend on the placement of the beam on the facet of the GI-MMF.

the distance of the beam waist from the input facet of the GI-MMF, respectively, as shown in Figure 3.1. In the case of GI-MMFs with parabolic index profiles, for radially offset beams with zero angular offset, i.e. $\theta_0 = 0$, in order to excite as few principal mode groups, i.e. groups of modes with similar propagation coefficient, as possible, the beam waist should lie on the fiber facet (zero axial offset) with its radius given by [82]

$$w_0 = c(\rho_0) w_{\mathrm{fm}}, \tag{3.1}$$

$$\text{where} \quad w_{\mathrm{fm}} = \sqrt{\frac{2a}{k_0 \, \mathrm{NA}_{\text{GI-MMF}}(0)}} \tag{3.2}$$

is the mode field radius of the fundamental mode. Here, a is the radius of the GI-MMF core, $\mathrm{NA}_{\text{GI-MMF}}(0)$ is the central numerical aperture of the GI-MMF and k_0 is the free space wave-vector. Further, $0 < c(\rho_0) \leq 1$ and the suggested value is $c(\rho_0) = 0.6$, which is nearly optimal for the excitation of higher order modes ($\rho_0 > 0.3a$) and still retains almost 80% of the launched power in the fundamental mode when $\rho_0 = 0$ [82]. A good compromise is to use an SMF.

In the next section, an $N \times N$ MGDM link is discussed, employing N radially offset beams with zero angular offset. As will be shown, this ensures high coupling efficiency for large ρ_0 and yields a matrix $\mathbf{H}$ which is not practically affected by the GI-MMF length for up to 1 km, when silica-based GI-MMF is considered.

3.2 A link with radially offset input beams

In the following, a 3×3 MGDM link is described, serving as an example for the design of an $N \times N$ one. At the transmitting side of the link, three radially offset beams are launched, and at the receiving side, a three-segment detector is proposed. The segment areas are chosen so as to minimize, on average, the optical cross-talk at the detector segments.

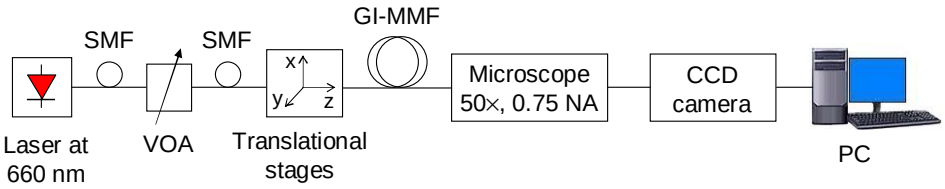

Figure 3.2: Experimental setup for the observation of the NFP on the output facet of a GI-MMF under selective excitation with a radially offset SMF.

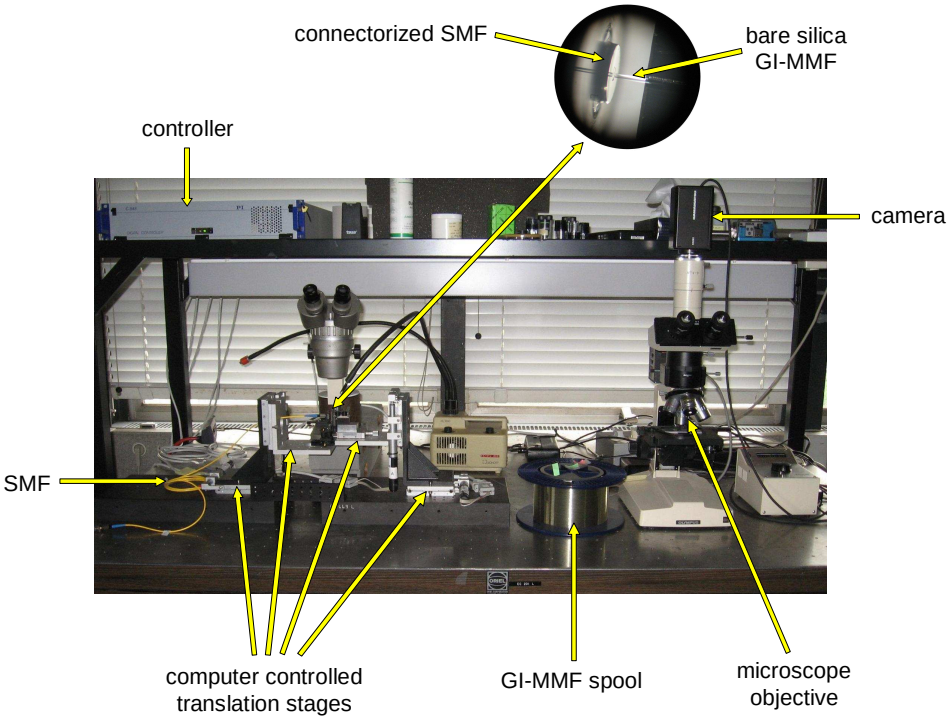

Figure 3.3: Photograph of the experimental setup used to observe the NFP on the output facet of a GI-MMF under selective excitation with a radially offset SMF.

3.2.1 Experimental NFP at the GI-MMF output

Figure 3.2 shows the experimental setup used to observe the near-field pattern (NFP) of the optical intensity on the output facet of a GI-MMF under selective excitation. A photograph of the actual setup in the laboratory is shown in Figure 3.3. A continuous wave 660 nm Fabry–Pérot laser pigtailed with a 1 m SMF

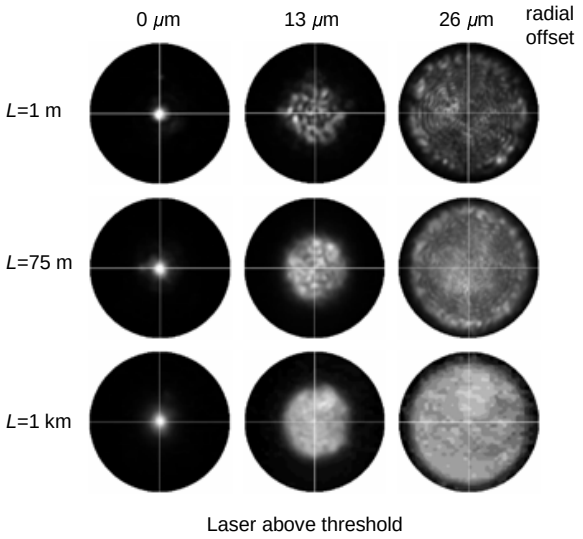

Figure 3.4: NFP on the output facet of a 1 m, 75 m and 1 km long 62.5/125 μm silica-based GI-MMF under selective excitation with a radially offset beam, at 660 nm wavelength. The radial offset was 0 μm, 13 μm and 26 μm and the laser was operating above threshold.

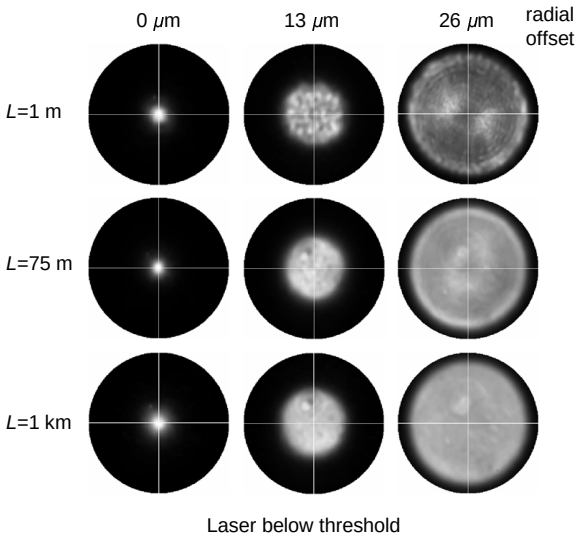

Figure 3.5: NFP on the output facet of a 1 m, 75 m and 1 km long 62.5/125 μm silica-based GI-MMF under selective excitation with a radially offset beam, at 660 nm wavelength. The radial offset was 0 μm, 13 μm and 26 μm and the laser was operating below threshold.

with a mode field diameter (MFD) of 4.2 μm and an NA of 0.12 was used to excite selectively a GI-MMF with core/cladding diameter of 62.5/125 μm and an NA of 0.275. A variable optical attenuator (VOA) with SMF pigtails, of similar MFD and NA as the laser pigtail, was used to control the level of the optical power. The radial offset of the SMF axis from the GI-MMF axis was set by means of computer-controlled translational stages. A microscope with 50× magnification and an NA of 0.75 projected the NFP on the GI-MMF output facet onto a charge-coupled device (CCD) camera. An image of the NFP was grabbed with video processing software. Three GI-MMFs were tested, of lengths $L = 1$ m, 75 m and 1 km, under excitation with the SMF at offset $\rho_0 = 0$ μm, 13 μm and 26 μm radial offset, corresponding to beams T_1, T_2 and T_3 of the investigated MGDM scheme [Figure 3.6(a)]. The NFP was observed for laser operation above as well as below threshold and the 75 m and 1 km GI-MMFs were placed around a 15 cm diameter drum. In a real MGDM link, the three beams should be launched simultaneously. This could be achieved by means of a laser array [83] or a planar waveguide [84].

The obtained NFP images are shown in Figures 3.4 and 3.5 for laser operation above and below threshold, respectively. The overall NFP has a disk-like shape, with a radius that depends on the radial offset of the input beam. It is evident that the disk radius is practically independent of the GI-MMF length, indicating that mode mixing is limited. If mode mixing is strong, the NFP hardly depends on the launch conditions. Further analysis on the impact of the propagation effects, including mode mixing, on the NFP will be presented in Chapter 4. The speckle contrast is larger for laser operation above threshold and for short GI-MMFs. This is because under these conditions the mutual coherence among the fields of the guided modes is strong [75]. It should be noted that in the results presented in Figures 3.4 and 3.5, an optical filter was used at the GI-MMF output, instead of the VOA shown in Figure 3.2. This was simply because there was no VOA available operating at red light at the time these results were obtained.

3.2.2 Transmission matrix and cross-talk estimation

Figure 3.6(b) shows the normalized annular power flux (NAPF) of the three MGDM channels for the case of the 75 m long GI-MMF and for laser operation above threshold. The annular power flux is the integrated light intensity I between radii r and $r + \mathrm{d}r$ over the output facet of the GI-MMF [85]. The NAPF due to T_j is given by

$$\mathrm{NAPF}_j(r, \mathrm{d}r) = \frac{\int_0^{2\pi} \int_r^{r+\mathrm{d}r} I_j(r', \phi) r' \, \mathrm{d}r' \, \mathrm{d}\phi}{\int_0^{2\pi} \int_0^{\alpha} I_j(r', \phi) r' \, \mathrm{d}r' \, \mathrm{d}\phi}. \tag{3.3}$$

where (r, ϕ) are polar coordinates on the GI-MMF facet with $r = 0$ on the GI-MMF axis. For the calculation of the curves of Figure 3.6(b), $\mathrm{d}r \approx 0.47$ μm. NAPF depends on the area of integration and therefore it will be very small close to the GI-MMF axis, even though the actual intensity there can be high.

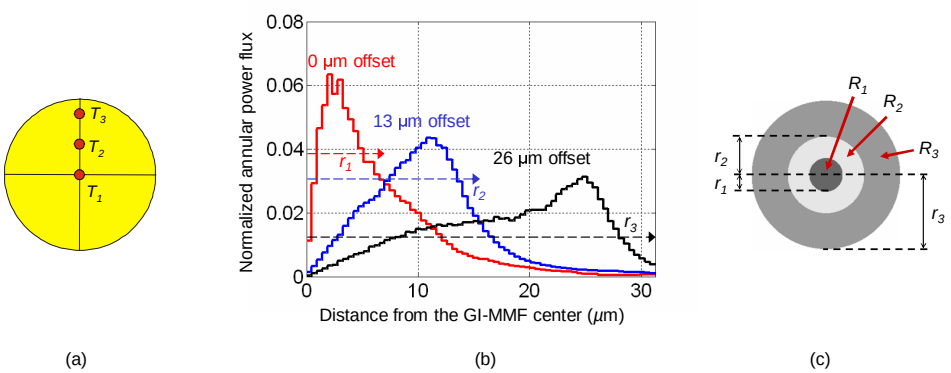

Figure 3.6: (a) Three launched beams on the front facet of a GI-MMF, with radial offsets 0 μm, 13 μm and 26 μm. (b) Measurements of the normalized annular power flux at the output of a 75 m long 62.5/125 μm silica-based GI-MMF under selective excitation with an SMF at 0 μm, 13 μm and 26 μm radial offset, at 660 nm wavelength. (c) Three-segment detector geometry based on the measurements of (b).

Due to the circular symmetry of the GI-MMF and the overall NFP, a circular three-segment detector geometry is proposed, consisting of three annular segments, as illustrated in Figure 3.6(c). The radii that define the detector segments are chosen close to the points of intersection of the three curves of the NAPF shown in Figure 3.6(b). This choice yields a diagonally dominant matrix. Further, the intersection points approximate the points for which cross-talk is minimized on average, as will be explained in Section 3.4. In the 3×3 example, the detector radii are $r_1 = 7$ μm, $r_2 = 16$ μm and $r_3 = 31.25$ μm. In legacy GI-MMFs, defects may occur in the refractive index profile, primarily close to the GI-MMF axis. An investigation of the impact of such defects will be presented in Chapter 4.

In Chapter 2, it was shown that under certain conditions it is possible to add up the three intensity distributions at the GI-MMF output. Assuming such conditions hold, the MGMD link is linear with the optical intensity and the $h_{i,j}$ coefficients can be estimated by

$$h_{i,j} = \frac{\int_0^{2\pi} \int_{r_{i-1}}^{r_i} I_j(r,\phi) r \, \mathrm{d}r \, \mathrm{d}\phi}{\int_0^{2\pi} \int_0^{\alpha} I_j(r,\phi) r \, \mathrm{d}r \, \mathrm{d}\phi}. \tag{3.4}$$

The resulting matrix for laser operation above threshold is

$$\mathbf{H} = \begin{pmatrix} 0.64 \ / \ 0.67 \ / \ 0.61 & 0.23 \ / \ 0.23 \ / \ 0.19 & 0.08 \ / \ 0.07 \ / \ 0.07 \\ 0.30 \ / \ 0.26 \ / \ 0.29 & 0.65 \ / \ 0.63 \ / \ 0.63 & 0.30 \ / \ 0.30 \ / \ 0.29 \\ 0.06 \ / \ 0.07 \ / \ 0.10 & 0.12 \ / \ 0.14 \ / \ 0.18 & 0.62 \ / \ 0.63 \ / \ 0.64 \end{pmatrix},$$

presented in the form $h_{i,j}\{75 \text{ m} \ / \ 1 \text{ m} \ / \ 1 \text{ km}\}$. The matrix is similar for laser

operation below threshold. The $h_{i,j}$ coefficients vary moderately with the GI-MMF length, which makes the choice for the values of the radial offsets of the input beams and the detector radii independent of the length of the silica-based GI-MMF, for at least up to 1 km.

The optical cross-talk (OC) in decibels at the ith detector segment R_i is

$$\mathrm{OC} = 10 \log_{10} \frac{\sum_{j \neq i} h_{i,j}}{h_{i,i}}. \tag{3.5}$$

For the 75 m GI-MMF, cross-talk at segment R_1, R_2 and R_3 is -3.1 dB, -0.3 dB and -5.4 dB, respectively.

3.3 Introducing an angular offset

Cross-talk could be reduced by bounding the propagating power in the jth mode group between r_{j-1} and r_j. Annular NFPs can be observed by introducing an angular offset to the input beams. To confine the radial spread of the NFP as much as possible $\theta_0 = \theta_0^{\mathrm{he}}$ in accordance with the launch of helical rays [86]. Helical rays are propagating rays with two caustic surfaces that coincide. The two caustic surfaces of a propagating ray are cylindrical surfaces that define the area of the GI-MMF core where the ray is bound [13, 15, 16]. The projection of the trajectory of a helical ray on a plane perpendicular to the GI-MMF axis is a circle. The launch of helical rays depends on the refractive index profile $n(r)$ and the

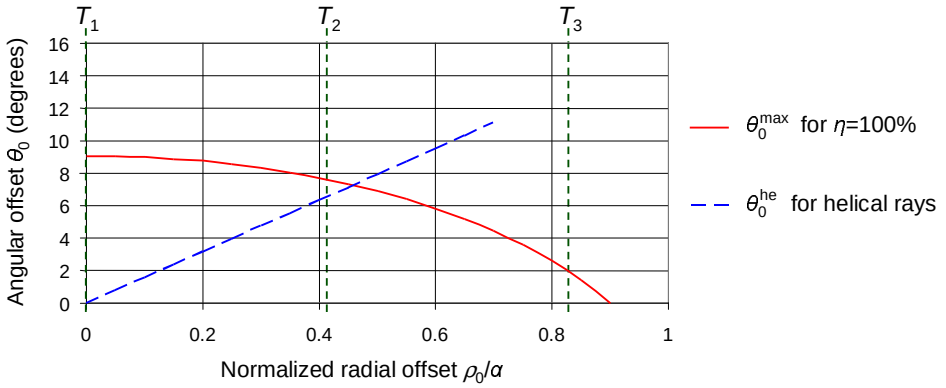

Figure 3.7: Solid curve: $\theta_0^{\max}$ that maintains $\eta = 100\%$, when η is calculated using only the NA as a criterion. Dashed curve: θ_0^{he} for the launch of a helical ray. For $\rho_0 > 0.7a$ it is not possible to launch a helical ray, due to the small value of the local NA. Both curves correspond to a GI-MMF with a parabolic refractive index profile.

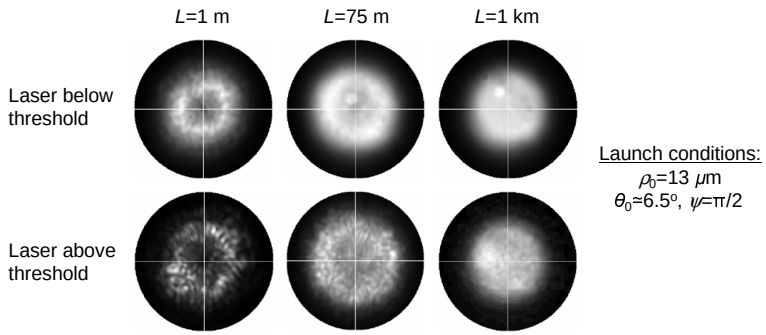

Figure 3.8: NFP on the output facet of a 62.5/125 μm silica-based GI-MMF under selective excitation with a beam, at 660 nm wavelength. The launch conditions of the input beam are in line with the launch of a helical ray.

radial offset ρ_0, while $\psi = \pi/2$. For an α-profile, the value of the angular offset θ_0^{he} is given by [86]

$$\theta_0^{\text{he}}(\rho_0) = \arcsin \sqrt{\frac{\alpha\, \text{NA}^2_{\text{GI-MMF}}(0)}{2} \left(\frac{\rho_0}{a}\right)^{\alpha}}. \tag{3.6}$$

According to Eq. (3.6), for $\rho_0 = 0$, $\theta_0^{\text{he}}(0) = 0$, and this case corresponds to the straight, axial ray.

In the case of the investigated 3×3 system, a non-zero angular offset could be introduced only in T_2. This is because an angular offset at T_3 would result in very low coupling efficiency due to the small local NA of the GI-MMF at $\rho_0 = 26$ μm. Figure 3.7 shows $\theta_0^{\text{he}}(\rho_0)$ required for a helical ray in the case of a parabolic-index GI-MMF, as well as the maximum θ_0, or $\theta_0^{\max}(\rho_0)$, that can be introduced in order to maintain 100% coupling efficiency (η). The latter was calculated only with the NA value as a criterion. In particular, for the solid curve of Figure 3.7, the input beam was considered as a cone with $\text{NA}_{\text{beam}} = 0.12$ and the maximum θ_0 that still keeps the beam within the local NA was calculated. In other words,

$$\theta_0^{\max}(\rho_0) = \theta_{\text{GI-MMF}}(\rho_0) - \theta_{\text{beam}}, \tag{3.7}$$

where θ_{beam} is the angular divergence of the input beam given by

$$\theta_{\text{beam}} = \arcsin(\text{NA}_{\text{beam}}), \text{ with } 0 \leq \theta_{\text{beam}} \leq \pi/2 \tag{3.8}$$

and $\theta_{\text{GI-MMF}}$ denotes the angular acceptance of the GI-MMF due to the local NA, calculated as

$$\theta_{\text{GI-MMF}}(\rho_0) = \arcsin \sqrt{n^2(\rho_0) - n^2(a)}. \tag{3.9}$$

Equation (3.7) is meaningful only when $\theta_0^{\max}(\rho_0) > 0$ and Eq. (3.6) can be used as long as $\theta_0^{\text{he}}(\rho_0) \leq \theta_{\text{GI-MMF}}(\rho_0)$, i.e. $\theta_0^{\text{he}}(\rho_0)$ falls within the local NA.

The NFP on the output facet of the GI-MMFs used in Section 3.2 was observed when the launch conditions of T_2 approximate the launch of a helical ray, i.e. $\rho_0 = 13\ \mu$m, $\theta_0 \simeq 6.5^o$ and $\psi = \pi/2$. The NFP images for laser operation above and below threshold are shown in Figure 3.8. When the laser operates below threshold, for the 1 m long GI-MMF, a clear doughnut-like image is observed. However, this image is hardly maintained after 75 m of propagation and completely turns into a disk after 1 km of propagation. Similar observations have been presented in Ref. [86]. The same holds true for laser operation above threshold, although the strong speckle contrast of the NFP on the output facet of the 1 m long GI-MMF makes the shape of the NFP more obscure. Overall, introducing an angular offset to improve the separation of the MGDM channels is not of particular interest due to restrictions related with the coupling efficiency and the dependence of the NFP on the length of the GI-MMF. This dependence may be due to differential mode attenuation or some mode mixing.

3.4 Cross-talk and power penalty minimization

Design considerations for a mode group diversity multi/demultiplexer have been hitherto given and the optical cross-talk in a 3×3 link has been estimated. To recover the input signals, electrical processing is required. In particular, as discussed in the previous chapters, matrix inversion is used, which is a zero-forcing method in line with the requirement of signal format transparency. Matrix inversion recovers the transmitted signals, however at the same time it induces an optical power penalty. In Chapter 2, Eqs. (2.18) and (2.19), this power penalty at the thermal noise and shot noise limits, respectively, was shown to be in decibels,

$$\left.\frac{\bar{P}_j}{\bar{P}}\right|_{\text{thermal}} = 10\log_{10}\sqrt{\sum_{k=1}^{N}(h^{\dagger}_{j,k})^2} \tag{3.10}$$

$$\left.\frac{\bar{P}_j}{\bar{P}}\right|_{\text{shot}} = 10\log_{10}\left[\sum_{k=1}^{N}\sum_{l=1}^{N}(h^{\dagger}_{j,k})^2 h_{k,l}\right] \tag{3.11}$$

In Section 3.2, a 3×3 link was discussed. In this section, the radial offsets of the input beams and the radii of the detector segments that minimize, on average, cross-talk and the power penalty due to the electronic matrix inversion in an $N \times N$ system are approximated for $N = 2 \ldots 5$. Table 3.1 shows the optical power penalty and optical cross-talk for an $N \times N$ system with $N = 2 \ldots 5$. The average and maximum value of the power penalty and cross-talk across the N calculated values are presented. Table 3.1 also gives the corresponding geometric parameters for the design of the $N \times N$ link. The matrix elements $h_{i,j}$ have been estimated using the experimental NFP of the 75 m long GI-MMF without loss of generality, since in Section 3.2, it was shown that the dependence of $h_{i,j}$ on the GI-MMF length is minimal.

Table 3.1: Average (maximum) optical power penalty and optical cross-talk, together with the geometric design parameters for an $N \times N$ MGDM system over 62.5/125 μm silica-based GI-MMF.

$N \times N$	Power penalty at shot noise limit (dB)	Power penalty at thermal noise limit (dB)	Optical cross-talk (dB)
2×2	2.3 (2.3)	1.2 (1.4)	-6.7 (-5.7)
3×3	5.7 (7.2)	2.9 (3.2)	-2.8 (-0.4)
4×4	8.3 (10.3)	4.2 (4.7)	-0.8 (1.5)
5×5	11.3 (13.3)	5.6 (6.3)	0.8 (2.7)

$N \times N$	Radial offsets (μm)	Detector radii (μm)
2×2	0, 26	12, 31.25
3×3	0, 15, 26	7, 17, 31.25
4×4	0, 10, 19, 26	5, 12, 20, 31.25
5×5	0, 10, 15, 21, 26	5, 10, 16, 22, 31.25

In the results of Table 3.1, apart from optimizing the detector radii, optimal offsets of the input beams have been approximated as well. The optimization process is with respect to the minimization, on average, of cross-talk and power penalty. This process has not been done in a strict mathematical way, but rather by empirically testing different values. The starting point for the values of the detector radii has been the intersection points of the NAPF curves. Other criteria for optimization could have been used, such as an equal value of the optical cross-talk at each detector segment. For example, for a 3×3 MGDM system, for radial offsets of 0 μm, 15 μm and 26 μm, and detector radii of 10 μm, 12 μm and 31.25 μm, the optical cross-talk at R_1, R_2 and R_3 is -1.6 dB, -1.4 dB and -1.6 dB, respectively, and hence very similar at the three detector segments. However, the average (maximum) power penalty at the shot noise limit is 10.5 dB (13 dB) and the average (maximum) power penalty at the thermal noise limit is 6.9 dB (8.8 dB). These values are much larger than the ones in Table 3.1 for a 3×3 system. The more diagonally dominant the system matrix, the lower the power penalty due to the electronic matrix inversion.

The specification of the geometric parameters included in Table 3.1 can be used for the manufacture of MGDM components. An evaluation of such a system is provided by the calculated values of optical cross-talk and power penalty. In some cases, the optical cross-talk has a positive value in decibels. This indicates that in

detector segment i, the power from the ith mode group is lower than the aggregate interference from the other mode groups. The power penalty grows significantly with the number of channels N and this, in practice, can deteriorate N. At the same time, the sensitivity of the power penalty to changes in the value of $h_{i,j}$ is a very important factor, as will be discussed in the following section.

3.5 Sensitivity to misalignments

A feature of GI-MMF links is tolerance in alignment. Misalignments can be found at the launching or detecting side of a GI-MMF link, can be caused when connecting GI-MMFs, or can be even due to fiber concentricity. In an MGDM system, in order to maintain tolerance in alignment, the largest radial offset for the input beams should be $\rho_{\max} = \rho_\eta - d_{\text{tol}}$, where ρ_η is the maximum radial offset ensuring a desired η and d_{tol} the required tolerance in alignment. However, misalignments will change the sets of excited modes and consequently the NFP. Figure 3.9 shows the NFP on the output facet of the 75 m long GI-MMF for ± 2 μm misalignment at the input end of the GI-MMF. These changes in the NFP will affect cross-talk and hence the power penalty due to the electronic matrix inversion. Figure 3.10 shows the influence of misalignments on the power penalty of channel 1 (T_1, R_1), which is the most affected channel of the proposed MGDM link with $N = 3$ and $N = 4$. The same tolerance $d_{\text{tol}} = 2$ μm has been used at both the transmitting side and the receiving side. The 3×3 link is much more robust than the 4×4 one. The latter link is primarily affected by the -2 μm misalignment at the transmitting end, since a smaller part of the GI-MMF core is used to propagate the optical power, as can be seen in Figure 3.9. Therefore, the spatial overlap among the intensity profiles of the excited mode groups increases. Obviously, channel separation would fail with a -5 μm misalignment at the transmitting end of the 4×4 link.

The sensitivity of the link to misalignments depends on the transmission matrix $\mathbf{H}$. In particular, the more diagonally dominant $\mathbf{H}$ tends to be, the more robust the link is to changes in the value of the $h_{i,j}$ coefficients. Figure 3.10 clearly shows that for $N \geq 4$ the proposed MGDM link will be very sensitive to changes in the value of the $h_{i,j}$. This certainly limits the scalability of the link with respect to the number of channels. To combat this restriction, in Chapter 6, we introduce a new optical technique, namely mode-selective spatial filtering, to reduce the optical cross-talk and therefore increase the robustness of the link.

3.6 Passive optical components

3.6.1 Topologies of local area networks

GI-MMFs are mainly used in local area networks (LANs). In LANs, bus, star and ring topologies are often employed, typically at the electrical signal level (Figure 3.11). MGDM requires mode-selective components. Design considerations for

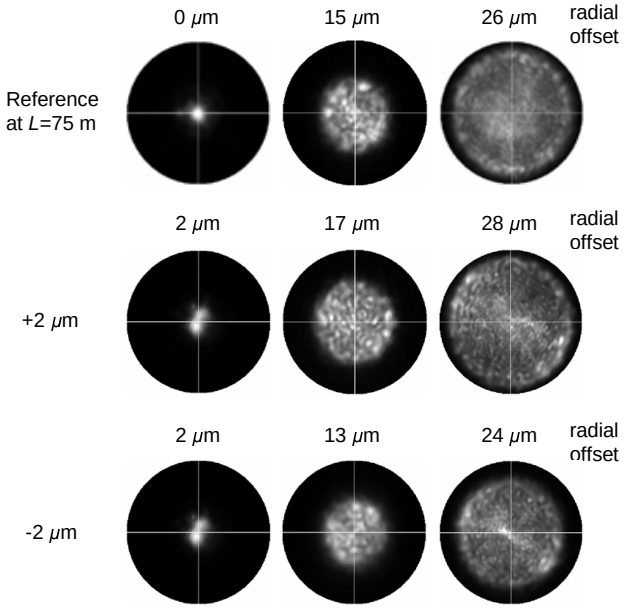

Figure 3.9: NFP on the output facet of a 75 m long 62.5/125 μm silica-based GI-MMF under selective excitation with three radially offset beams, at 660 nm wavelength, when considering ± 2 μm misalignment at the GI-MMF input.

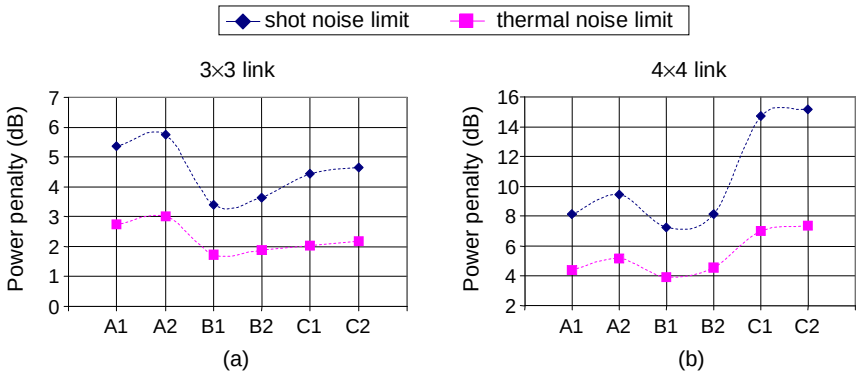

Figure 3.10: Influence of misalignments on the power penalty of the most affected channel of a (a) 3×3 and (b) 4×4 MGDM link over a 75 m long 62.5/125 μm silica-based GI-MMF. A1 corresponds to no misalignment (Table 3.1). B1 and C1 correspond to $+2$ μm and -2 μm misalignment at the transmitting side. A2, B2 and C2 correspond to A1, B1 and C1 with 2 μm misalignment at the receiving side.

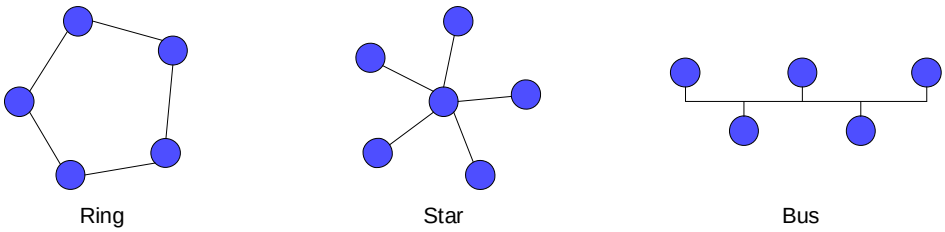

Figure 3.11: Common basic topologies in local area networks.

an MGDM link over GI-MMFs have been presented in the preceding sections, with radially offset beams on the GI-MMF input facet and a multi-segment detector with annular segments responding to the NFP on the GI-MMF output facet. The annular power flux of the NFPs of the detected mode groups determines the area of the detector segments. To apply MGDM in optical bus, star or ring LAN topologies, passive optical components, such as optical couplers, are required. Optical couplers may be also used in a bidirectional MGDM link. In this section, we present an experimental investigation of the effect of several standard passive optical components, i.e. components not designed for restricted mode excitation, on the NFP at the output end of GI-MMF links under selective excitation with an SMF.

3.6.2 Experimental results

The experimental investigation of the NFP was realized with the setup illustrated in Figure 3.12. An external cavity type, tunable, semiconductor, continuous wave laser was used to excite selectively a 1 m long 50/125 μm silica-based GI-MMF with NA = 0.2. The wavelength of the laser was tuned at 1310 nm and its linewidth is 85 kHz. The laser is pigtailed with an SMF of 9.3 μm MFD at 1310 nm wavelength. The SMF and GI-MMF axes were parallel and their lateral distance was set by computer-controlled translational stages. The 1 m long GI-MMF was connected to a GI-MMF passive optical component followed by a 100 m long GI-MMF. All GI-MMFs were of the same type as the 1 m long GI-MMF. The optical components

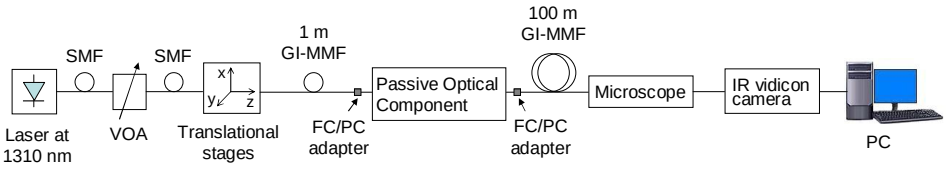

Figure 3.12: Experimental setup for the investigation of the effect of passive optical components on the NFP at the output end of GI-MMF links.

Table 3.2: Description of the cases presented in Figure 3.13.

Case	Passive component
2	2 m long 50/125 μm GI-MMF
3	monolithic 50/50 coupler, input 1 to output 1
4	monolithic 50/50 coupler, input 1 to output 2
5	monolithic 90/10 coupler, input 1 to output 1
6	monolithic 90/10 coupler, input 1 to tap 1
7	three-port circulator, port 1 to port 2
8	three-port circulator, port 2 to port 3

were connected with fixed-connection/physical-contact (FC/PC) adapters. At the output of the 100 m long GI-MMF, the NFP was observed with an infrared vidicon camera and a microscope (50×, 0.75-NA). An image of the NFP was grabbed with video-processing software.

The NFP was observed when the radial offset of the SMF axis with respect to the GI-MMF one was 0 μm, 12 μm and 21 μm, and for different passive optical components. The obtained NFP images are shown in Figure 3.13, for several cases described in Table 3.2. The speckle contrast of the NFPs is very strong, due to the very narrow linewidth of the laser. A 2 m long GI-MMF, a monolithic 50/50 coupler[1], a monolithic 90/10 coupler[2] and a three-port circulator[3] were tested. The couplers and the circulator are optimized for use at 1310 nm. When the 2 m long GI-MMF was tested (case 2), the overall shape of the NFP was very similar to the corresponding NFP on the output facet of the 1 m long GI-MMF (case 1). This is meant to show the limited effect of the FC/PC adapters, present in every case. The NFP in cases 3, 4 and 5 appears to be nearly as in cases 1 and 2. In cases 7 and 8, the overall NFP for 0 μm radial offset at the input end of the GI-MMF link is slightly expanded, while for the other two offsets it remains similar. Finally, in case 6, the shape of the NFP seems to be independent of the offset of the input SMF.

In order to use passive optical components in a GI-MMF network with selective excitation, these components should not alter significantly the modal distribution and furthermore, their specifications, such as the coupling ratio and the insertion loss, should be maintained. Apart from MGDM, this is of interest for the offset launch technique, which has been proposed to increase the bandwidth of IM-DD, single-input, single-output GI-MMF links [77]. From the components that were

[1]Comcore Technologies, Inc., product number MBS7250PD2L01.
[2]Comcore Technologies, Inc., product number MBS7290PD2L01.
[3]Agiltron, Inc., product number OCMM-303115422.

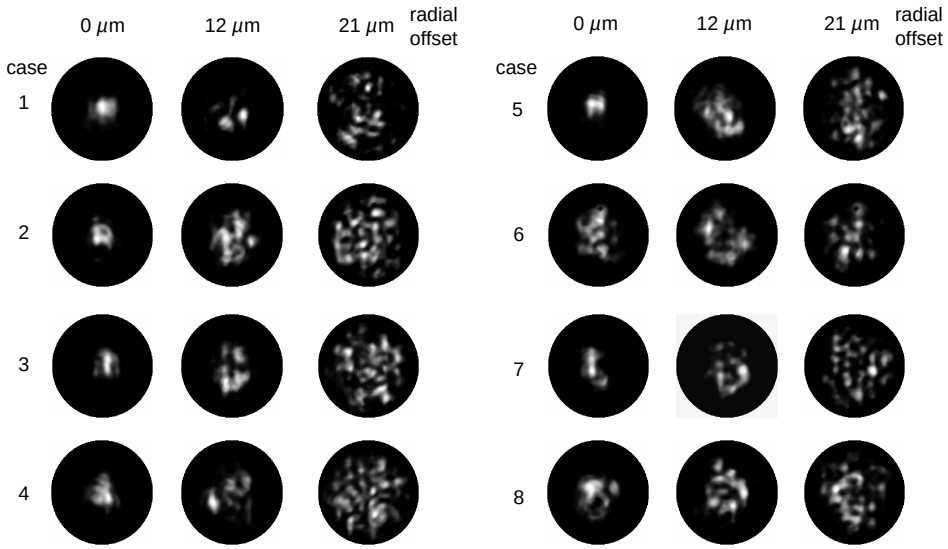

Figure 3.13: NFP on the output facet of (1) the 1 m long GI-MMF, (2-8) the 100 m long GI-MMF used in the setup of Figure 3.12, at 1310 nm wavelength. The passive components used in cases 2-8 are described in Table 3.2.

tested, only the circulator maintained its specifications for all offsets. The couplers did not exhibit a consistent coupling ratio, even though in several cases they did not change the overall NFP. For example, a 3-dB difference was observed in the optical power between the two output ports of the 50/50 coupler (cases 3 and 4) for 12 μm offset launch. According to the specifications of such a coupler, the power at the two output ports should be equal.

The above investigation indicates that the tested standard GI-MMF components are not suitable for GI-MMF networks using techniques with selective excitation. Laser optimized components, i.e. components optimized for restricted excitation, would be required [87]. The primary reason is that the tested components, although in most cases do not change dramatically the NFP, and thus the modal distribution, do not respond according to their specifications. These specifications are usually given for overfilled launch conditions. The latter can be achieved with a source of high angular divergence, e.g. a light emitting diode, or a mode scrambler at the GI-MMF input [88]. Finally, it should be noted that for MGDM transmission, even in the case where laser optimized components are used, the tolerance in misalignments at the GI-MMF connections should be small. This would be a strong requirement especially in links with many passive optical components [89].

3.7 Conclusions

The design of an $N \times N$ MGDM system is a non-trivial issue. An approach was proposed, with N radially offset Gaussian-like beams on the input facet of the GI-MMF exciting N mode groups and a multi-segment detector with N annular segments responding to the NFP on the output facet of the GI-MMF. This scheme was shown to yield a transmission matrix which is not practically affected by the GI-MMF length for at least up to 1 km, in the case of silica-based GI-MMFs. Further, the scheme is in line with high coupling efficiency at the transmitting side of the link. For a system using standard 62.5/125 μm silica-based GI-MMF, with $N = 2 \ldots 5$, the areas of the detector segments as well as the radial offsets of the input beams were estimated so as to minimize, on average, the optical cross-talk and the optical power penalty due to the electronic matrix inversion. The estimation was based on experimental measurements of the NFP on the output facet of a GI-MMF under selective excitation with a radially offset SMF. These results can be used for the manufacture of a mode group diversity multi/demultiplexer. The introduction of an angular offset at the input beams was found to be only of marginal interest for reducing the optical cross-talk. That was because the NFP shows a strong dependence on the GI-MMF length and the coupling efficiency at the input end of the GI-MMF decreases significantly as the radial offset increases. The requirements in alignment were shown to be tight and for $N \geq 4$, even a 2 μm misalignment changes the power penalty due to matrix inversion considerably and hence the power budget of the system. Such a system would require great precision to be stable and reliable. Therefore the proposed method is more suitable for $N \leq 3$. Finally, several standard passive GI-MMF components were tested to check whether they could be used in GI-MMF networks where techniques with selective excitation, such as MGDM, are employed. The result was negative because some of these components can alter the NFP and further, they do not always maintain their specifications, such as the coupling ratio in the case of an optical splitter.

Chapter 4

Near-field pattern of silica GI-MMFs with restricted excitation

An analysis of the near-field pattern (NFP) on the output facet of silica-based GI-MMFs excited by a radially offset SMF is presented. Simulation results exhibit all of the features displayed by experimental ones. It turns out that differential mode attenuation and delay, full intra-group mode mixing, and small deviations in the refractive index profile of the GI-MMF do not affect the overall NFP, which is determined by the radial offset of the input SMF. In particular, the NFP is confined within a disk, the radius of which depends on the radial offset of the launched beam. The effect of defects in the refractive index profile, such as deviation of the α-parameter from its optimal value and a central dip or peak, is also examined. The analysis presented in this chapter gives insight into light propagation in GI-MMFs and supports that the design method proposed in Chapter 3 for an MGDM link yields a robust system with the GI-MMF length, at least for up to 1 km.

4.1 Selective excitation of GI-MMFs with an SMF

Optical transmission systems with GI-MMFs are mostly based on the intensity-modulation direct-detection (IM-DD), single-input single-output (SISO) approach. In this case, the bandwidth limitation comes from inter-modal dispersion, which is caused by the differential propagation delay of the propagating modes. One way to enhance the 3-dB bandwidth of IM-DD SISO links with GI-MMF is to restrict the launch conditions, aiming at the excitation of a subset of modes with similar propagation delay. Selective excitation with an SMF at the input end of a GI-MMF

Parts of this chapter are published in Ref. [2,15] of Appendix B.

is a simple way to achieve this [77, 78, 90, 91]. A radial offset at the launch position of the SMF with respect to the GI-MMF axis may be required, depending on the refractive index profile of the GI-MMF. Central launch can be combined with detectors for SMF systems offering a similar advantage. Subcarrier multiplexing beyond the 3-dB bandwidth [31, 92] and spatially resolved equalization [93] can also enhance the transmission bandwidth of GI-MMF links.

Besides the above methods, MIMO techniques are gaining interest to create parallel channels over the same MMF, by exploiting the propagating spatial modes [52, 61, 63, 66, 67]. In all MIMO approaches, selective excitation is required. MGDM is an IM-DD MIMO technique and, as proposed in Chapter 3, it can be implemented with radially offset Gaussian-like beams on the input facet of a GI-MMF and spatially selective detection of the NFP at the GI-MMF output end. The field profile of the single spatial mode of an SMF approximates a Gaussian beam. This implementation is based on the experimental observation that for silica-based GI-MMFs, at least up to 1 km long, the NFP of the optical intensity on the GI-MMF output facet remains confined within a disk with a radius that depends on the radial offset of the input beam.

The analysis presented in this chapter has been motivated by the aforementioned interest in selective excitation of GI-MMFs with an SMF. The effect of such an excitation scheme on the bandwidth of IM-DD SISO links has been widely addressed [77, 78, 90, 91]. Although its effect on the NFP has been observed experimentally in Chapter 3, as well as in Refs. [68, 89, 94], no extended analysis has been reported, to the best of the author's knowledge. In this chapter, an experimental and theoretical investigation of the NFP is presented. It is shown that the overall NFP is not affected by differential mode delay and attenuation, small deviations in the refractive index profile of the GI-MMF, or full intra-group mode mixing. The latter refers to mixing among modes with similar propagation coefficient, as will be explained in the following sections. Further, the effect of refractive index profile defects is examined. These defects include deviation of the α-parameter from its optimal value that minimizes differential mode delay, as well as a central dip or peak in the refractive index profile. Such defects are common in legacy GI-MMFs.

4.2 Experimental investigation

Figure 4.1 shows the experimental setup used to observe the NFP on the output facet of a GI-MMF under selective excitation with an SMF. An external cavity type, tunable, semiconductor, continuous wave laser was used to excite selectively a GI-MMF with core/cladding diameter of 62.5/125 μm and a numerical aperture (NA) of 0.275. The linewidth of the laser is 85 kHz and its wavelength was tuned to 1310 nm. The laser is pigtailed with a 1 m long standard SMF with a mode field diameter of 9.3 μm at 1310 nm. A variable optical attenuator (VOA) with SMF pigtails was used to control the level of the optical power. The radial offset

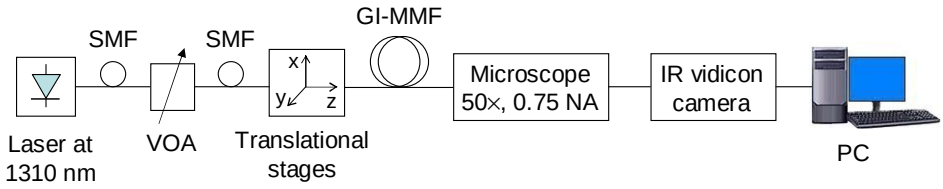

Figure 4.1: Experimental setup for the observation of the NFP on the output facet of a GI-MMF under selective excitation with a radially offset SMF.

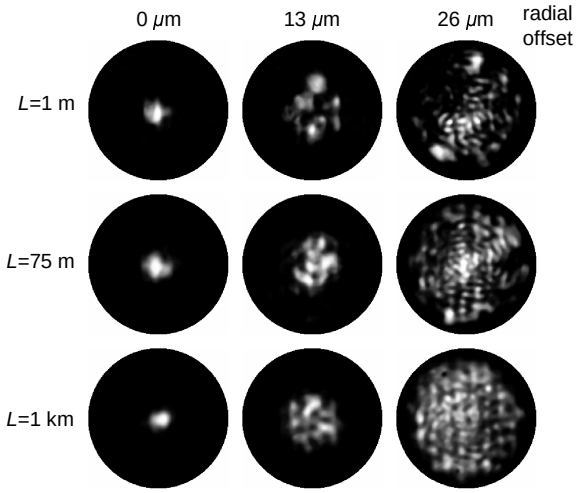

Figure 4.2: Experimental NFP on the output facet of a 1 m, 75 m and 1 km long 62.5/125 μm silica-based GI-MMF, under selective excitation with a radially offset SMF, at 1310 nm wavelength. The radial offset was 0 μm, 13 μm and 26 μm.

of the SMF axis from the GI-MMF axis was set by means of computer-controlled translational stages. A microscope with 50× magnification and NA = 0.75 projected the NFP at the GI-MMF output end onto an infra-red vidicon camera. An image of the NFP was grabbed with video processing software.

The obtained NFP images are shown in Figure 4.2. Three GI-MMFs were tested, of lengths 1 m, 75 m and 1 km, under excitation with the SMF of the VOA at 0 μm, 13 μm and 26 μm radial offset, similarly to Chapter 3, where a 660 nm laser was used instead. The speckle contrast of the images is very strong even in the case of the 1 km long GI-MMF. This is due to the very narrow linewidth of the laser that results in highly coherent radiation [75]. Similar results have been previously obtained at 660 nm (Chapter 3), 850 nm [89], 1300 nm [94], and 1540 nm [68]. The images of Figure 4.2 indicate that propagation does not affect the overall NFP, which remains confined within a disk. The radial offset of the

SMF determines the radius of the disk. This indicates that mode mixing is limited, since in the presence of strong mode mixing, light would span most of the area of the GI-MMF core and the radial dependence of the intensity profile would tend to resemble the refractive index profile [95]. To investigate the impact of separate propagation effects as well as of the refractive index profile on the NFP, numerical simulations are required.

4.3 Numerical investigation

The numerical simulations presented in this chapter have been carried out in cooperation with the Electromagnetics Group of the Eindhoven University of Technology. A mode solver that had originally been developed for the investigation of differential mode delay in MMFs was used to simulate the NFP on the output facet of GI-MMFs. In the simulations, continuous wave, monochromatic light at 1310 nm is considered.

4.3.1 Differential mode delay

Important effects in MMFs are dispersion, attenuation and mode mixing. Intermodal dispersion is usually the dominant source of dispersion. Chromatic dispersion depends on the wavelength and the linewidth of the optical source. In our experiment, we used a 1310 nm laser with an 85 kHz linewidth and therefore chromatic dispersion can be neglected. We employ cylindrical polar coordinates r, ϕ, z, with the z-axis coinciding with the MMF axis. At the MMF input end $z = 0$ and at the MMF output end $z = L$. The propagating electric ($\mathbf{E}$) and magnetic ($\mathbf{H}$) complex fields are [13–16]

$$\begin{bmatrix} \mathbf{E}(r,\phi,z,t) \\ \mathbf{H}(r,\phi,z,t) \end{bmatrix} = \sum_{\nu,\mu} c_{\nu,\mu}(z) \begin{bmatrix} \mathbf{e}_{\nu,\mu}(r,\phi) \\ \mathbf{h}_{\nu,\mu}(r,\phi) \end{bmatrix} \exp(\mathrm{j}\omega t). \tag{4.1}$$

Here, $\mathbf{e}_{\nu,\mu}$, $\mathbf{h}_{\nu,\mu}$ are the modal electric and magnetic fields of the (ν,μ) guided mode, where ν and μ are the azimuthal and radial mode numbers. The modal fields $\mathbf{e}_{\nu,\mu}(r,\phi)$, $\mathbf{h}_{\nu,\mu}(r,\phi)$ are normalized to unit power and $c_{\nu,\mu}(z)$ is the complex modal amplitude at z, its modulus expressing the fractional modal power. Further, ω is the optical angular frequency and j is the imaginary unit.

The intensity distribution at the MMF output is given by

$$\begin{aligned} I(r,\phi,L) \quad = \quad & \frac{1}{2}\mathrm{Re}\left[\sum_{\nu,\mu} \mathbf{e}_{\nu,\mu}(r,\phi,L) \times \mathbf{h}^*_{\nu,\mu}(r,\phi,L)\cdot \hat{u_z} \right. \\ & \left. + \sum_{\substack{\nu\neq\nu' \\ \mu\neq\mu'}} \mathbf{e}_{\nu,\mu}(r,\phi,L) \times \mathbf{h}^*_{\nu',\mu'}(r,\phi,L)\cdot \hat{u_z}\right]. \end{aligned} \tag{4.2}$$

On the right hand side of Eq. (4.2), the first term is the summation of the intensity distributions due to each mode separately and the second term expresses the variations in the total intensity distribution due to the interference of the modal fields.

In the absence of mode mixing, the modal amplitude is given by

$$c_{\nu,\mu}(z) = c_{\nu,\mu}(0)\exp(-\mathrm{j}\beta_{\nu,\mu}z)\exp(-\gamma_{\nu,\mu}z), \tag{4.3}$$

where $\beta_{\nu,\mu}$, $\gamma_{\nu,\mu}$ are the propagation and attenuation coefficients of the (ν,μ) mode. We assume that losses are limited, so that they can be treated as a perturbation of the lossless case [13]. The modal amplitude in the plane of excitation, $c_{\nu,\mu}(0)$, depends on the excitation condition. In particular, the orthogonality of the modal fields at $z = 0$ reads

$$c_{\nu,\mu}(0) = \int_0^{2\pi}\int_0^{\infty} \mathbf{e}_{in}(r,\phi) \times \mathbf{h}^*_{\nu,\mu}(r,\phi)\cdot\hat{u}_z r\mathrm{d}r\mathrm{d}\phi \tag{4.4}$$

where $\mathbf{e}_{in}(r,\phi)$ is the excitation electric field at the MMF input end.

4.3.2 Mode mixing

Mode mixing is the gradual redistribution of the optical power among the propagating modes. It can be separated into two categories, namely intra-group and inter-group mode mixing, referring to mixing among modes of the same principal mode group (PMG), and among modes of different PMGs, respectively. PMGs consist of modes with very similar propagation coefficient. Under the weakly guiding approximation, the modes that constitute a PMG are the degenerate (ν,μ) modes of the linearly polarized $\mathrm{LP}_{\ell,\mu}$ modes with LP mode number $M_{\mathrm{LP}} = \ell + 2\mu$, where ℓ is related to ν [15]. The manufacturing process of silica-based GI-MMFs allows for an accurate formation of the refractive index profile, with very low dependence on z. Therefore mode mixing is limited in silica-based GI-MMFs, with intra-group mixing occurring earlier than inter-group mixing [96]. For our analysis, we consider the effect of full intra-group mode mixing, as a case of practical importance. We calculate the total power launched in a PMG and redistribute it evenly among the modes of the PMG. In other words, the modulus of the amplitude $c^n_{\nu,\mu}(L)$ of all modes in the nth PMG will be

$$\left|c^n_{\nu,\mu}(L)\right| = \sqrt{\frac{\sum_{\nu,\mu}\left|c^n_{\nu,\mu}(0)\right|^2}{M_n}}, \tag{4.5}$$

where M_n is the number of modes in the nth PMG. The phase of $c^n_{\nu,\mu}(L)$ is chosen randomly with a uniform distribution over $[0, 2\pi)$.

The modal field distributions $\mathbf{e}_{\nu,\mu}(r,\phi)$, $\mathbf{h}_{\nu,\mu}(r,\phi)$ and the propagation coefficient $\beta_{\nu,\mu}$ depend on the wavelength and the refractive index profile $n(r)$. We

assume that $n(r)$ follows the power-law profile, i.e.,

$$n(r) = \begin{cases} n_0\sqrt{1-2\Delta\left(\frac{r}{a}\right)^{\alpha}}, & r < a, \\ n_0\sqrt{1-2\Delta}, & r \geq a, \end{cases} \tag{4.6}$$

where $\Delta = [n_0^2 - n^2(a)]/(2n_0^2)$ and a is the GI-MMF core radius. The central NA of the GI-MMF is NA $= n_0\sqrt{2\Delta}$. For our simulations, $n_0 = 1.474$ and NA $= 0.275$. The α-parameter was 1.97, 2 and 2.06. The value $\alpha = 2$ corresponds to the parabolic index profile. For $\alpha = 1.97$ and $\alpha = 2.06$, differential mode delay is minimized at 1300 nm and 850 nm wavelength, respectively [97, 98], and therefore these values are of special interest in the design of GI-MMFs. To account for the radial dependence of the refractive index in the core, the computation of the propagation coefficient $\beta_{\nu,\mu}$ and the modal fields $\mathbf{e}_{\nu,\mu}(r,\phi)$, $\mathbf{h}_{\nu,\mu}(r,\phi)$ is performed by a direct numerical integration of Maxwell's equations in their full-wave form [99]. Models based on ray optics could have also been used to give the near-field intensity yielded by a mode group, however, in that approach, excitation of a large number of modes is assumed and the phase of the modal amplitudes is not taken into consideration [67, 100, 101].

4.3.3 Differential mode attenuation

Each mode experiences different attenuation due to propagation. In other words, different propagating rays travel along paths with different length and therefore their effective propagation length is not the same. This makes attenuation mode-dependent. In addition, losses will be higher where the concentration of dopant (e.g. Germanium), in order to form the refractive index profile, is larger. This renders an analysis of the losses even more difficult. The following relation can be used to give the attenuation coefficients:

$$\gamma_n(\lambda) = \gamma_0(\lambda) + \gamma_0(\lambda) I_9\left[7.35\left(\frac{n-1}{M_0}\right)^{2\alpha/(\alpha+2)}\right], \tag{4.7}$$

where $n = 1, 2, \ldots$, and I_9 is the 9th-order modified Bessel function of the first kind. This relation has been proposed in Ref. [97] using experimental data from Ref. [102]. According to Eq. (4.7) differential mode attenuation becomes significant in higher order modes. Here, λ is the wavelength and $\gamma_0(\lambda)$ the attenuation of the lowest-order mode which travels the shortest optical path. At 1310 nm it corresponds to 0.35 dB/km. For $n = 1$, $\gamma_1(\lambda) = \gamma_0(\lambda)$. M_0 is the total number of PMGs. The value of $\gamma_n(\lambda)$ depends on n and therefore is the same for all modes in the nth PMG. Consequently, in the calculation of $\exp(-\gamma_{\nu,\mu} z)$ in Eq. (4.3), when full intra-group mode mixing is considered, we may take $z = L$ for all modes.

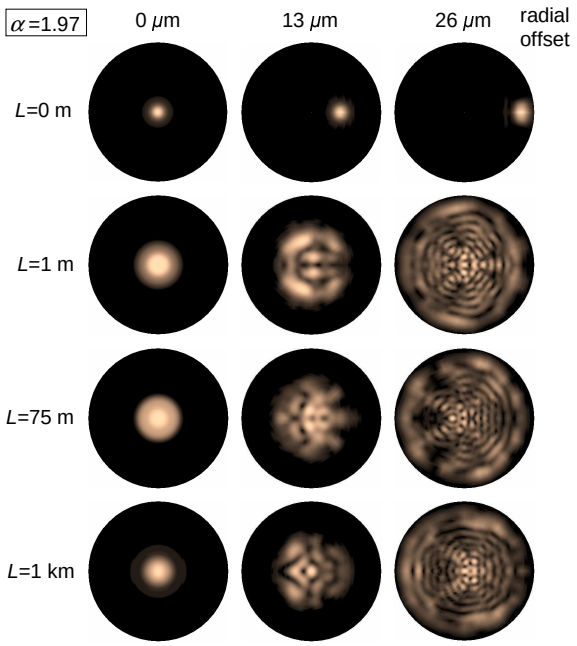

Figure 4.3: Simulated NFP on the output facet of a 62.5/125 μm silica-based GI-MMF with refractive index parameter $\alpha = 1.97$, at 1310 nm wavelength. Each row corresponds to a different GI-MMF length (L) and each column to a different radial offset of the input SMF. Mode mixing is not taken into account.

4.3.4 Results

The simulated NFPs are shown in Figures 4.3, 4.4, 4.5, 4.6 and 4.7. Figures 4.3, 4.4 and 4.5 illustrate the NFP considering differential mode attenuation and delay, but not taking into account mode mixing. The mode field diameter of the input SMF was 9.3 μm at 1310 nm and the radial offset was 0 μm, 13 μm and 26 μm. The NFP was calculated for $L = 0$ m, 1 m, 75 m and 1 km. Figure 4.3 corresponds to $\alpha = 1.97$, Figure 4.4 to $\alpha = 2$ and Figure 4.5 to $\alpha = 2.06$. The speckle pattern clearly depends on the refractive index profile. However, for all three index profiles, the overall NFP is confined within a disk with a radius that depends on the offset of the input SMF, but not on the α-parameter. It should be noted that although the values of the α-parameter used in the simulations have no significant effect on the overall NFP, they can strongly influence the GI-MMF bandwidth [97]. In Figures 4.6 and 4.7, full intra-group mode mixing is taken into account. The same offsets of the input SMF and the same index profiles are considered. The NFP is shown at the output of a 75 m and a 1 km long GI-MMF. Full intra-group mixing does not change the overall NFP either. A distinct difference between

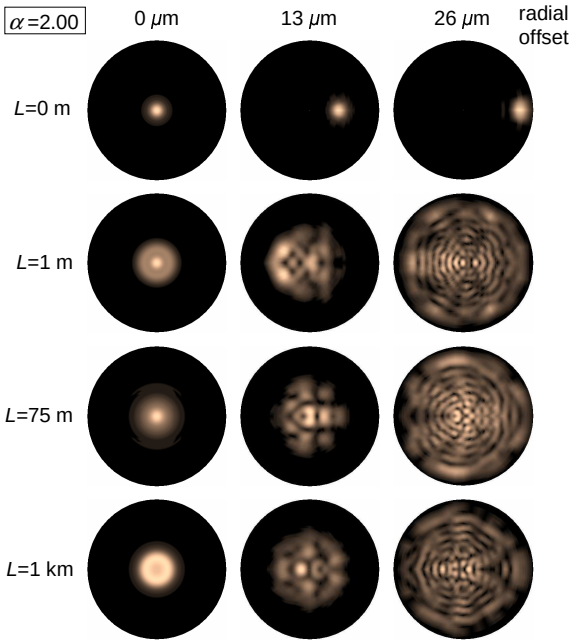

Figure 4.4: Simulated NFP on the output facet of a 62.5/125 μm silica-based GI-MMF with refractive index parameter $\alpha = 2$, at 1310 nm wavelength. Each row corresponds to a different GI-MMF length (L) and each column to a different radial offset of the input SMF. Mode mixing is not taken into account.

the images of Figures 4.3, 4.4, 4.5 and those of Figures 4.6, 4.7 is that in the case of Figures 4.6 and 4.7, the speckle contrast is less strong. This is related to the phase of $c^n_{\nu,\mu}(L)$ which is taken randomly in the results of Figure 4.6 and 4.7. The effect is similar to that of incoherent radiation that yields a very smooth NFP, as can be seen in the experimental NFPs of Figure 3.5 for laser operation below threshold. In all figures, differential mode attenuation does not influence the overall NFP, even in the case of an input beam with a radial offset of 26 μm, where light propagates primarily in higher order modes. In principle, the NFP is not symmetric. However, the simulations give symmetric NFPs. This symmetry is due to the symmetric excitation field, since, in the simulations, the polarization of the input beam was set in the radial direction of the GI-MMF. This simulation approach has the practical advantage of reducing the computational time, since only half of the NFP has to be simulated.

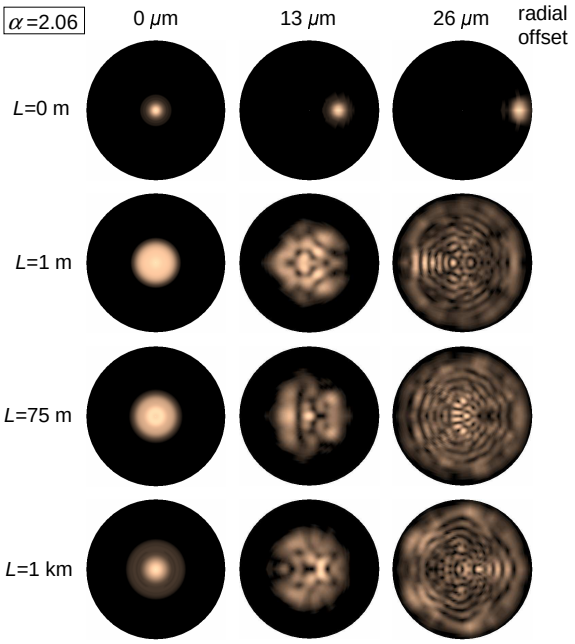

Figure 4.5: Simulated NFP on the output facet of a 62.5/125 μm silica-based GI-MMF with refractive index parameter $\alpha = 2.06$, at 1310 nm wavelength. Each row corresponds to a different GI-MMF length (L) and each column to a different radial offset of the input SMF. Mode mixing is not taken into account.

4.4 Refractive index profile defects

4.4.1 Modeling

In the preceding section, simulation results of the NFP on the output facet of silica-based GI-MMFs were presented. Three different refractive index profiles were tested. These profiles follow the well-known power-law relation and each profile is characterized by a different parameter α. One profile corresponds to the parabolic one, while the other two are of great interest in the manufacturing of high-quality silica-based GI-MMFs, as the GI-MMF used in our experiment. However, the refractive index profile of field installed GI-MMFs may have stronger defects than a simple variation of the parameter α. Such defects are included in the 108-fiber set introduced in Ref. [70] and expanded by the IEEE 802.3aq committee [103].

In this section, we use the defect parameters of two fibers from the 108-fiber set, namely fibers 26 and 78. In the following part of this subsection, we derive the total refractive index profile $n_{tot}(r)$ of fibers 26 and 78. The refractive index profile is divided into two regions, one described by parameter α_1 and the other

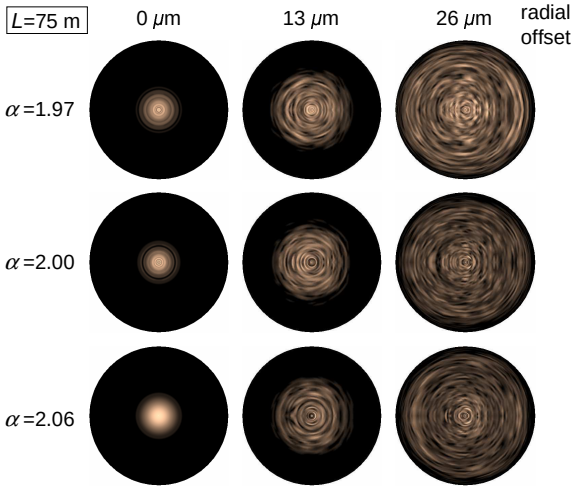

Figure 4.6: Simulated NFP on the output facet of a 75 m long 62.5/125 μm silica-based GI-MMF, assuming full intra-group mode mixing, at 1310 nm wavelength. Each row corresponds to a different refractive index parameter (α) and each column to a different radial offset of the input SMF.

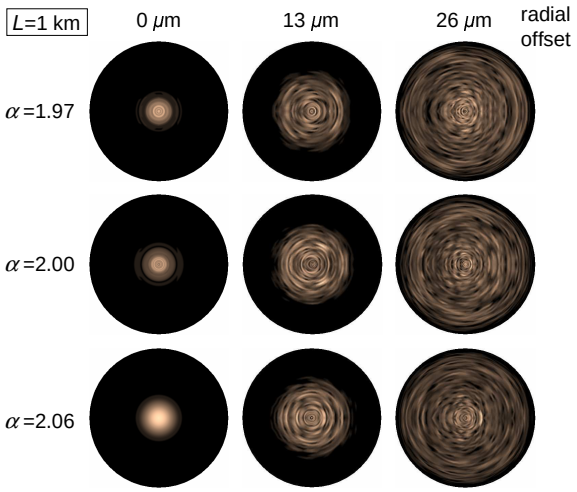

Figure 4.7: Simulated NFP on the output facet of a 1 km long 62.5/125 μm silica-based GI-MMF, assuming full intra-group mode mixing, at 1310 nm wavelength. Each row corresponds to a different refractive index parameter (α) and each column to a different radial offset of the input SMF.

by α_2. In fibers 26 and 78, the difference in the values of α in these two regions is the largest assured difference in the 108-fiber set, viz. $\alpha = 1.89$ and $\alpha = 2.05$. In particular, for fiber 26 (78), $\alpha_1 = 1.89$ (2.05) and $\alpha_2 = 2.05$ (1.89). The refractive index profile is described by the following equation

$$n_\alpha(r) = \begin{cases} n_1(r) &= n_{01}\sqrt{1 - 2\Delta_1 \left(\frac{r}{a}\right)^{\alpha_1}}, & 0 \le r \le a/2, \\ n_2(r) &= n_{02}\sqrt{1 - 2\Delta_2 \left(\frac{r}{a}\right)^{\alpha_2}}, & a/2 \le r \le a, \\ n_{clad} &= n_{01}\sqrt{1 - 2\Delta_1}, & a \le r, \end{cases} \tag{4.8}$$

where $\Delta_1 = (n_{01}^2 - n_{clad}^2)/(2n_{01}^2)$ and $\Delta_2 = (n_{02}^2 - n_{clad}^2)/(2n_{02}^2)$. Continuity at $r = a/2$, i.e. $n_1(a/2) = n_2(a/2)$, yields

$$n_{02} = \sqrt{\frac{n_1^2(a/2) - n_{clad}^2 0.5^{\alpha_2}}{1 - 0.5^{\alpha_2}}} \tag{4.9}$$

In our simulations, $n_{01} = 1.4740$ and $n_{clad} = 1.4481$. Fibers 26 and 78 include a kink perturbation in the profile at $r_k = 27$ μm and $r_k = 19$ μm, respectively. If $\Delta_\alpha(r) = [n_\alpha^2(r) - n_{clad}^2]/[2n_\alpha^2(r)]$ and $\Delta(r) = [n^2(r) - n_{clad}^2]/[2n^2(r)]$, where $n(r)$ is the refractive index profile with the kink perturbation, then $\Delta(r)$ is given by

$$\Delta(r) = \Delta_\alpha(r) + a_k \left[e^{-b_k \left| \frac{r - r_k}{a} \right|} - e^{-b_k \left| \frac{a - r_k}{a} \right|} \right] \Delta_1 \tag{4.10}$$

where $a_k = 0.03$ and $b_k = 20 \cdot 5/31.25$. The refractive index profile is then

$$n(r) = \frac{n_{clad}}{\sqrt{1 - 2\Delta(r)}}. \tag{4.11}$$

Additionally, the index profile of fiber 26 has a central (on-axis) dip, while the profile of fiber 78 shows a central peak. The dip and peak with a full width at half maximum FWHM = 3 μm are modeled as follows

$$n_{axis}(r) = Ae^{-\frac{r^2}{\delta^2}}, \quad \text{where} \quad \delta = \frac{\text{FWHM}}{2\sqrt{\ln 2}}. \tag{4.12}$$

In the case of a dip, $A = -0.004$, whereas in the case of a peak, $A = 0.002$. The total refractive index profile is given by

$$n_{tot}(r) = n(r) + n_{axis}(r). \tag{4.13}$$

Figures 4.8 and 4.10 show the total refractive index profiles of fibers 26 and 78, respectively.

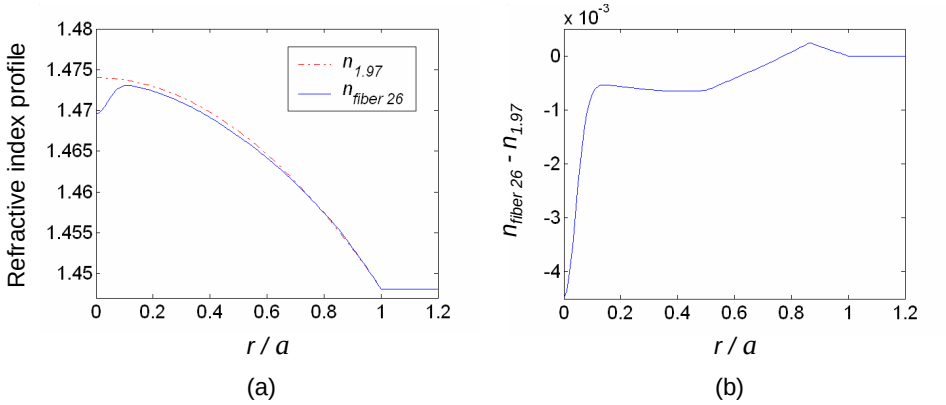

Figure 4.8: (a) Refractive index profile for $\alpha = 1.97$ (dot-dashed curve) and for fiber 26 from the 108-fiber set (solid curve). (b) Difference in the refractive index profiles presented in (a).

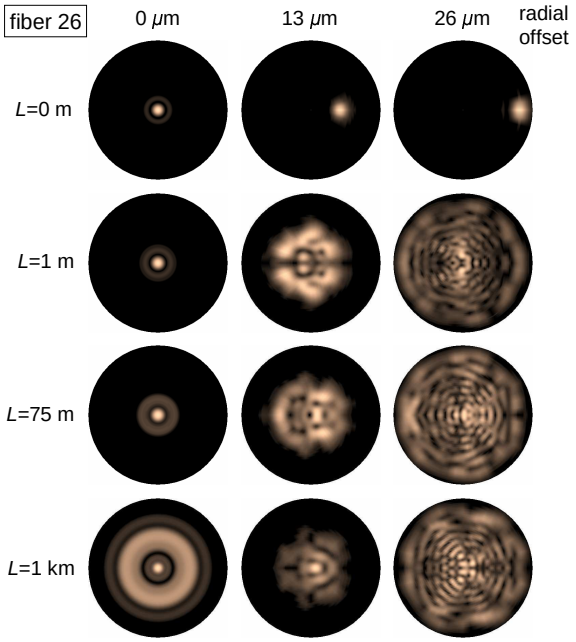

Figure 4.9: Simulated NFP on the output facet of a 62.5/125 μm silica-based GI-MMF using fiber 26 from the 108-fiber set, at 1310 nm wavelength. Each row corresponds to a different GI-MMF length (L) and each column to a different radial offset of the input SMF. Mode mixing is not taken into account.

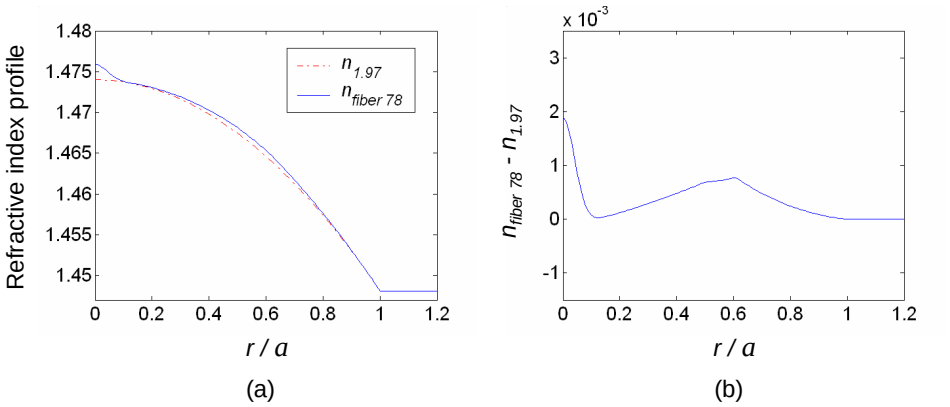

Figure 4.10: (a) Refractive index profile for $\alpha = 1.97$ (dot-dashed curve) and for fiber 78 from the 108-fiber set (solid curve). (b) Difference in the refractive index profiles presented in (a).

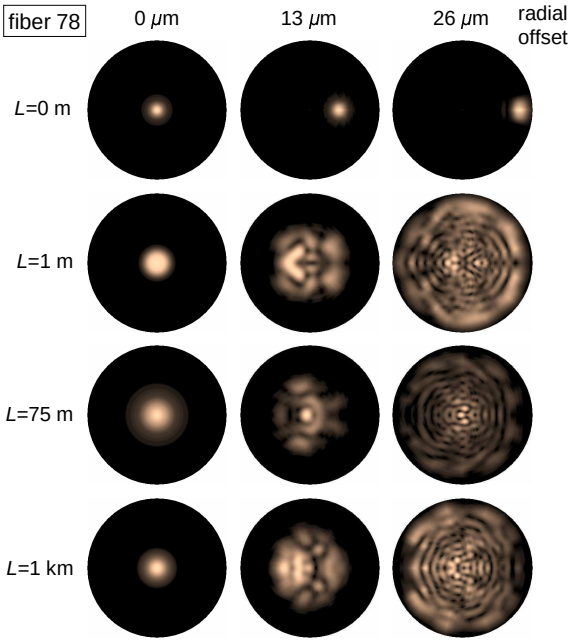

Figure 4.11: Simulated NFP on the output facet of a 62.5/125 μm silica-based GI-MMF using fiber 78 from the 108-fiber set, at 1310 nm wavelength. Each row corresponds to a different GI-MMF length (L) and each column to a different radial offset of the input SMF. Mode mixing is not taken into account.

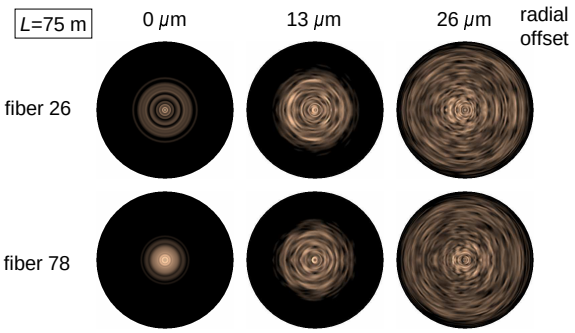

Figure 4.12: Simulated NFP on the output facet of a 75 m long 62.5/125 μm silica-based GI-MMF, assuming full intra-group mode mixing, at 1310 nm wavelength. The first (second) row corresponds to fiber 26 (78) and each column to a different radial offset of the input SMF.

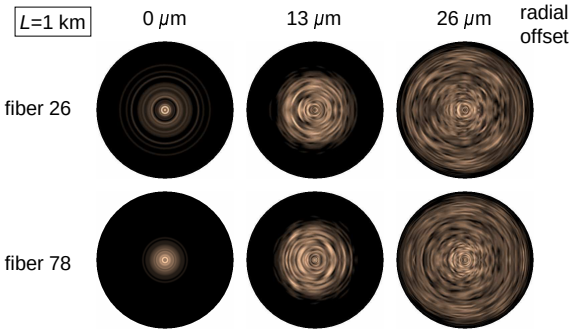

Figure 4.13: Simulated NFP on the output facet of a 1 km long 62.5/125 μm silica-based GI-MMF, assuming full intra-group mode mixing, at 1310 nm wavelength. The first (second) row corresponds to fiber 26 (78) and each column to a different radial offset of the input SMF.

4.4.2 Results

The simulated NFPs, at 1310 nm wavelength, are shown in Figures 4.9 and 4.11, as well as Figures 4.12 and 4.13, considering no mode mixing and full intra-group mode mixing, respectively. The speckle patterns are different compared to the results of Section 4.3. However, the overall NFP is affected only for fiber 26 with central excitation as can be seen in Figures 4.9, 4.12 and 4.13. In this case, the NFP can expand significantly and span over an area similar to the area of the NFP yielded by the 13 μm offset input beam. This will affect an MGDM link, and if such a fiber would be used, central excitation should be avoided. The results

obtained with fiber 78 are very similar to the ones in Section 4.3 for all input beams.

The limited effect of a central peak (fiber 78) on the overall NFP under central excitation, as opposed to the stronger effect of a central dip (fiber 26), is most likely because light guided by total internal reflection tends to propagate in areas of higher refractive index. Furthermore, the absolute amplitude of the dip in fiber 26 is $|A| = 0.004$, while in fiber 78, the absolute amplitude of the peak is only half, i.e. $|A| = 0.002$.

4.5 Conclusions

Experimental and simulation results of the NFP on the output facet of silica-based GI-MMFs were presented and compared. Selective excitation with a radially offset SMF was considered. The NFP is confined within a disk, the radius of which depends on the radial offset of the input SMF. It was shown that differential mode delay and attenuation, as well as full intra-group mode mixing do not change the overall NFP, although they do affect the speckle pattern. The same holds for small deviations of the refractive index profile. This supports the proposition that the MGDM link described in Chapter 3 is tolerant as regards the GI-MMF length. Finally, it was shown that when the refractive index profile exhibits a central dip, the overall NFP under central excitation can significantly expand, while in the case of a central peak, the overall NFP remains practically intact. Therefore, in an MGDM link over a GI-MMF with a central dip, on-axis excitation is better to be avoided.

Chapter 5

A stable 2×2 MGDM system

The temporal stability of an MGDM link is examined. The transmission matrix is vulnerable to mode mixing as well as changes of the coupling of light at the input and output ends of the GI-MMF. An experimental 2×2 *MGDM link has been built. Measurements of the transmission matrix of this link over a 12.7 h period in a not-environmentally-controlled experimental setup show that an MGDM link can be very stable. Further, the electrical cross-talk is estimated as a function of the period of estimation of the transmission matrix, assuming that the transmitted signals are demultiplexed with electronic matrix inversion. The linearity of this* 2×2 *link is examined and the sources of signal distortion are identified. Finally, an analog approach for electronic demultiplexing is described, which was used to build the first basic MGDM demonstrator, supporting the transmission of two low-bandwidth signals.*

5.1 Introduction

The performance of every optical communication system can be affected by several factors. Temperature changes, wavelength drifting or mechanical vibrations can have a severe impact on the performance of a system. For example, temperature changes can affect the level of the optical power emitted by a semiconductor laser. Temperature controllers or automatic power control loops can be used to combat this problem. Wavelength drifting, which can be temperature-induced, may affect systems with wavelength-selective components, such as the ones used in wavelength division multiplexing transmission. Further, wavelength drifting due to laser chirping widens the spectrum of the transmitted signal. Mechanical vibrations can alter the MMF propagation characteristics or the coupling of light.

In an MGDM system, the above factors can also induce varying mode mixing conditions during propagation and hence change the performance of the link.

Parts of this chapter are published in Refs. [3,7,8,10,13] of Appendix B.

Overall, in MGDM transmission, any variation can translate into changes in the transmission matrix of the system. To accommodate such changes, adaptivity in the estimation of the transmission matrix is required. Adaptivity can be achieved by updating the value of the transmission matrix coefficients at the receiving side of the MGDM link. This approach would suffice for a link which is fairly stable and therefore would not require a feedback control loop from the receiving side to the transmitting side. In this chapter, a 2×2 MGDM link is described and it shown to be stable, requiring adaptivity only at the receiving side.

5.2 The impact of variations of the transmission matrix

As discussed in Chapter 2, in an $N \times N$ MGDM system, vector $\mathbf{s}_R(t)$ of the received electrical signals is related to vector $\mathbf{s}_T(t)$ of the transmitted electrical signals via a real-valued $N \times N$ transmission matrix $\mathbf{H}(t) = \{h_{i,j}(t)\}$, i.e.

$$\mathbf{s}_R(t) = \mathbf{H}(t)\mathbf{s}_T(t) + \mathbf{n}(t),$$

where $\mathbf{n}(t)$ is a noise term. The matrix elements express the spatial diversity and the signal mixing. When $\mathbf{H}(t)$ is known, the transmitted signals can be recovered by electronic matrix inversion, a method consistent with the requirement of service transparency. The estimated transmitted signals are then

$$\begin{aligned} \hat{\mathbf{s}}_T(t) &= \hat{\mathbf{H}}^{-1}(t)\mathbf{s}_R(t) + \mathbf{n}_{de}(t) \Rightarrow \\ \hat{\mathbf{s}}_T(t) &= \hat{\mathbf{H}}^{-1}(t)\mathbf{H}(t)\mathbf{s}_T(t) + \hat{\mathbf{H}}^{-1}(t)\mathbf{n}(t) + \mathbf{n}_{de}(t), \end{aligned} \tag{5.1}$$

where $\hat{\mathbf{H}}^{-1}(t)$ is an estimate of the inverse of $\mathbf{H}(t)$ and $\mathbf{n}_{de}(t)$ the noise from the electronic circuit that performs the demultiplexing based on matrix inversion.

From Eq. (5.1), it is evident that any temporal variations in the elements of $\mathbf{H}(t)$, and consequently of $\hat{\mathbf{H}}^{-1}(t)$, will change the noise level through the factor $\hat{\mathbf{H}}^{-1}(t)\mathbf{n}(t)$ and thus the power budget of the link. Furthermore, if the estimation of $\mathbf{H}(t)$ is not ideal, i.e. if $\hat{\mathbf{H}}^{-1}(t) \neq \mathbf{H}^{-1}(t)$, then cross-talk will remain among the channels, since the inner product $\hat{\mathbf{H}}^{-1}(t)\mathbf{H}(t)$ will not result in the $N \times N$ identity matrix $\mathbf{I}_{N \times N}$.

The rate of the temporal variations is an important parameter. Very fast variations may not be trackable and therefore will be manifest as noise. Slow variations can be tracked and therefore can be compensated. If these variations are strong, then due to the power budget dependence on $\mathbf{H}(t)$, the system may require feedback to adjust the transmitted power. This would increase the complexity of the system considerably. As already mentioned in Chapter 1, our investigation aims at a system without a feedback control loop from the receiver to the transmitter. Therefore, it is in our interest to show that an MGDM link can be stable.

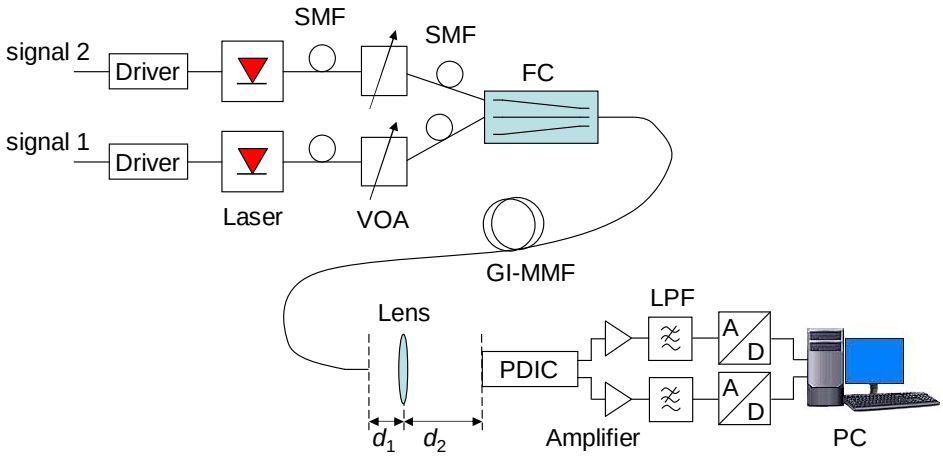

Figure 5.1: Experimental setup of a 2×2 MGDM link.

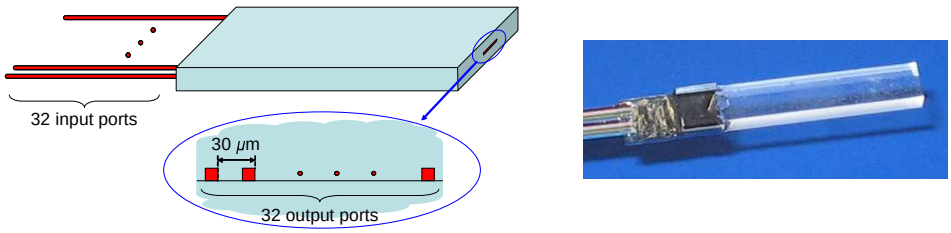

Figure 5.2: (a) An illustration and (b) a photograph of the fiber concentrator (FC). The FC is used at the transmitting side of the 2×2 MGDM link.

5.3 Experimental setup

MGDM is a new technique and consequently there are no MGDM-specific components available. Therefore, components originally developed for other applications were employed, in an effort to approximate the design guidelines presented in Chapter 3. Figure 5.1 shows the experimental setup of a 2×2 MGDM link.

At the transmitting side of the link, a fiber concentrator (FC) was used to excite simultaneously two groups of modes. Figure 5.2 shows the FC. The FC is a linear array of standard single-mode waveguides, i.e. waveguides with a single-mode cut-off at around 1200 nm. At the concentrated side of the FC, the distance between adjacent waveguides is only 30 μm. It is then possible to launch light into thick core GI-MMFs with 0 μm and 30 μm radial offset from the GI-MMF axis. Let transmitter one (Tx1) correspond to the 0 μm offset launch and transmitter

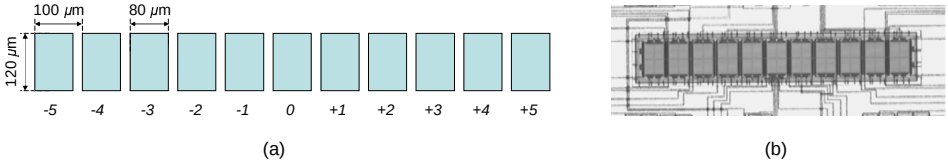

Figure 5.3: (a) An illustration and (b) a photograph of the photodiode integrated circuit (PDIC). The PDIC was used at the receiving side of the 2 × 2 MGDM link.

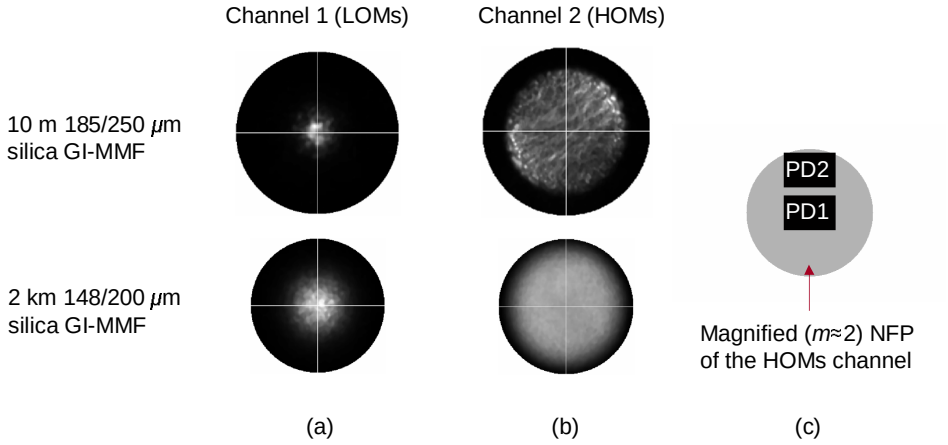

Figure 5.4: NFP of the (a) lower and (b) higher order modes channel on the output facet of the 10 m and 2 km long thick core GI-MMFs. (c) Geometry of the receiving side of the link when a lens is used to magnify the NFP by a factor of $m \approx 2$. Gray color indicates the area of the magnified NFP of the higher order modes channel and black the PDIC photodiodes.

two (Tx2) to the 30 μm offset launch. Two uncooled, directly modulated, 635 nm continuous wave, Fabry–Pérot multiquantum-well lasers were connected to two adjacent ports of the FC. The level of the optical power was controlled with VOAs. It should be noted that the FC waveguides are not single-mode, but support a few modes at 635 nm wavelength. Consequently, the selective excitation of GI-MMFs is not exactly the same as the one investigated in Chapters 3 and 4. However, as will be shown, it is still adequate to demonstrate a stable 2 × 2 MGDM link.

At the receiving side of the link, a lens projected the NFP at the output end of the GI-MMF onto a photodiode integrated circuit (PDIC) with preamplifiers [104]. The PDIC has an array of eleven photodiodes of rectangular shape with dimensions 80×120 μm and highest responsivity at visible light. This is the main reason for using lasers at 635 nm, although this wavelength is not a standard one in optical telecommunication systems. Figure 5.3 shows the PDIC. The distances of

the lens from the output end of the GI-MMF (d_1) and the PDIC (d_2) were such as to magnify the NFP by a proper factor (m) and use two out of the eleven PDIC photodiodes, as shown in Figure 5.4(c). The dimensions of the PDIC photodiodes and the size of the NFP imposed that the magnification factor is $m \approx 2$. Photodiode one (PD1) primarily detects light that propagates in the lower order modes (LOMs) and photodiode two (PD2) responds more to light from the higher order modes (HOMs). The two electrical outputs of the PDIC were each followed by a transimpedance amplifier and a low-pass filter (LPF). Therefore receiver one (two) Rx1 (Rx2), consisted of PD1 (PD2) with a preamplifier, a transimpedance amplifier and a LPF. The output of each receiver was connected to a personal computer (PC) through an analog-to-digital (A/D) converter for further electrical processing.

A 10 m long silica-based GI-MMF with a core/cladding diameter of 185/250 μm and a 2 km long 148/200 μm silica-based GI-MMF were tested. The link was then studied under two extreme conditions. In the 10 m long GI-MMF, limited mode mixing takes place and the NFP on the GI-MMF output facet exhibits a strong speckle contrast. In the case of the 2 km long GI-MMF, there is significant mode mixing and the NFP on the GI-MMF output facet is smoother. Figures 5.4(a) and 5.4(b) show the NFP on the output facet of the two GI-MMFs as observed with a CCD camera through a microscope (20×, 0.40-NA). Each launched mode group yields a distinguishable NFP for both GI-MMFs.

5.4 Measurements of the transmission matrix

One way to measure $h_{i,j}(t)$ is to apply a different sinusoidal pilot tone to each transmitter and measure the level (amplitude) of these pilot tones at the output of each receiver. Following this method, which is illustrated in Figure 5.5, 7 MHz and 8 MHz sinusoidal signals were used to directly modulate the laser of Tx1 and Tx2, respectively. For example, the level of the 7 MHz tone at the output of Rx2 gives the value of $h_{2,1}(t)$. The level of the pilot tones at the receiving side of the link was measured by performing a fast Fourier transform (FFT) of the received electrical signals. Approximately 2.5 measurements per second were taken, with an integration time of 82 μsec for each measurement.

Figures 5.6 and 5.7 show the measured $h_{i,j}(t)$ during a period of 12.7 h for the two GI-MMFs, together with temperature variations in the same period. The four coefficients $h_{i,j}(t)$ are plotted normalized to the average $\langle h_{1,j} + h_{2,j} \rangle$ across the 12.7 h period, i.e.,

$$h_{i,j}^{\mathrm{nor}}(t) = \frac{h_{i,j}(t)}{\langle h_{1,j} + h_{2,j} \rangle}. \tag{5.2}$$

The normalization value in Eq. (5.2) is proportional to the average total received

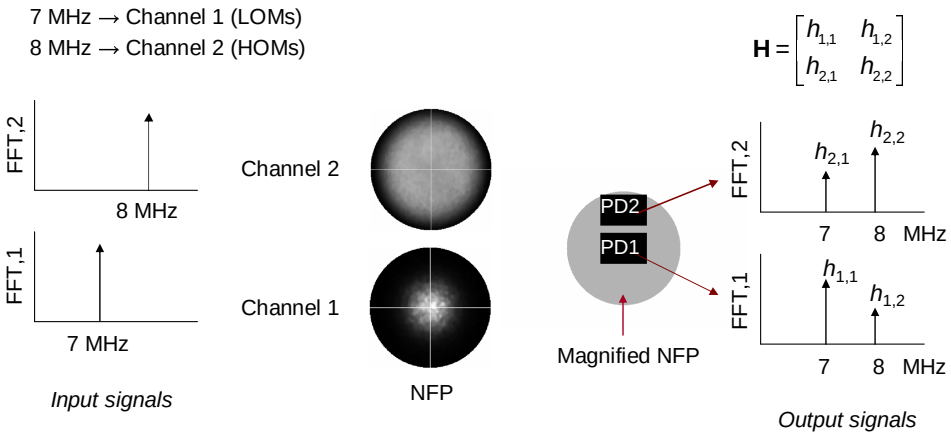

Figure 5.5: Experimental method used to measure the transmission matrix of the 2×2 MGDM link.

optical power which is emitted by the laser of transmitter j. In this way, the value of $h_{i,j}^{\mathrm{nor}}(t)$ expresses the spatial diversity irrespective of the average received power. At the same time, variations in the emitted power can be also visualized, giving an indication of the power stability of the link. The link uses uncooled lasers and no power stabilization technique, such as an electrical automatic power control loop at each transmitter. To solely express the spatial diversity, normalization to the instantaneous sum $h_{1,j}(t) + h_{2,j}(t)$ should be applied. However, in that way, temporal variations in the instantaneous total received optical power could not have been shown.

From the measurements of Figures 5.6 and 5.7, it seems that $h_{i,j}(t)$ varies moderately over the 12.7 h period. Long term fluctuations of the coefficients $h_{i,j}(t)$ can be associated with temperature changes. This is very clear in the case of the 2 km long GI-MMF. Apart from the mode distribution and the coupling of light at the input and output ends of the GI-MMF, temperature variations affect the optical power emitted by the lasers. In principle, in semiconductor lasers, as temperature increases, the emitted optical power drops because the threshold current increases and the P-I slope may decrease. The temporal variations of $h_{i,j}(t)$ can be reduced by using connectorized components at the input and output ends of the GI-MMF, as well as an electrical feedback control loop at each transmitter to stabilize the level of the emitted optical power.

In general, it is difficult to explain thoroughly the fluctuations in the curves of Figures 5.6 and 5.7, due to the multitude of factors involved. The significance of the results lies in the observed stability of the link. Taking into account that our link does not use MGDM-specific components, even better performance should be expected in an optimally implemented system.

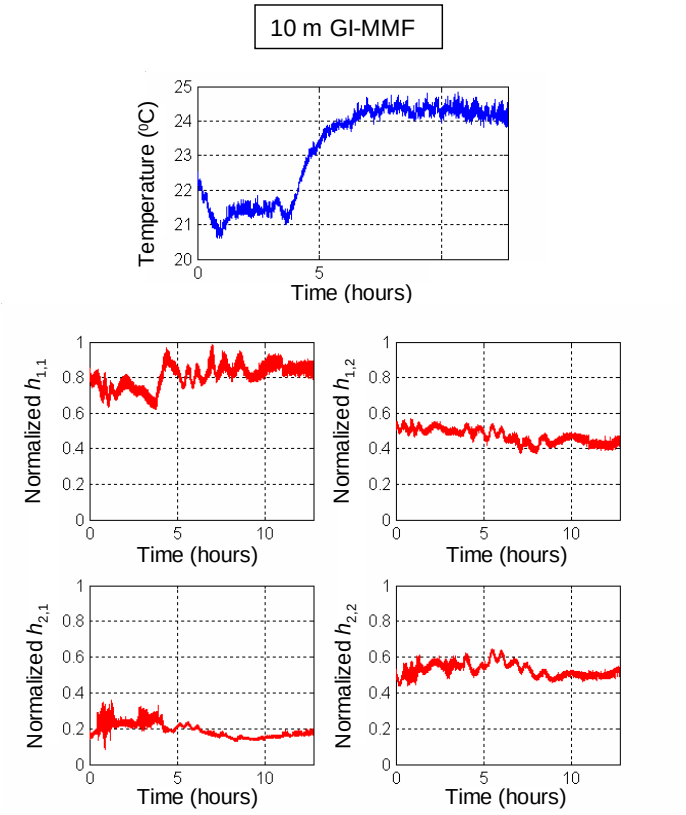

Figure 5.6: Measurements of the transmission matrix elements $h_{i,j}(t)$ over 12.7 h, when the 10 m long 185/250 μm silica-based GI-MMF is used, together with the temperature variations during the same period. The value of $h_{i,j}(t)$ is normalized to the average $\langle h_{1,j} + h_{2,j} \rangle$.

5.5 Electrical cross-talk after demultiplexing

The $h_{i,j}(t)$ coefficients can be used to estimate the electrical cross-talk between the two MGDM channels, assuming matrix inversion as the demultiplexing algorithm. If $\mathbf{G}(t) = \hat{\mathbf{H}}^{-1}(t)\mathbf{H}(t) = \{g_{i,j}(t)\}$, the electrical cross-talk $C_1(t)$ and $C_2(t)$ at the LOMs and the HOMs channel, respectively, is defined in decibels as

$$C_1(t) = 20 \log_{10} \left| \frac{g_{1,2}(t)}{g_{1,1}(t)} \right|, \tag{5.3}$$

$$C_2(t) = 20 \log_{10} \left| \frac{g_{2,1}(t)}{g_{2,2}(t)} \right|. \tag{5.4}$$

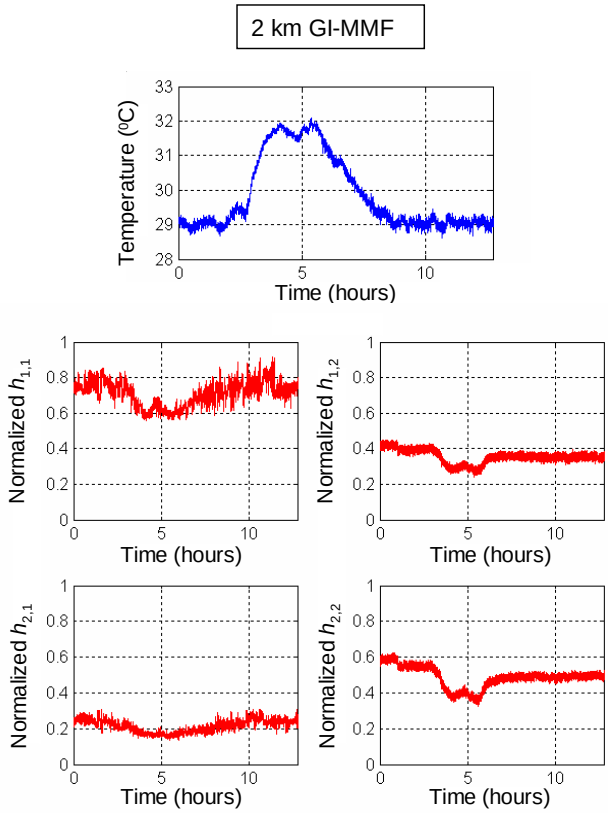

Figure 5.7: Measurements of the transmission matrix elements $h_{i,j}(t)$ over 12.7 h, when the 2 km long 148/200 μm silica-based GI-MMF is used, together with the temperature variations during the same period. The value of $h_{i,j}(t)$ is normalized to the average $\langle h_{1,j} + h_{2,j} \rangle$.

When both the estimation of the transmission matrix and matrix inversion are ideal, cross-talk is equal to $-\infty$ dB.

To give a figure of merit of the rate of the transmission matrix changes, the electrical cross-talk has been calculated for different periods of estimation of the transmission matrix (Δt). Specifically, it is assumed that the measured normalized $\mathbf{H}(t)$ is ideal and $\hat{\mathbf{H}}^{-1}(t)$ is calculated every Δt sec during the 12.7 h measurement of $h_{i,j}(t)$. Cross-talk is then estimated by Eqs. (5.3) and (5.4). Figure 5.8 shows the average and maximum values of the calculated cross-talk during the 12.7 h period for different Δt. Cross-talk clearly depends on Δt. Continuous estimation ($\Delta t = 0$) can ensure the best transmission performance and can therefore allow for transmission of services that require a very high SNR. For example, analog

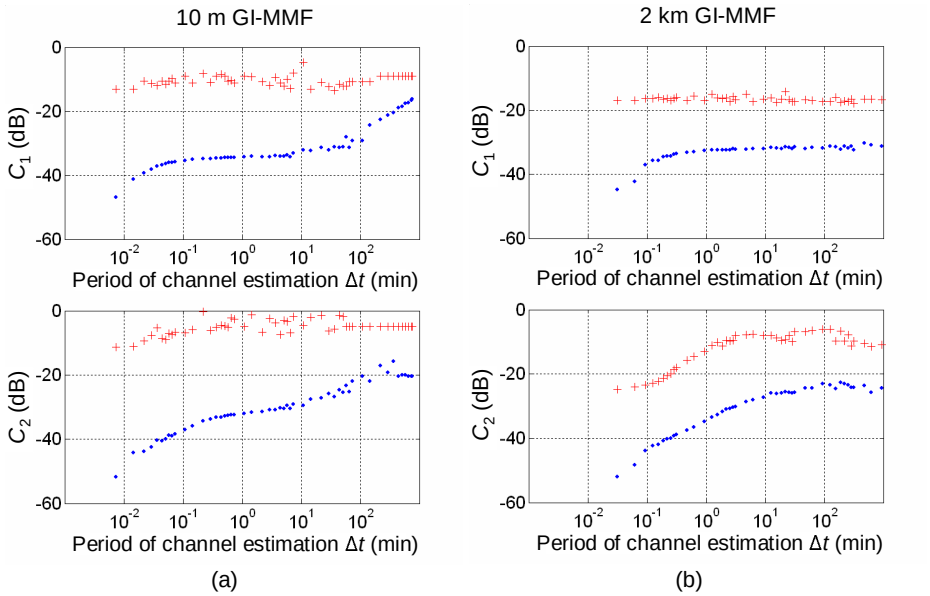

Figure 5.8: Calculated average ($\cdot$) and maximum ($+$) electrical cross-talk versus the period Δt of estimation of the transmission matrix, during the 12.7 h period in which $h_{i,j}(t)$ was measured, for the (a) 10 m (b) 2 km long GI-MMF. Matrix inversion was assumed to demultiplex the received electrical signals.

transmission may require an SNR as high as 40 dB, while transmission of an on-off keying bit sequence can be successful with an SNR of 10 to 15 dB.

5.6 Linearity and distortion in the 2×2 MGDM link

The 2×2 MGDM link described above was also used to transmit two analog low-bandwidth signals, as will be discussed in Section 5.7. Analog transmission is very demanding with respect to SNR and linearity. In this section, the 2×2 link is examined with respect to linearity and signal distortion.

5.6.1 Signal distortion

In Chapter 2, factors that may cause interaction among the MGDM channels were investigated. In the most general scenario, mutually incoherent optical sources are required to build an MGDM system which is linear with the optical intensity. This allows for a simple matrix to characterize the transfer function of the system.

Cross-talk is then expressed in the non-diagonal elements of $\mathbf{H}(t)$.

Similarly to other optical communication systems, the signal in every single MGDM channel can be distorted. Signal distortion can be caused either by linear or non-linear effects. Overall, MMFs can be viewed simply as dispersive, lossy media. Loss can be compensated by increasing the transmitting optical power. Dispersion limits the bandwidth of IM-DD transmission. It can also induce harmonic distortion when combined with laser chirping [105–108]. In general, direct modulation results in stronger chirping than external modulation. The signal is more distorted as chirping and dispersion increase. An MGDM system, with a real-valued $\mathbf{H}(t)$, operates below the dispersion limit. This limit depends on the transmission format and it is also determined by the tolerance of the provided services to dispersion-induced harmonic distortion.

Non-linear characteristics of the system can introduce harmonic and intermodulation distortion. Such non-linear characteristics can be in the P-I curve of the laser, the dependence of the responsivity of the photodiode on the optical intensity and non-linear responses in the electronic circuitries of the system. Usually, non-linearities from the laser prevail over the ones from the photodiode. A non-linear response can be also due to some degree of mutual coherence among the fields of the detected mode groups that can cause beat noise, as was shown in Chapter 2.

5.6.2 System response

To examine the linearity and signal distortion in the 2×2 experimental link, a simple measurement was performed. At first, the laser bias current and the amplitude of the modulating electrical pilot tone were determined so as to optimize the linearity of the response. At the bias point, the optical power at the output end of the SMF patch-cord of the laser was 2 mW, while the amplitude of the modulating signal corresponded to 1 mW optical power (thus 2 mW peak-to-peak). Figures 5.9 and 5.10 show the electrical spectrum of a back-to-back measurement. In particular, they show the spectrum at the output of one receiver of the link when the lasers of Tx1 and Tx2, respectively, were modulated with a pilot tone of 1 MHz. The photodiode of the receiver responded to light from the SMF patch-cord of the laser. In both cases, more than 44 dB difference was achieved between the amplitude of the 1 MHz tone and the amplitude of the highest harmonic.

A similar measurement was carried out using the 2 km long 148/200 μm silica-based GI-MMF and exciting simultaneously both the LOMs channel and the HOMs channel. The laser of Tx1 (Tx2) was modulated with a pilot tone of 1 (1.5) MHz. The electrical spectra at the output of Rx1 and Rx2 are shown in Figures 5.11, 5.12, 5.13, and 5.14. More specifically, Figure 5.11 (5.12) shows the spectra when only the LOMs (HOMs) channel is excited and Figure 5.13 shows the spectra when both channels are active at the same time. Figure 5.14 corresponds to the case when both channels are idle (the lasers are switched off), in order to show the response of the A/D converters when no signal is transmitted.

In Figures 5.11, 5.12 and 5.13, the pilot-to-the-strongest-harmonic ratio is de-

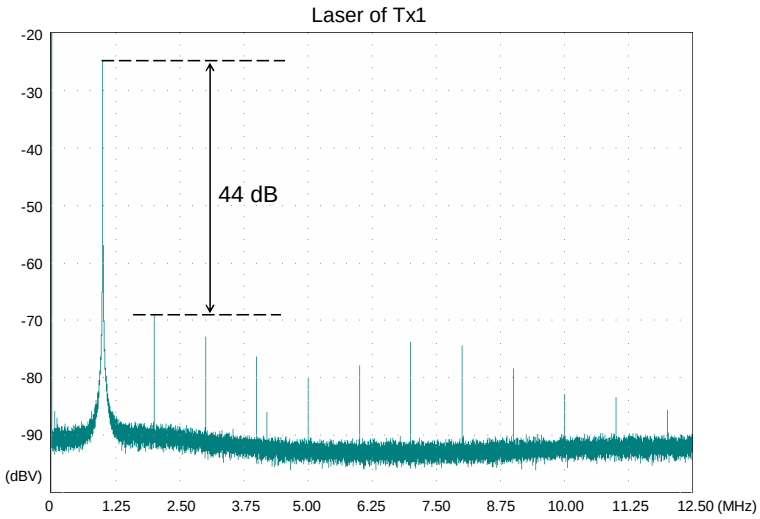

Figure 5.9: Back-to-back measurement of the electrical spectrum at the output of one receiver of the 2×2 MGDM link. The photodiode of the receiver responds directly to light from the SMF patch-cord of the laser of Tx1, which is modulated with a 1 MHz pilot tone.

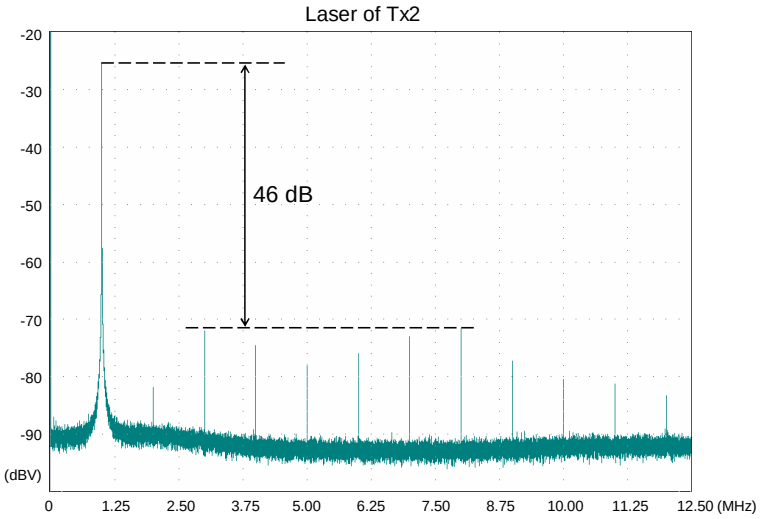

Figure 5.10: Back-to-back measurement of the electrical spectrum at the output of one receiver of the 2×2 MGDM link. The photodiode of the receiver responds directly to light from the SMF patch-cord of the laser of Tx2, which is modulated with a 1 MHz pilot tone.

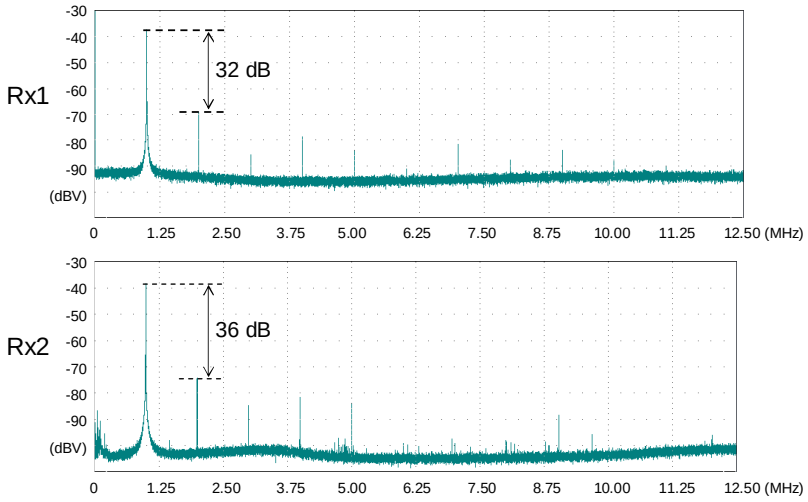

Figure 5.11: Electrical spectrum at the output of Rx1 and Rx2 of the 2 × 2 MGDM link with the 2 km long 148/200 μm silica-based GI-MMF, when only the LOMs channel is excited. The laser of Tx1 is modulated with a pilot tone of 1 MHz.

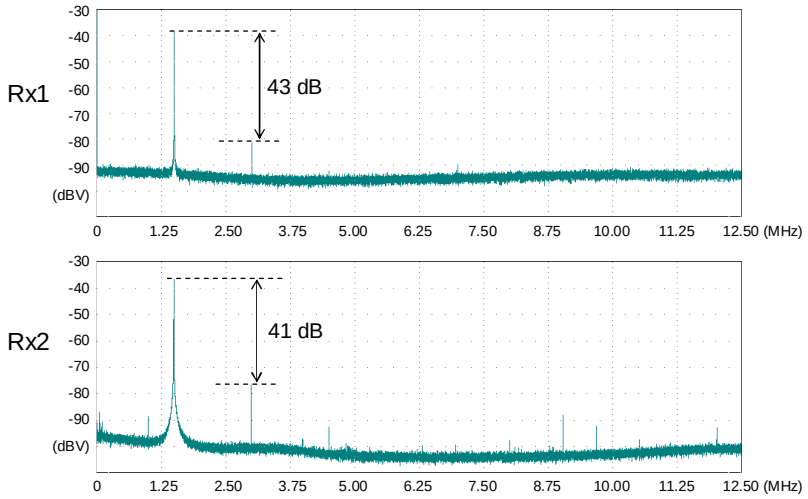

Figure 5.12: Electrical spectrum at the output of Rx1 and Rx2 of the 2 × 2 MGDM link with the 2 km long 148/200 μm silica-based GI-MMF, when only the HOMs channel is excited. The laser of Tx2 is modulated with a pilot tone of 1.5 MHz.

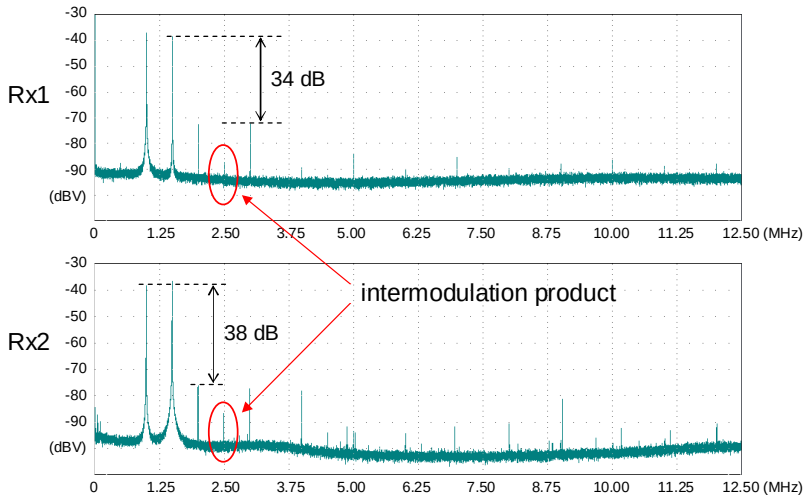

Figure 5.13: Electrical spectrum at the output of Rx1 and Rx2 of the 2 × 2 MGDM link with the 2 km long 148/200 μm silica-based GI-MMF, when both the LOMs and HOMs channels are excited. The laser of Tx1 (Tx2) is modulated with a pilot tone of 1 (1.5) MHz.

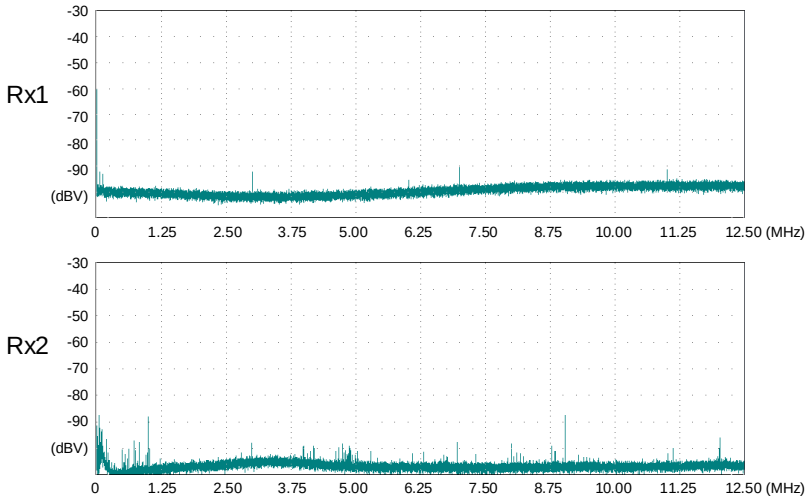

Figure 5.14: Electrical spectrum at the output of Rx1 and Rx2 of the 2 × 2 MGDM link when both the LOMs and HOMs channels are idle (the lasers are switched off).

graded compared to the results of Figures 5.9 and 5.10. This degradation can be attributed to the combined effect of laser chirping and dispersion in the 2 km long silica-based GI-MMF [105–108]. It should be noted that at 635 nm, chromatic dispersion is much higher than in the standard telecommunication windows. This degradation is different in each of the four propagation paths, namely from Tx1 to Rx1 and Rx2, and from Tx2 to Rx1 and Rx2. Harmonic distortion is stronger in the LOMs channel than in the HOMs channel. Therefore, it seems that dispersion in the LOMs channel is stronger than in the HOMs channel. Further, in Figure 5.13, an intermodulation product at 2.5 MHz can be observed. However, the amplitude level of this term is approximately 48 dB lower compared to the level of the weakest pilot tone. It should be mentioned that fiber displacements could easily yield different spectra with respect to the level of the harmonics and the intermodulation product. This may be due to varying mode mixing conditions that can affect the dispersion of each propagation path and therefore the level of the induced distortion. In contrast, when the 10 m long 185/250 μm silica-based GI-MMF was tested, the response of the link was much more stable and similar to the back-to-back case. Further, no significant difference was observed in the level of the harmonics at the electrical outputs of Rx1 and Rx2.

5.7 Analog transmission

In this section, the integration of the optical system that was described in the preceding sections and the electronic system implemented by the Signal Processing Systems group of the Eindhoven University of Technology is presented. The first approach was to realize a non-adaptive demultiplexer [109] and the second step was to implement an adaptive one [110]. In both cases, the demultiplexer was designed to accommodate the transmission of analog video and/or audio signals. Both demultiplexing circuits were analog with a bandwidth of about 6 MHz to meet the bandwidth requirement of the video signal, since the audio signal had a bandwidth of about 50 kHz.

The demultiplexing of the MGDM channels is achieved by multiplying the received electrical signals by the inverse transmission matrix $\mathbf{H}^{-1}(t)$. The transmission matrix can be measured with the use of pilot tones, as was already shown in Section 5.4. In the case of a 2×2 system, $\mathbf{H}^{-1}(t)$ is given by

$$\mathbf{H}^{-1}(t) = \frac{1}{|\mathbf{H}(t)|} \begin{bmatrix} h_{2,2}(t) & -h_{1,2}(t) \\ -h_{2,1}(t) & h_{1,2}(t) \end{bmatrix}, \tag{5.5}$$

where $|\mathbf{H}(t)|$ is the determinant of $\mathbf{H}(t)$. Therefore the measurement of $\mathbf{H}(t)$ gives in a very straightforward way $\mathbf{H}^{-1}(t)$.

Figure 5.15 shows the experimental setup including the electronic demultiplexing unit. A photograph of the actual setup in the laboratory is shown in Figure 5.16. Analog video and/or audio signals were transmitted in the two channels

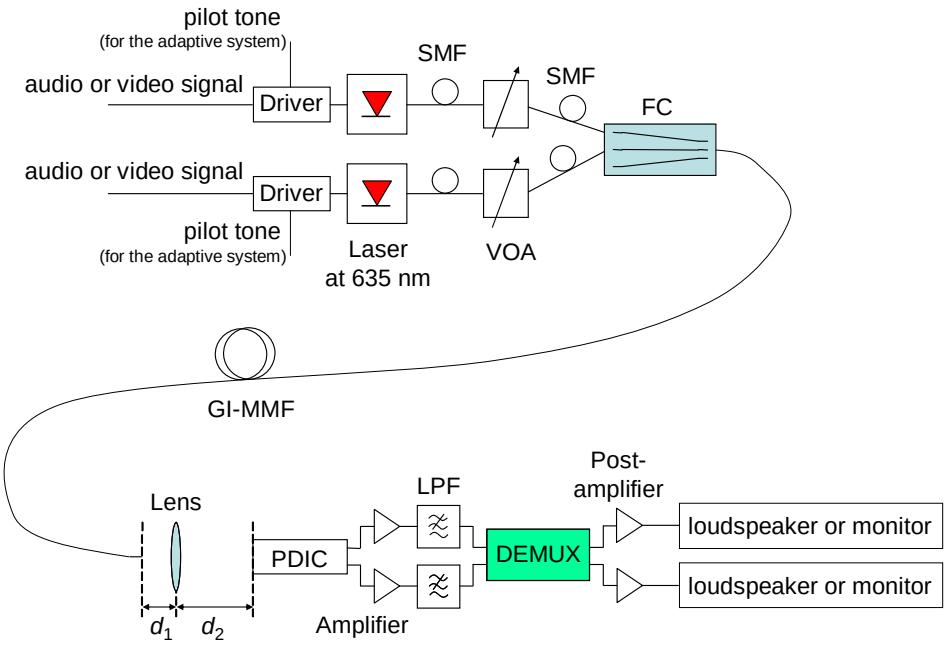

Figure 5.15: Transmission of two low-bandwidth, analog signals (audio, video) over the 2×2 MGDM system.

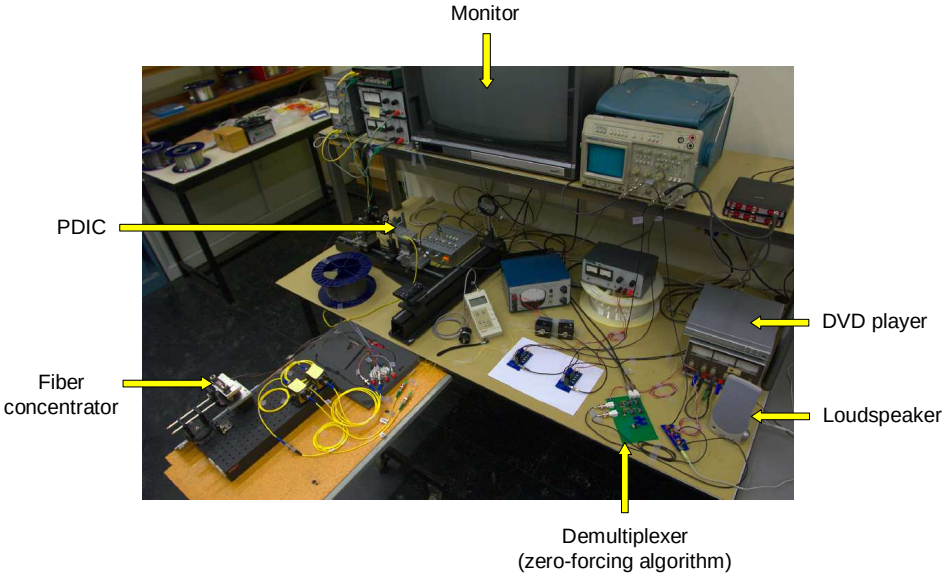

Figure 5.16: Photograph of the 2×2 MGDM system in the laboratory.

and the demultiplexed electrical signals were used as input signals to a loudspeaker or a monitor. That proved to be an easy and practical way to realize a transmission experiment, given the low bandwidth of the electronic circuitry. In the transmission experiment with the non-adaptive demultiplexer, the lasers were modulated only with the transmitted signals, since $\hat{h}_{i,j}^{-1}$ were set manually [109]. In the case of the adaptive demultiplexer, the lasers were modulated both with the transmitted signals and out-of-band pilot tones at 6.06 MHz and 7.12 MHz [110].

5.7.1 Non-adaptive demultiplexing

In the non-adaptive scheme [109], demultiplexing was achieved using potentiometers to manually adjust the value of $\hat{h}_{i,j}^{-1}$. Four analog multipliers were then used to perform the multiplication of the received signals by $\mathbf{H}^{-1}(t)$. One way to evaluate the reduction of cross-talk is to transmit a pilot tone at each channel and measure the level (amplitude) of each pilot tone at the electrical inputs and outputs of the demultiplexing unit. The measurement of the level of the pilot tones was done similarly as in Section 5.4. In particular, the laser of the LOMs (HOMs) channel was directly modulated by a sinusoidal pilot tone of 1 MHz (1.664 MHz) and the level of the pilot tones was measured at the input and output ports of the demultiplexing circuit. Figure 5.17 illustrates this measurement approach. An FFT of the signals was performed with about 11 measurements per second and an integration time of 2.6 msec for each measurement. Cross-talk before the electronic demultiplexing unit is estimated as

$$C_1^{\mathrm{be}}(t) = 20\log_{10}\left|\frac{h_{1,2}(t)}{h_{1,1}(t)}\right|, \tag{5.6}$$

$$C_2^{\mathrm{be}}(t) = 20\log_{10}\left|\frac{h_{2,1}(t)}{h_{2,2}(t)}\right|, \tag{5.7}$$

while cross-talk after the electronic demultiplexing unit is given by Eqs. (5.3) and (5.4).

Figure 5.18 shows the cross-talk measurements before and after the demultiplexer over a period of 14 h, when a 50 m long 93/125 μm silica-based GI-MMF was used. An average cross-talk of -28.1 dB and -21.8 dB at the LOMs and HOMs channel, respectively, was achieved after the electronic demultiplexer. The measurements of Figure 5.18 provide more strong evidence of how stable an MGDM link can be, especially considering that these measurements are taken using a non-adaptive demultiplexer and in a not-environmentally-controlled laboratory setup. Cross-talk remains low during the 14 h, more so in the LOMs channel. However, the value of cross-talk varies a lot due to lack of adaptivity. These cross-talk variations can span even 25 dB. These large variations should be attributed to the algorithm of demultiplexing, i.e. matrix inversion. Matrix inversion is a rather sensitive operation. As will be discussed in Chapter 6, the more diagonally dominant the transmission matrix tends to be, the more robust the MGDM link becomes, in

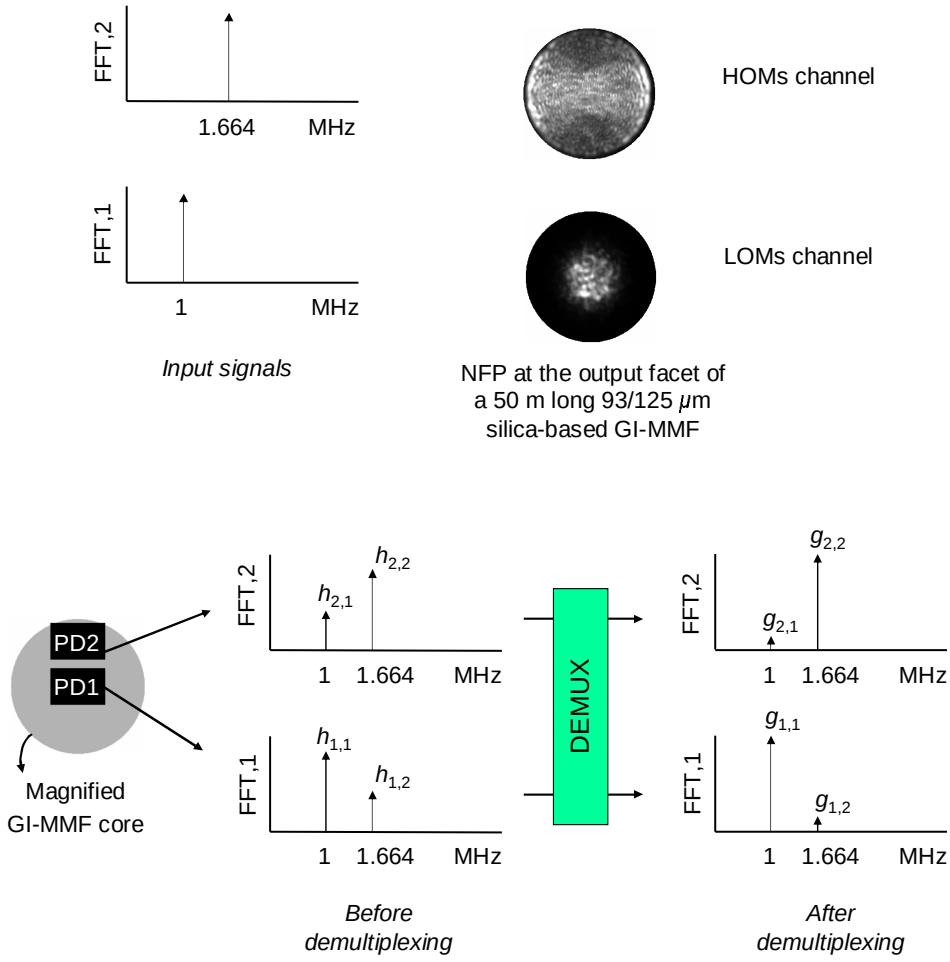

Figure 5.17: Experimental method used to measure cross-talk before and after the electronic demultiplexer of the 2×2 MGDM system.

the sense that changes in the value of $h_{i,j}(t)$ have less impact in the performance of the system. This sensitivity of an MGDM system in changes in the value of $h_{i,j}(t)$ was already observed in Section 3.5, in the calculations of the optical power penalty due to electronic matrix inversion, where the impact of misalignments was examined. In addition, in Section 5.5, a very large difference between the calculated values of the average and the maximum cross-talk was observed. This difference was around 30 dB in some cases.

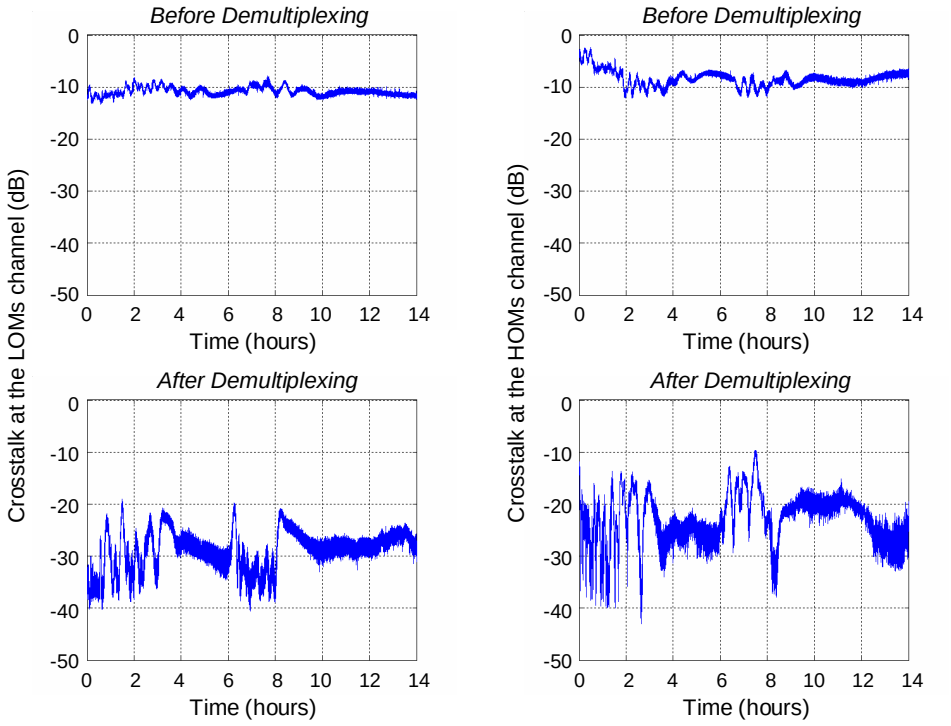

Figure 5.18: Measured cross-talk before and after the electronic demultiplexer of the 2 × 2 MGDM system, over a period of 14 h. A 50 m long 93/125 μm silica-based GI-MMF was used.

5.7.2 Adaptive demultiplexing

The difference between the adaptive and the non-adaptive 2 × 2 MGDM systems lies in the estimation of $h_{i,j}(t)$ and therefore of $h_{i,j}^{-1}(t)$ according to Eq. (5.5). The adaptive demultiplexer requires that the signals are transmitted together with out-of-band sinusoidal pilot tones, as is also shown in Figure 5.15. The received signals are then filtered and phase-locked loops are used to measure the value of $h_{i,j}(t)$. Details on the design, implementation and evaluation of this adaptive demultiplexer can be found in Ref. [110].

5.8 Conclusions

A demonstration of a 2×2 MGDM system was described, which showed quite stable operation, although the laboratory environmental conditions were not stabilized. To the author's knowledge, this is the first demonstration of a two-input, two-

output, transparent MGDM system.

Components originally made for other applications were used to build a 2×2 MGDM link, in a way that approximates the design guidelines of Chapter 3. The transmission matrix of this link was measured over a 12.7 h period, when a 10 m long 185/250 μm and a 2 km long 148/200 μm silica-based GI-MMF was used. In both cases, the links were shown to be stable. The stability of the links was evaluated in terms of cross-talk calculations as a function of the period of estimation of the transmission matrix, assuming electronic demultiplexing based on matrix inversion. The use of MGDM-specific connectorized components, as well as a feedback control loop at each transmitter to maintain the average emitted optical power constant can further increase the stability of an MGDM link. Furthermore, some simple measurements were performed to examine the linearity and signal distortion in the 2×2 MGDM link.

This stable 2×2 link was integrated with a non-adaptive as well as an adaptive analog electronic demultiplexer. These electronic circuits implement the demultiplexing of the channels based on matrix inversion and have a bandwidth of about 6 MHz. Both demultiplexing circuits were designed and implemented by the Signal Processing Systems group of the Eindhoven University of Technology. The transmission of two low-bandwidth analog signals (video and/or audio) was tested with both electronic demultiplexers. Cross-talk measurements over a 14 h period before and after the non-adaptive demultiplexer provided strong evidence of the stability of this 2×2 MGDM system. A 50 m long 93/125 μm silica-based GI-MMF was used in these measurements. The average cross-talk, during the 14 h period, after the demultiplexer was estimated to be -28.1 dB and -21.8 dB at the LOMs and HOMs channels, respectively.

Chapter 6

Mode-selective spatial filtering

Mode-selective spatial filtering (MSSF) is introduced and demonstrated. MGDM has initially been approached using electronic mitigation of cross-talk. The electronic mitigation is based on matrix inversion. MSSF is an optical method that reduces cross-talk among the channels. MSSF is achieved by projecting the near-field pattern at the GI-MMF output end onto the detectors via an imaging system with a lower numerical aperture (NA) than the central NA of the GI-MMF. The power penalty due to the electronic demultiplexing is then decreased and the robustness of the link is increased, although some of the optical power is lost. MSSF allows for a larger number of channels. With MSSF it would be possible to eliminate the need for electronic demultiplexing. This facilitates the combination of MGDM with wavelength division multiplexing, using a single laser source for each wavelength, together with an optical splitter and an external modulator at each MGDM channel. MSSF is a new optical technique, first proposed in the framework of the research presented in this dissertation.

6.1 Introduction

In Chapter 3, a method of designing an MGDM system was proposed. This method exploits the fact that an MGDM system requires no orthogonality of the received signals in the optical intensity domain. That led to a simple design approach, which can be used as long as the linearity of the link with the optical intensity has been properly addressed as an engineering task. This approach is based on the principle that for a MIMO system, cross-talk is not viewed as an impairment as it is in other systems, but rather that it bears useful information. Matrix inversion

Parts of this chapter are published in Ref. [1,6] of Appendix B.

is a zero-forcing method that uses the spatial information to cancel cross-talk regardless of the performance of the system in relation to noise [49]. In MGDM transmission, matrix inversion allows for transparency to the signal format.

Several factors may limit the performance of an MGDM transmission system based on the approach of Chapter 3. These transmission impairments are discussed in the following section. It becomes evident that an optical technique of reducing cross-talk can mitigate — partially or fully — these impairments. Subsequently, mode-selective spatial filtering (MSSF) is introduced and demonstrated as such a technique.

6.2 Transmission impairments in MGDM systems

As explained in Chapter 2, an MGDM system which is not dispersion-limited is described by a real-valued transmission matrix $\mathbf{H}$. In general, this requires that each channel uses a different laser source so that the fields of the detected mode groups are mutually incoherent and optical beating averages to zero. For a small number of channels and moderate transmission bandwidth, optical beating should pose no problem. However, if the use of MGDM is to be extended to applications where maximization of the aggregate bandwidth is of major concern, optical beating may limit the system performance. In Ref. [61], where dispersive multiplexing is proposed, it is suggested that to avoid this problem, the wavelengths of the lasers should not exactly overlap so that any beating term falls outside the transmission bandwidth of the system. Such a system still employs a detector which is wavelength-blind and therefore cost advantages related to the lack of optical filtering are maintained. However, if the MGDM technique is to be combined with wavelength division multiplexing (WDM), the use of a single laser source for each wavelength-channel and external modulation at each MGDM channel would be desired. In that case, optical beating can pose a limitation.

Assuming that an MGDM system is adequately characterized by a real-valued transmission matrix, the demultiplexing of the transmitted signals is based on electronic matrix inversion. This induces a power penalty, as was explained in Chapter 2. Analysis of an MGDM system using the design approach of Chapter 3 showed that as the number of channels increases, this penalty grows significantly and furthermore, the system becomes less robust to changes in the value of the transmission matrix elements. The robustness of the system depends on the condition number of $\mathbf{H}$, denoted as $\kappa(\mathbf{H})$. This number is defined as [71–73]

$$\kappa(\mathbf{H}) = \|\mathbf{H}\|\|\mathbf{H}^{-1}\|, \tag{6.1}$$

where $\|\cdot\|$ denotes a matrix norm [71–73]. The most usual matrix norms are the p-norms and the Frobenius norm [72, 73]. The above definition depends on the specific choice of the norm, but in general, $\kappa(\mathbf{H}) \geq 1$ and when $\mathbf{H}$ is singular $\kappa(\mathbf{H}) = +\infty$. The smaller the value of $\kappa(\mathbf{H})$ is, the better-conditioned the linear problem that describes an MGDM system is and therefore the more robust the

solution of the system is to changes in the value of the elements $h_{i,j}$. For example, the Frobenius norm of $\mathbf{H}$ is

$$\|\mathbf{H}\|_F = \sqrt{\sum_i \sum_j |h_{i,j}|^2}. \tag{6.2}$$

For the $N \times N$ MGDM systems described in Table 3.1 of Chapter 3, in which the whole near-field pattern (NFP) on the GI-MMF output facet is detected, the condition number of $\mathbf{H}$ using the Frobenius norm is $\kappa_F(\mathbf{H}) = 2.22$, 4.15, 6.74 and 10.46, for $N = 2$, 3, 4 and 5, respectively. As a point of reference, the $N \times N$ identity matrix $\mathbf{I}_{N\times N}$ has $\kappa_F(\mathbf{I}_{N\times N}) = N$.

Summarizing, the following factors can limit MGDM transmission:

- The need for mutual incoherence among the fields of the detected mode groups can limit the transmission bandwidth and complicates the combination of MGDM with WDM.
- The electronic matrix inversion yields a power penalty to maintain the SNR of the single channel case.
- The robustness of an MGDM system to changes in the value of $h_{i,j}$ depends on the condition number of $\mathbf{H}$.

The above factors limit the bandwidth of the system, the number of channels and pose some restrictions in the spectral content of the optical sources. If these issues are not properly addressed by the system designer, they can cause serious transmission impairments.

These limitations and the transmission impairments that they can cause can be overcome by reducing the spatial overlap among the intensity profiles of the detected mode groups. Indeed, the ideal case is $\mathbf{H} = \mathbf{I}_{N\times N}$. MSSF is a new technique that can be used to optically reduce cross-talk among the channels. Therefore it is of great significance in extending MGDM transmission to more demanding applications.

6.3 MSSF principle

Figure 6.1 illustrates the MSSF principle. Two propagating rays exit the GI-MMF output facet from points with similar distance from the GI-MMF axis [Figure 6.1(b)]. However, their angular divergence θ_1 and θ_2 from the GI-MMF axis is significantly different. If the MGDM multi-segment detector [Figure 6.1(a)] responds directly to the NFP, as was considered in Chapter 3, then both rays would be detected by the same segment R_2. Let us assume that a lens projects the NFP onto the MGDM detector. Let the numerical aperture of the lens at the side of the GI-MMF output end ($\mathrm{NA}_{\mathrm{lens}}$) correspond to an angle θ_{lens} such that $\theta_1 \leq \theta_{\mathrm{lens}} < \theta_2$. Only ray 1 is then gathered by the lens and subsequently detected

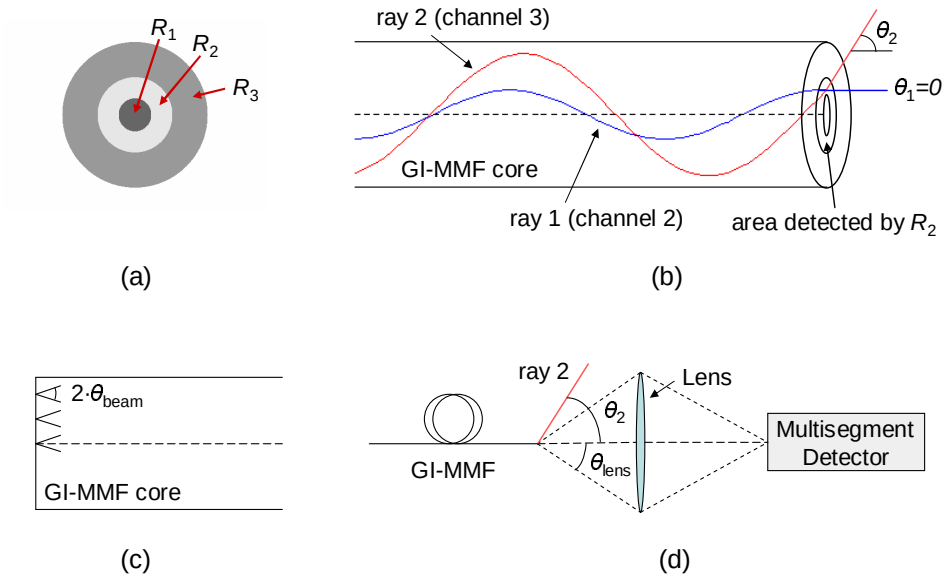

Figure 6.1: MSSF principle. (a) Geometry of a three-segment detector of a 3×3 MGDM system. (b) Two propagating rays in a GI-MMF. (c) Three input beams with different radial offset at the GI-MMF input end. (d) A lens projects light at the GI-MMF output end onto the multi-segment detector of an MGDM system.

by R_2. If $\mathrm{NA}_{\mathrm{lens}}$ is sufficiently low, R_3 (R_2) detects light related to ray 2 (1), while R_1 does not respond to light related with rays 1 and 2.

The NA of GI-MMFs $[\mathrm{NA}_{\text{GI-MMF}}(r)]$ has a maximum value on the GI-MMF axis ($r = 0$) and gradually drops to zero at the core-cladding interface ($r = a$). MSSF will be effective on the area of the GI-MMF core defined by $\mathrm{NA}_{\text{GI-MMF}}(r) > \mathrm{NA}_{\mathrm{lens}}$. As a rule of thumb

$$\mathrm{NA}_{\mathrm{beam}} < \mathrm{NA}_{\mathrm{lens}} < \mathrm{NA}_{\text{GI-MMF}}(0), \tag{6.3}$$

where $\mathrm{NA}_{\mathrm{beam}}$ is the NA of the radially offset input beams. The lower limit is because in GI-MMFs with limited mode mixing, light launched with a beam of $\mathrm{NA}_{\mathrm{beam}}$ at radial offset ρ_0 will tend to propagate with similar NA around ρ_0 and larger NA at points closer to the GI-MMF axis [Figure 6.1(b)].

MSSF introduces a power penalty since some of the optical power is not gathered. However, this power causes interference among the MGDM channels. Even if the total power penalty in an MGDM link with MSSF is comparable to the total power penalty in an MGDM link without MSSF, the link that uses MSSF is more robust since $\mathbf{H}$ is better-conditioned. The value of $\mathrm{NA}_{\mathrm{lens}}$ is a tradeoff between the total power penalty and the condition number of $\mathbf{H}$. In general, $\mathrm{NA}_{\mathrm{lens}}$ will decrease as the number of channels increases.

6.4 Experimental results

Figure 6.2 shows the experimental setup used for the investigation of MSSF. A 635 nm continuous wave, Fabry–Pérot multi-quantum-well laser was used to excite selectively a silica-based GI-MMF with a core/cladding diameter of 62.5/125 μm and NA = 0.275. The laser is pigtailed with an SMF with a mode field diameter (MFD) of 4.2 μm and an NA of 0.12, at 635 nm. A VOA with SMF pigtails, of similar MFD and NA as the laser pigtail, was used to control the level of the optical power. A microscope projected the NFP at the GI-MMF output end onto a CCD camera. An image of the projected pattern was grabbed with video processing software. Two GI-MMF samples were tested, of lengths 1 m and 1 km, under excitation with the SMF of the VOA at 0 μm, 10 μm, 15 μm, 21 μm, and 26 μm radial offset, following the design parameters for a 5×5 MGDM system of Chapter 3. The radial offset of the SMF axis from the GI-MMF axis was set by means of computer-controlled translational stages. Two microscope objectives were used. A 50× one with $\mathrm{NA_{lens}} = 0.75$, capturing all the NFP, and a 5× one with $\mathrm{NA_{lens}} = 0.10$, achieving MSSF, its NA being close to the limit $\mathrm{NA_{beam}} = 0.12$. According to Eq. (6.3), $\mathrm{NA_{lens}} > 0.12$. However, the next option in our laboratory setup would be to use a microscope objective with $\mathrm{NA_{lens}} = 0.25$, for which the effect of MSSF is very limited.

The experimental results are shown in Figure 6.3. The NFP on the output facet of the GI-MMF (50× objective) is confined within a disk which is transformed into a doughnut when the 5× objective is used. It is clear that MSSF is highly effective for both the 1 m long GI-MMF and the 1 km long GI-MMF, and a robust MGDM system with five channels could be realized. For a smaller number of channels, e.g. three, MSSF could fully mitigate cross-talk. Quantitative evaluation of MSSF would require a careful analysis that takes into account both the power penalty due to the electronic demultiplexing based on matrix inversion and the power penalty due to MSSF. The optimal value of $\mathrm{NA_{lens}}$ should be also defined for a certain number of channels. This could be done either with an experimental setup where $\mathrm{NA_{lens}}$ can vary over a large range, or with simulations. The low magnification factor of 5× does not allow for a good estimation of the power penalty due to the electronic matrix inversion, similarly to the analysis of Chapter 3, since the obtained images have a low resolution. The results of Figure 6.3, though, clearly

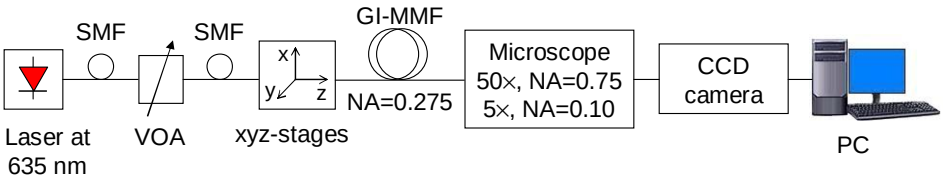

Figure 6.2: Experimental setup for the investigation of the effect of MSSF.

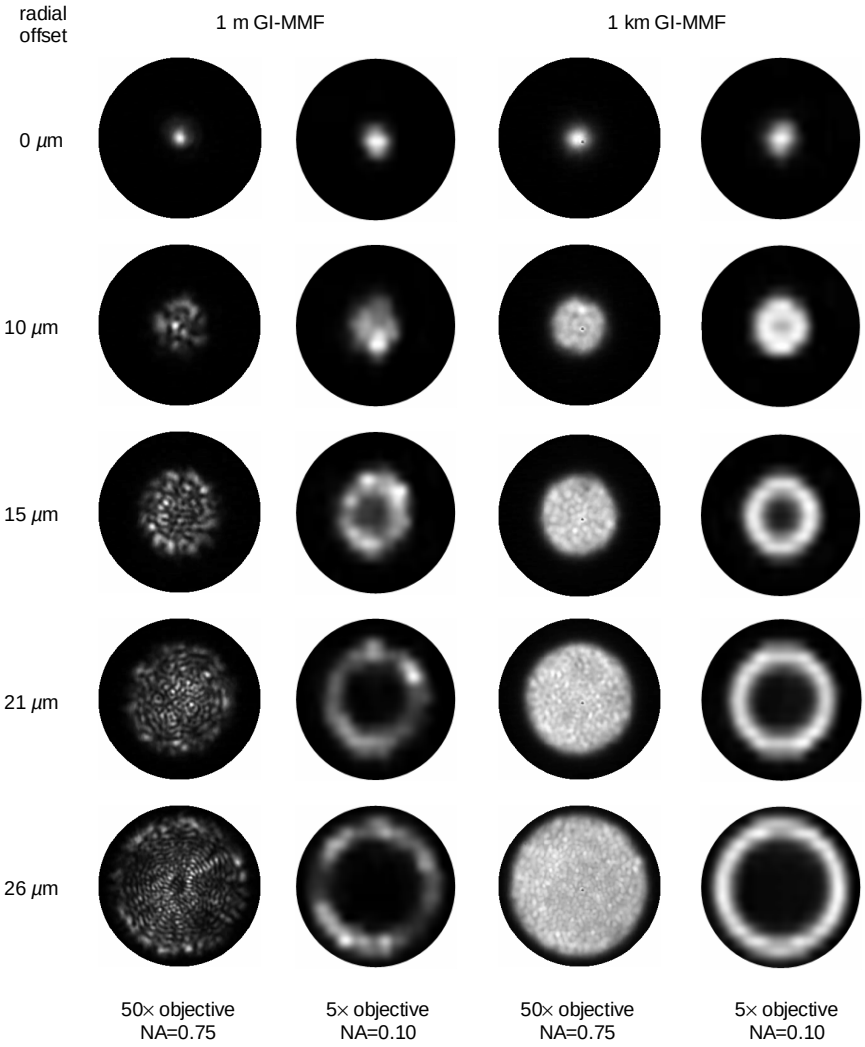

Figure 6.3: Experimental NFP observations, clearly illustrating the effectiveness of MSSF. Each row corresponds to a different radial offset of the input SMF. The first two columns show the results with a 1 m long, 62.5/125 μm, 0.275-NA, silica-based GI-MMF and the last two columns show the results with a 1 km long GI-MMF of the same type. The wavelength of light is 635 nm. MSSF is achieved when the microscope objective with 0.10-NA is used. The image seen with the objective of 0.75-NA corresponds to the whole NFP.

show the effectiveness and great potential of MSSF.

A coarse estimation of the optical power loss due to MSSF, in the case of a 5×5 MGDM system that could be realized based on the experimental results of Figure 6.3, can be done by comparing the area of the disk-like surface of the whole NFP to the area of the doughnut-like surface of the corresponding pattern when MSSF is applied. In particular, from Figure 6.3, for 26 μm radial offset at the input SMF, the doughnut-like area where light is distributed when MSSF is applied appears to be approximately twice smaller than the disk-like area of the whole NFP. This means that the loss due to MSSF is approximately 3 dB. For the other input beams, loss is smaller, while for central excitation it would appear that there is no loss due to MSSF. Certainly, though, this approach underestimates the loss due to MSSF. For example, since $\mathrm{NA_{lens}} = 0.10 < 0.12 = \mathrm{NA_{beam}}$, for central excitation there is some power loss. However, this coarse estimation shows that the loss due to MSSF is much lower than the power penalty due to matrix inversion in an MGDM system without MSSF. In Chapter 3, in Table 3.1, for a 5×5 MGDM system, the maximum optical power penalty at the shot (thermal) noise limit is 13.3 dB (6.3 dB).

6.5 A 2×2 MGDM link with MSSF

In Chapter 5, a stable 2×2 MGDM link was demonstrated. In this section, the effect of MSSF is incorporated in the same experimental setup and the stability of the link is again investigated. The setup used in Chapter 5 included a lens to project the NFP on the output facet of the GI-MMF onto the photodiode integrated circuit (PDIC), as can be seen in Figure 5.1. This lens was used with the purpose of magnifying the NFP by a factor $m \approx 2$, so that two PDIC photodiodes could be used [Figure 5.4(c)]. In this section, the parameter $\mathrm{NA_{lens}}$ is also exploited to achieve MSSF.

Figure 6.4 shows the experimental setup. Figures 6.4(a) and 6.4(c) show the transmitting side and receiving side of the 2×2 MGDM link, respectively. Further explanation of this setup can be found in Chapter 5. Two thick core silica-based GI-MMFs were used, as in Chapter 5, namely a 10 m long 185/250 μm one and a 2 km long 148/200 μm one. The NA of these GI-MMFs is 0.22. Two mode groups were excited simultaneously using two subsequent ports of the fiber concentrator (FC). In particular, a lower order modes (LOMs) group and a higher order modes (HOMs) group were excited with light launched at 0 μm and 30 μm radial offset on the input facet of the GI-MMFs, respectively. The NFPs at the output end of the GI-MMFs were observed with a CCD camera through a microscope [Figure 6.4(b)]. Similarly to the results of the previous section, the disk-like NFP of the HOMs group turns into a doughnut-like image when the NA of the microscope objective is sufficiently low. The results are shown in Figure 6.5. In particular, when $\mathrm{NA_{lens}} = 0.10$, two MGDM channels are implemented with a very high degree of spatial complementarity in the optical intensity domain.

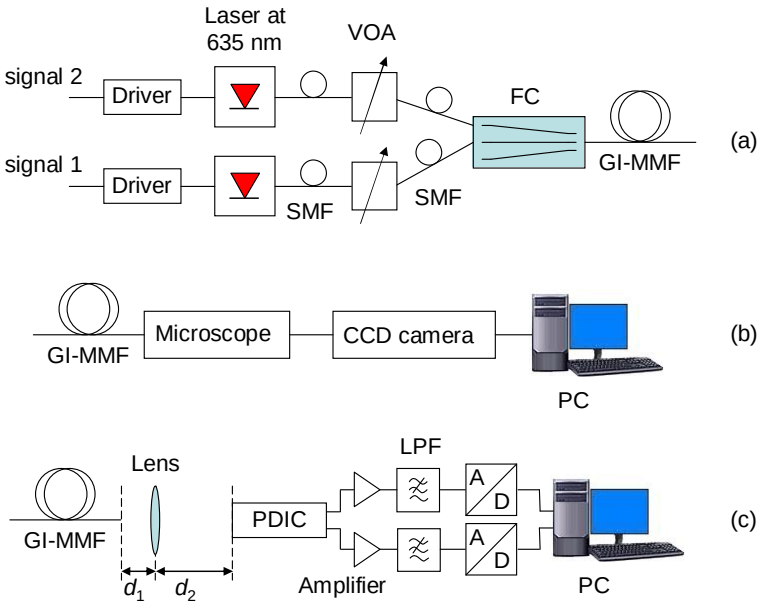

Figure 6.4: Experimental setup for the investigation of a 2×2 MGDM link with MSSF. (a) Transmitting side. (b) Observation of the NFP at the output end of the GI-MMF. (c) Receiving side.

Variations in the optical path from transmitter j to receiver i, due to changes either in the coupling of light at the GI-MMF ends or in the mode mixing conditions, cause the time-dependence of $\mathbf{H}(t)$. The former can be minimized with MGDM-specific, connectorized components, while the effect of the latter depends on the GI-MMF length. MSSF may affect the value of $h_{i,j}(t)$, since fluctuating mode mixing conditions can be translated into intensity variations. If these variations are very fast, and therefore not tractable, they will be manifest as modal noise.

We have measured $\mathbf{H}(t)$ of the 2×2 MGDM link with MSSF. Figure 6.4(c) shows the receiving side of the link. The lens and its distance from the GI-MMF end (d_1) and the PDIC (d_2) were chosen empirically, in order to achieve MSSF as well as properly magnify the NFP so as to use two PDIC photodiodes, as is shown in Figure 6.6. In the final implementation, $d_1 = 38$ mm, $d_2 = 83$ mm and therefore the magnification factor was $m = 2.18$. The value of $h_{i,j}(t)$ was measured using the same approach as in Chapter 5. The lasers of channels one (LOMs) and two (HOMs) were directly modulated with sinusoidal pilot tones of 1 MHz and 1.664 MHz, respectively. The level (amplitude) of each pilot tone at the two electrical outputs of the link was measured with a fast Fourier transform (FFT) and it corresponds to the value of $h_{i,j}(t)$. The FFT used approximately 11

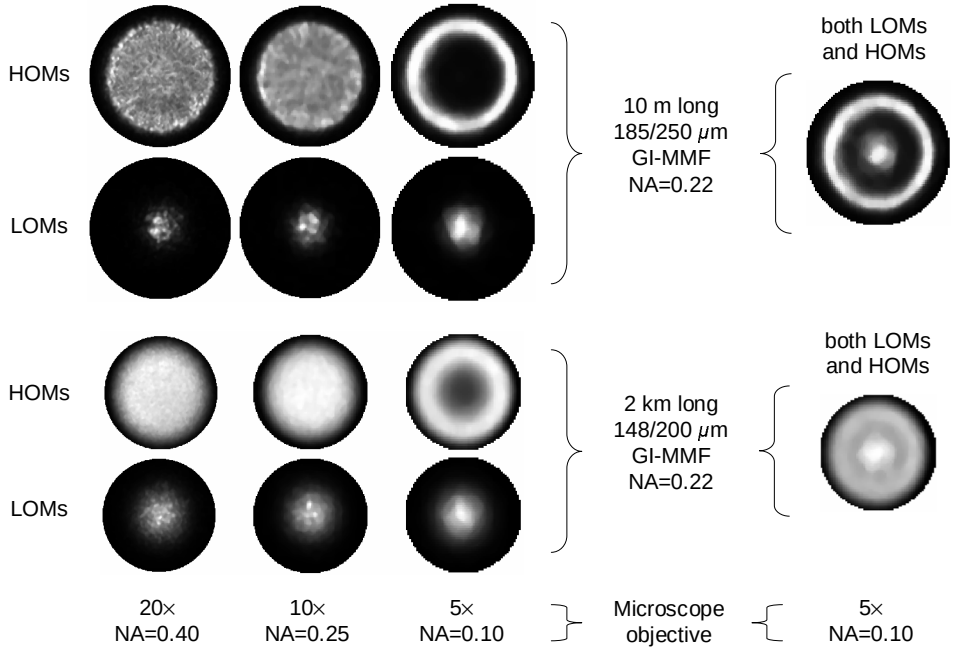

Figure 6.5: Observed NFPs at the output end of two thick core silica-based GI-MMFs, using different microscope objectives, when light propagates in LOMs and HOMs. The wavelength of light is 635 nm.

measurements per second and an integration time of 82 μsec.

Figures 6.6(a) and 6.6(b) show the measured normalized $h_{i,j}(t)$ over a period of 25 h, as well as the temperature variations during this period, when the 10 m and 2 km long GI-MMF was used, respectively. The normalization is with respect to the average $\langle h_{1,j} + h_{2,j} \rangle$, as is expressed in Eq. (5.2) of Chapter 5. It is clear that $h_{2,2}(t) > h_{1,2}(t)$, while in the absence of MSSF $h_{2,2}(t) \approx h_{1,2}(t)$. In the measurement shown in Figure 5.7 of Chapter 5, it appears that $h_{2,2}(t) > h_{1,2}(t)$. This may be due to MSSF, although the latter was not intentionally achieved. The results of Figure 6.6 reveal remarkable stability. The stronger variations appear with the 2 km long GI-MMF. This can be attributed to time-varying mode mixing conditions.

6.6 Conclusions

MSSF is a new optical method that can be used to reduce cross-talk among the channels of an MGDM system. It requires that the NFP on the output facet of a GI-MMF is projected onto the MGDM detector by an imaging system with

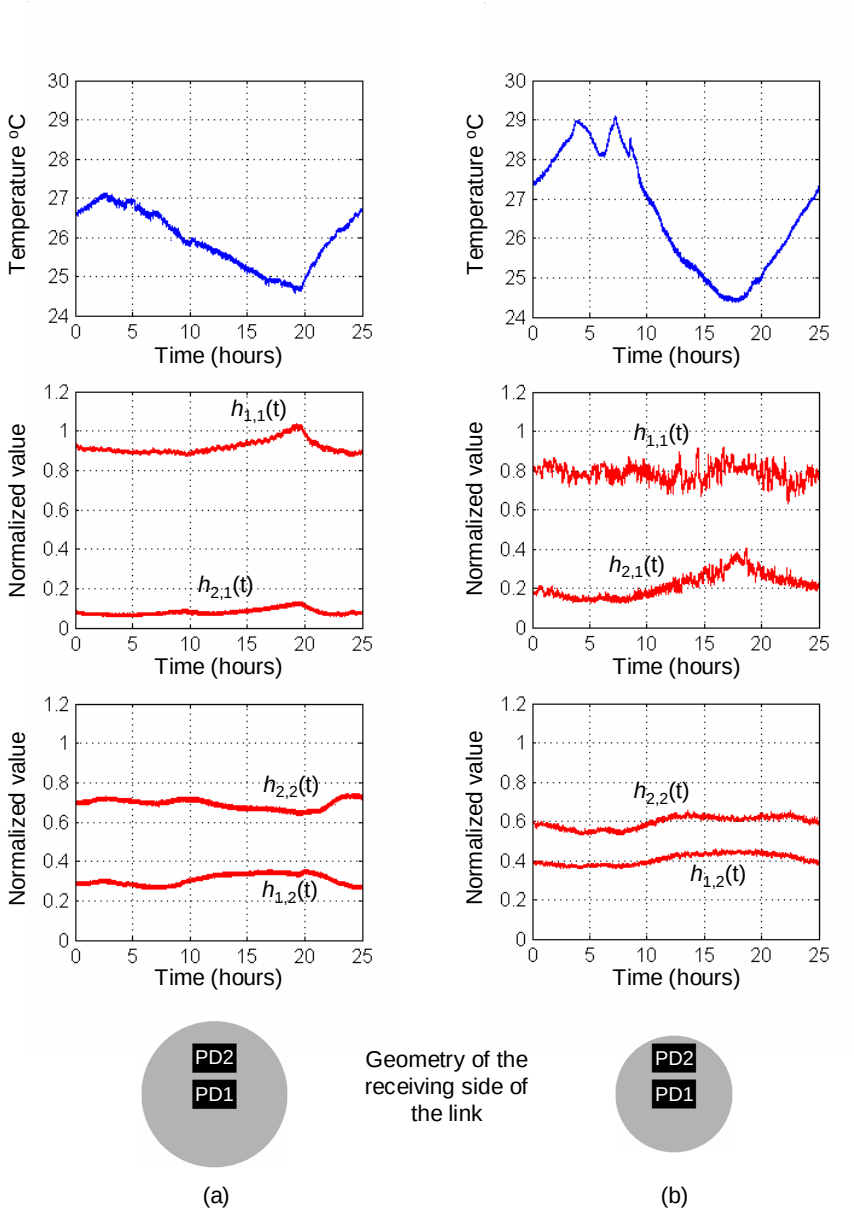

Figure 6.6: Measured $\mathbf{H}(t)$ of a 2×2 MGDM link with MSSF, over a 25 h period, using a (a) 10 m long 185/250 μm and (b) 2 km long 148/200 μm silica-based GI-MMF. The temperature variations during this period are shown as well. The geometry at the receiving side of the link is also illustrated, where gray color indicates the area of the magnified core of the GI-MMF and black the PDIC photodiodes (PDs).

a lower NA than the central NA of the GI-MMF. Such an imaging system can be a single lens. Selective excitation of GI-MMFs with an SMF yields an NFP which is confined within a disk. This disk-like pattern turns into a doughnut-like pattern when MSSF is applied, therefore reducing cross-talk. This means that some of the optical power does not reach the MGDM detector. However, despite this loss, this optical mitigation of cross-talk offers very significant advantages. In particular, it reduces the power penalty due to the electronic demultiplexing based on matrix inversion, increases the robustness of the system to changes in the value of $h_{i,j}(t)$ and relaxes the requirement of mutual incoherence among the fields of the detected mode groups. Consequently, the system admits more channels. For a small number of channels, e.g. three, over standard 62.5/125 μm silica-based GI-MMF, MSSF can eliminate the need for electronic demultiplexing. This greatly facilitates the combination of MGDM with WDM using a single laser source for each wavelength. MSSF was shown to be very effective for a five-channel system with standard 62.5/125 μm silica-based GI-MMF. Furthermore, the 2×2 system that was demonstrated in Chapter 5 was expanded to include MSSF. The transmission matrix of this 2×2 link with MSSF was measured over a period of 25 h and it was shown to be remarkably stable. All these features make MSSF a very reliable and promising technique.

Chapter 7

MGDM in GI-POF links

Polymer-based GI-MMF or GI polymer optical fiber (POF) is considered a very suitable medium for in-building and in-house optical networks. This is due to the flexibility of GI-POF that facilitates installation in ducts. Especially polymethylmethacrylate (PMMA)-based GI-POF has typically a large core diameter and high numerical aperture that allow for easy coupling of light and handling. The possibility of using MGDM transmission in GI-POF, mainly PMMA-based one, systems is investigated. The basic ideas are found to apply. However, mode mixing poses a strong restriction. Furthermore, although the flexibility of the PMMA material is an advantage concerning installation, it could cause deformations of the refractive index profile that can seriously affect the near-field pattern at the output end of the GI-POF. This influences the transmission matrix of an MGDM system and hence its performance.

7.1 Introduction

GI-MMFs can be silica- and/or polymer-based, as has been mentioned in Chapter 1. However, in the investigation presented in the preceding chapters, only silica-based GI-MMFs were considered and used. This was mainly due to the following reasons:

1. Mode mixing is very limited in silica-based GI-MMFs. In MGDM transmission, mode mixing is a restricting factor. Studying MGDM over silica-based GI-MMFs allows the investigation of the technique under almost ideal conditions from the mode mixing point of view.

2. Silica-based GI-MMFs are commonly used in short reach optical networks and connections. Therefore any results obtained with such fibers can be directly evaluated in terms of application in existing systems.

Parts of this chapter are published in Ref. [11] of Appendix B.

3. Previous modal multiplexing techniques have been studied using silica-based GI-MMFs. Hence, the results obtained for MGDM can be compared with the previous approaches.

In the present chapter, considerations for the use of graded-index polymer optical fibers (GI-POFs) are given. GI-POFs differ from silica-based GI-MMFs, or alternatively GI glass optical fibers (GI-GOFs), in the material and therefore absorption and scattering of light are not the same in the two GI-MMF types. This means that attenuation and mode mixing are different. As far as MGDM transmission is concerned, the MGDM model presented in Chapter 2 stands for both GOFs and POFs. Therefore, the issue to be investigated is what the near-field pattern (NFP) at the output end of GI-POFs under selective excitation looks. In the following sections, characteristics of GI-POFs and relevant literature results are explored. Polymethylmethacrylate (PMMA)-based GI-POF is suggested to be a suitable option for MGDM transmission, especially in the context of a transparent in-house network, and some experimental results are presented for this type of GI-POF.

7.2 PMMA- and PF-based GI-POFs

POFs are most commonly based on the PMMA material. The use of step-index (SI) POFs is more widespread than that of GI-POFs, the latter being developed to meet the needs of high speed, short range optical connections. A lot of work has been carried out on the control and optimization of the refractive index profile of PMMA-based GI-POFs [23, 111–113]. The core diameter of a PMMA-based GI-POF is around 500 μm, although there are no standards as there are in the case of SI-POFs with a core/cladding diameter of 980/1000 μm. Mode mixing in PMMA-based GI-POFs is much stronger compared to silica-based GI-MMFs. In several experiments, the NFP at the output end of PMMA-based GI-POFs under selective excitation has been observed [67, 113, 114]. In those studies, selective excitation was achieved using a silica-based SMF at visible light. The reported NFPs strongly depend on the excitation conditions, even after 100 m of propagation, which indicates that the optical power is not equally spread among the modes. Therefore, there seems to be room for MGDM transmission over short PMMA-based GI-POF links. This is especially interesting taking into account that the attenuation spectrum of this fiber does not allow for extensive use of wavelength division multiplexing (WDM) [24].

GI-POF based on perfluorinated (PF) polymer has more recently emerged as a low loss, high bandwidth transmission medium [115, 116]. PF polymer is a more expensive material than PMMA. As is the case for PMMA-based GI-POFs, mode mixing in PF-based GI-POFs is much stronger than in silica-based GI-MMFs. Observation of the NFP at the output end of PF-based GI-POFs shows that mode mixing is not full for a fiber length up to 108 m [117]. In Ref. [117], selective excitation with a silica-based SMF at 1300 nm wavelength was used.

This supports MGDM transmission. However, when compared with the results reported using PMMA-based GI-POF [67, 113, 114], it seems that greater spatial separation can be achieved among MGDM channels with PMMA-based rather than PF-based GI-POF. In contrast with PMMA-based GI-POF, the attenuation spectrum of PF-based GI-POF allows transmission in a very wide wavelength range from about 600 nm to approximately 1300 nm, with less than 100 dB/km attenuation. Therefore, it is easier to apply WDM transmission over PF-based than PMMA-based GI-POF.

A significant difference between PMMA-based and PF-based GI-POF lies in their size. As was mentioned in Chapter 1, PMMA-based GI-POF has usually a much larger core radius and higher numerical aperture (NA). Typical values were shown in Table 1.2. In particular, for PMMA-based GI-POF, the core radius is $a = 250$ μm and NA $= 0.29$, while for PF-based GI-POF, $a = 60$ μm and NA $= 0.171$. In order to facilitate the use of high speed transceivers at 1300 nm, PF-based GI-POFs with $a = 25$ μm, a typical value for GI-GOFs, have been recently used [35]. The large core radius and high NA of PMMA-based GI-POFs give them their special advantages related to the ease of light coupling and relaxed alignment. In contrast, PF-based GI-POF appears more as a competitor of GI-GOF, and its smaller core radius and low NA, together with high mode mixing do not make it a very appealing medium for MGDM transmission in in-house networks.

7.3 Selective excitation of PMMA-based GI-POFs with an SMF

In the previous section, it was suggested that PMMA-based GI-POF is a more suitable candidate for an MGDM system than PF-based GI-POF, especially when in-house networking is concerned. To investigate the possibility of MGDM transmission over PMMA-based GI-POF, an experimental investigation of the NFP at the output end of PMMA-based GI-POF has been attempted. The experimental setup is shown in Figure 7.1. A 635 nm continuous wave, Fabry–Pérot multi-quantum-well laser was used to selectively excite a GI-POF with core radius $a \approx 200$ μm and NA $= 0.274$. Perdeuterated PMMA (PMMA-d8) was used to fabricate this GI-POF[1] [112]. The laser is pigtailed with an SMF, with a mode field diameter (MFD) of 4.2 μm and an NA of 0.12, at 635 nm. The level of the optical power was controlled with a variable optical attenuator (VOA). The MFD and NA of the SMF pigtails of the VOA match the MFD and NA of the laser pigtail. A microscope projected the NFP on the GI-POF output facet onto a CCD camera. An image of the projected pattern was grabbed with video processing software. Two microscope objectives were used. A 20×, 0.40-NA one gathering all light at

[1] This PMMA-based GI-POF sample was provided by Dr. Takaaki Ishigure (Keio University, Japan).

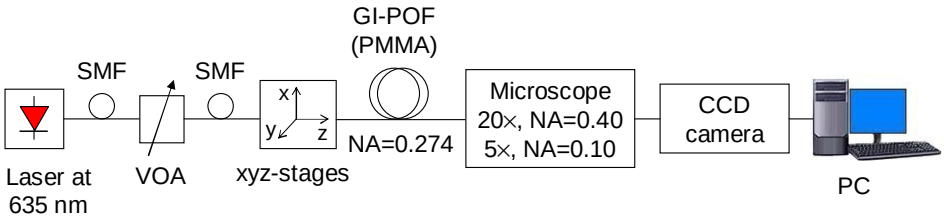

Figure 7.1: Experimental setup for the observation of the NFP, with and without the effect of MSSF, at the output end of a GI-POF under selective excitation with a radially offset SMF.

the output end of the GI-POF and a 5×, 0.10-NA one achieving mode-selective spatial filtering (MSSF).

The observed images are shown in Figures 7.2 and 7.3 for the cases of a 1 m and a 199 m long GI-POF, respectively. The two GI-POF samples are from the same spool and therefore they have the same characteristics. The results obtained with the 1 m long GI-POF are very similar to the ones obtained with the GI-GOF in Chapter 6. In particular, the NFP on the output facet of the GI-POF has a disk-like shape, with its radius depending on the radial offset of the input SMF. This disk-like pattern turns into a doughnut-like pattern when MSSF is applied. The transformation of the pattern due to MSSF is more evident for large radial offsets of the input SMF. The NFPs on the output facet of the 199 m long GI-POF exhibit similar characteristics, although indicating at the same time that mode mixing is very strong. The dependence of the NFP on the launch conditions, i.e. the radial offset of the input SMF, is much weaker than in the case of the 1 m long GI-POF. In the case of the 199 m long GI-POF as well, MSSF affects the observed images and improves the spatial separation of the patterns. It would seem that the images of Figures 7.2 and 7.3 do not exactly duplicate the results reported in Refs. [67, 113, 114]. In particular, in the case of Figures 7.2 and 7.3, doughnut-like patterns are observed only after applying MSSF, while in Refs. [67, 113, 114], similar doughnut-like patterns are simply mentioned as the NFP, without any indication to spatial filtering similar to MSSF. However, in Refs. [67, 113, 114], there is no detailed data on the NA of the imaging system used to observe the NFP nor on the value of the radial offset of the input SMF when exciting higher order modes.

The experimental results of Figures 7.2 and 7.3 show that it is possible to apply MGDM transmission over PMMA-based GI-POFs. Unfortunately, though, unlike the case of GI-GOFs, the transmission matrix would strongly depend on the length of the GI-POF. This is because mode mixing is very strong in GI-POFs. For the two GI-POF samples used, it appears from Figures 7.2 and 7.3 that a five and two channel MGDM system would be possible over the 1 m and the 199 m long GI-POF, respectively. This dependence on the GI-POF length renders it compli-

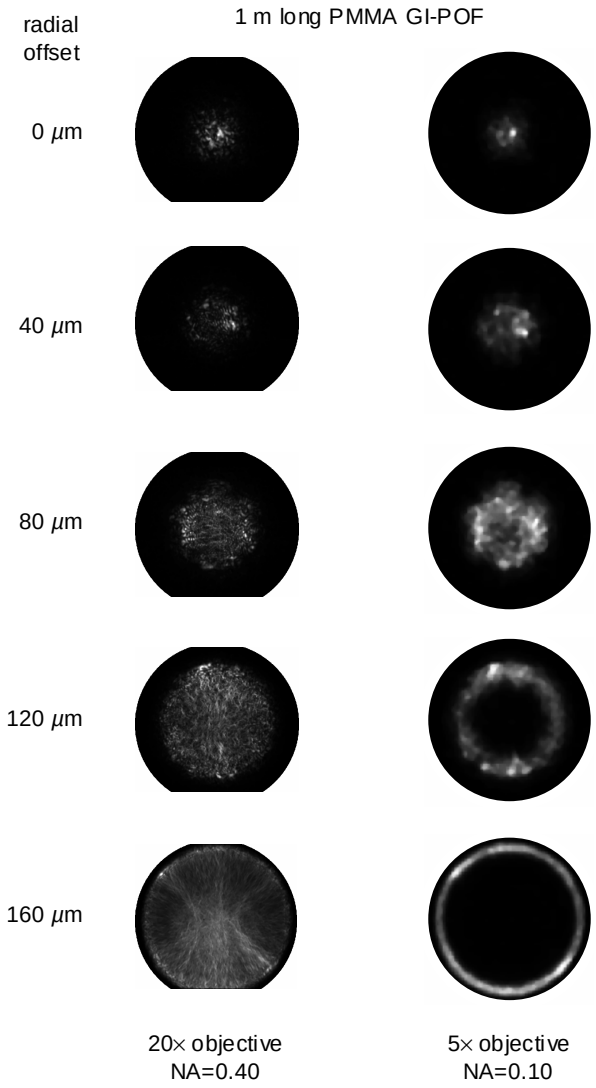

Figure 7.2: Observed NFPs at the output end of a 1 m long PMMA-based GI-POF with a core radius of about 200 μm and an NA of 0.274, using the setup of Figure 7.1. The wavelength of light is 635 nm. Each row corresponds to a different radial offset of the input SMF. The first column shows the results obtained with the 20×, 0.40-NA microscope objective that captures all light at the output end of the GI-POF. The second column shows the corresponding results when MSSF is applied. The latter is achieved with a 5×, 0.10-NA microscope objective. The 20× magnified core exceeds the dimensions of the CCD camera (left column).

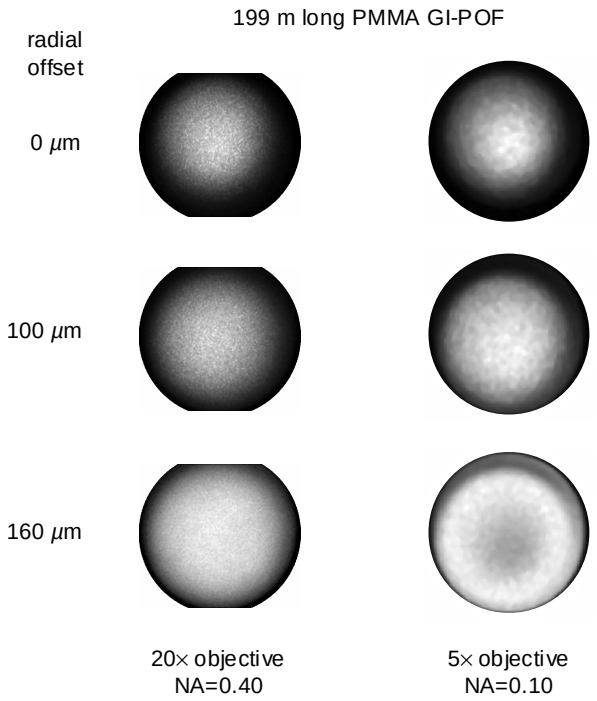

Figure 7.3: Observed NFPs at the output end of a 199 m long PMMA-based GI-POF with a core radius of about 200 μm and an NA of 0.274, using the setup of Figure 7.1. The wavelength of light is 635 nm. Each row corresponds to a different radial offset of the input SMF. The first column shows the results obtained with the 20×, 0.40-NA microscope objective that captures all light at the output end of the GI-POF. The second column shows the corresponding results when MSSF is applied. The latter is achieved with a 5×, 0.10-NA microscope objective. The 20× magnified core exceeds the dimensions of the CCD camera (left column).

cated to specify the geometric parameters of an MGDM multi/demultiplexer, in a similar way as in the case of GI-GOFs in Chapter 3. These parameters consist of the radial offsets of the input beams and the radii that define the annular segments of the MGDM detector. Mode mixing is not the sole factor that limits the maximum length of the PMMA-based GI-POF in MGDM transmission. Attenuation is another significant factor. The PMMA-based GI-POF sample under investigation has a loss of less than 100 dB/km at 635 nm [112].

It should be noted that there is a difference between the launch conditions of the tested PMMA-based GI-POF and the standard 62.5/125 μm GI-GOF used in Chapters 3 and 6. The SMF at the input end of both the GI-GOF and the GI-POF is the same, having a mode field radius of 2.1 μm at 635 nm. However, the mode

field radius of the fundamental mode in the two GI-MMF types is different. As was mentioned in Chapter 3, the mode selectivity of the excitation scheme that uses a Gaussian-like beam depends on the mode field radius of the fundamental mode (w_{fm}) of the GI-MMF and the mode field radius of the input beam (w_0). Equation (3.2) gives the value of w_{fm} for a parabolic index MMF. According to Eq. (3.1), in order to excite as few principal mode groups as possible, the radius of the input beam should be $w_0 = 0.6w_{\mathrm{fm}}$. For the parameters of the GI-POF under investigation, $w_0 \approx 7.3$ μm at 635 nm, which is much larger than the value of 2.1 μm of the mode field radius of the input SMF. In the case of the standard 62.5/125 μm GI-GOF, $w_0 \approx 2.9$ μm at 635 nm, a value much closer to the value of 2.1 μm. Consequently, excitation with the SMF pigtail of the 635 nm laser is more mode selective in the case of the GI-GOF than the GI-POF. The above calculations assume a parabolic index profile, i.e. $\alpha = 2$ in the power-law expression of Eq. (1.1). This is very close to the actual profile of the GI-GOF. The profile of the GI-POF under investigation is characterized by $\alpha = 2.3$ in the region close to its axis, while close to the core-cladding interface $\alpha = 3$. This means that the value of w_0 for the GI-POF is underestimated in the above calculation.

The two GI-POFs under test were bare, i.e. there was no coating around their cladding, and their ends were not connectorized. The 62.5/125 μm GI-GOFs used in the investigation of Chapters 3, 4 and 6 had a thin plastic coating around their cladding. These GI-GOF samples had also no connectors at their ends, which were stripped of the coating. Unlike the case with the GI-GOF samples, a strange phenomenon was observed with the GI-POFs. Fiber displacements easily affected the NFP. More careful investigation showed that the effect on the NFP was apparent when these displacements influenced the position of the end part of the GI-POF that was reaching the microscope stage. In particular, bending of the GI-POF at a distance of the order of 1 cm from its output end changed the overall NFP. Typical patterns, for central excitation, are shown in Figures 7.4(a), 7.4(c) and 7.4(d). When the end part of the GI-POF reaches the microscope stage in a straight position, the overall NFP is confined within a disk which is concentric with the GI-POF core. However, bending of this end part of the GI-POF moves the overall NFP, which does not remain concentric. This is very clear in Figure 7.4(a) that corresponds to the 1 m long GI-POF. It is also shown in Figure 7.4(c) and the left picture of Figure 7.4(d) for the 199 m long GI-POF. For offset launch, differentiation of the NFP also occurred for similar bending close to the GI-POF output end. This is shown in Figure 7.4(b) for the 1 m long GI-POF. Figure 7.5 shows two photographs of the GI-POF as it reaches the microscope stage in a straight and a bent position. The end part of the GI-POF in Figure 7.5(b) is not in a straight position and this kind of bending causes the changes in the NFP.

At the same time, when similar bending was forced at a larger distance from the GI-POF end, changes were observed only in the speckle pattern and not in the overall NFP, which remained stable. It seems therefore reasonable to assume that this bending does not really cause strong mode mixing. It rather causes macroscopic deformations in the refractive index profile that change the path of

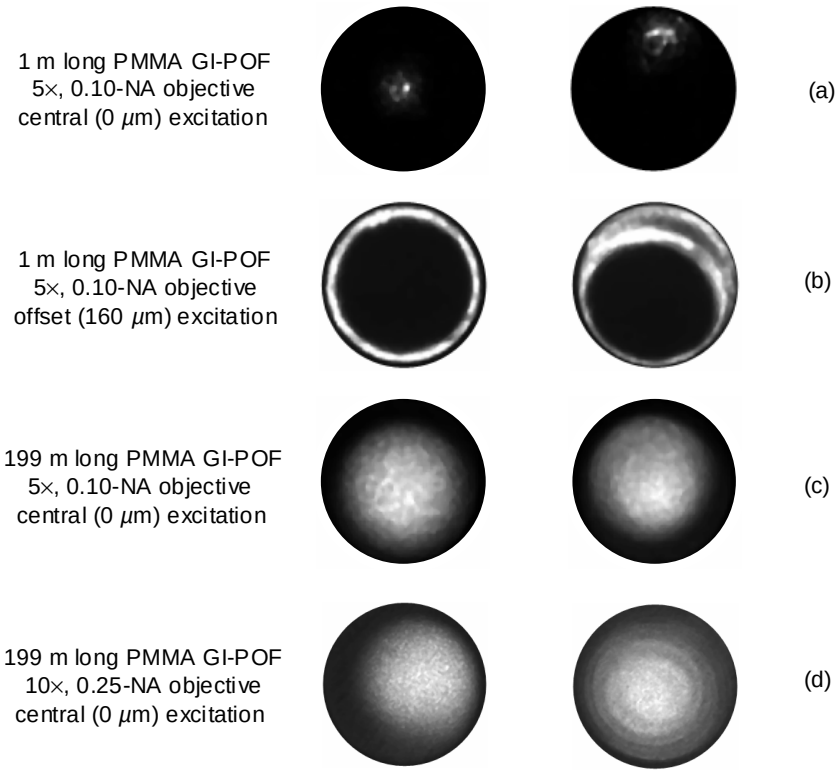

Figure 7.4: Experimental results showing changes in the observed NFP at the output end of a (a,b) 1 m and (c,d) 199 m long PMMA-based GI-POF, at 635 nm wavelength. The images were obtained using the setup of Figure 7.1 with (a,c,d) central and (b) 160 μm offset excitation with an SMF. A 5×, 0.10-NA microscope objective and a 10×, 0.25-NA one were used. Similar results were obtained with a 20×, 0.40-NA microscope objective. In all images, except the right one in (d), the changes in the intensity patterns are due to a bend of the end part of the GI-POF as it reaches the microscope stage, such as the one shown in Figure 7.5(b). The right image in (d) is after the GI-POF is pressed with the fingers at a distance around 30 cm from its output end.

light locally. These deformations are not sufficient to cause strong mode mixing, however, when taken place close to the GI-POF end, their impact becomes visible. It is probably the flexibility of the PMMA material and the large size of the GI-POF that cause large strain, and consequently large refractive index deformations. Silica is a much stiffer material and GI-GOFs are much thinner. These two characteristics make GI-GOFs more tolerant to bending. Since the effect becomes visible

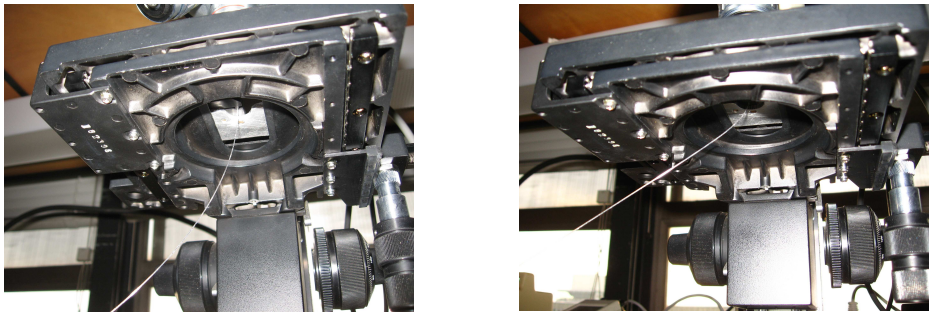

(a) (b)

Figure 7.5: Photographs of the microscope stage, where the GI-POF reaches in a (a) straight and (b) bent position.

when the bending occurs very close to the GI-POF output end, using a connector at this end may reduce or even eliminate this problem. Such a sensitivity of the NFP at the output end of GI-POFs has never been reported before and it would be interesting if it were examined further.

Finally, the right picture of Figure 7.4(d) shows the NFP, for central excitation, when the 199 m long GI-POF is pressed with the fingers at a distance of about 30 cm from its output end. The induced change in the NFP indicates that the applied stress causes mode mixing. Again, this was not observed with GI-GOFs.

7.4 Conclusions

PMMA-based GI-POF is considered a promising medium for short-reach in-building networks, such as in-house networks. This is due to its large core diameter and high NA that relax the accuracy in coupling and alignment and facilitate handling. In contrast, GI-POF based on PF polymer has a smaller core diameter and lower NA which, together with its lower attenuation, make it more interesting for longer connections, such as in campus networks. In both types of GI-POF, mode mixing is much stronger than in GI-GOFs. PMMA-based GI-POF was tested as a possible GI-MMF type in MGDM transmission. An experimental investigation of the NFP at the output end of PMMA-based GI-POF under selective excitation with a radially offset SMF showed that the NFP exhibits similar characteristics as in the case of GI-GOFs. MSSF also applies in a similar fashion as in GI-GOFs. However, due to the strong mode mixing, the overall NFP is strongly dependent on the GI-POF length. This hampers the design of an MGDM mutli/demultiplexer that holds independently of the GI-POF length, similarly to GI-GOFs. At the same time, the number of channels depends on the length of the GI-POF. It was shown that a 1 m long PMMA-based GI-POF could support five MGDM chan-

nels, while this number reduces to two for a 199 m long PMMA-based GI-POF. In addition, the size and flexibility of the PMMA-based GI-POF, although they offer advantages with respect to installation and handling, make the overall NFP sensitive to bending that occurs very close to the output end of the GI-POF. Further, putting the PMMA-based GI-POF under stress induces readily mode mixing that alters the NFP. These effects could be minimized when connectors are used at the GI-POF ends and coating layers protect the GI-POF. In principle, MGDM systems with PMMA-based, as well as PF-based, GI-POF are feasible. However, the high level of mode mixing and the sensitivity of the NFP to bending that occurs very close to the output end of the PMMA-based GI-POF as well as to external stress can cause practical difficulties for a reliable MGDM system with PMMA-based GI-POF.

Chapter 8

Conclusions and recommendations

The conclusions from the theoretical and experimental investigation of the mode group diversity multiplexing (MGDM) technique are summarized. The significance of mode-selective spatial filtering (MSSF) in mitigating transmission impairments in MGDM systems and offering scalability with the number of channels is underlined. Having reached a point at which it is fairly clear what MGDM can achieve, a comparison with other multiplexing techniques is made. The combination of MGDM with other techniques, such as subcarrier multiplexing and wavelength division multiplexing, appears to be an interesting option. MSSF has a key role in such combinations. Finally, it is suggested that future research on the design and manufacture of MGDM components, both optical and electronic ones, can proceed towards robust adaptive system solutions and thus can further explore the actual enhancement in the aggregate transmission bandwidth that can be achieved with MGDM.

8.1 Conclusions

Characteristics of MGDM

An important feature of an N-input, M-output mode group diversity multiplexing (MGDM) link with intensity-modulation and direct detection (IM-DD) is that it is described by an $M \times N$ linear system of equations, as long as the effect of optical beating is restricted. The matrix of this system, i.e. the transmission matrix $\mathbf{H}$, is real-valued when the effect of dispersion can be neglected. Indeed, a real-valued $\mathbf{H}$ cannot account for differential delays in the system. In the most general case, irrespective of the amount of spatial overlap among the fields of the N detected mode groups, these N fields should be mutually incoherent. Furthermore,

although in principle $M \geq N$, it is beneficial for the SNR that $M = N$.

Another characteristic of MGDM is that it supports signal format transparency. The channels are demultiplexed with electronic signal processing based on matrix inversion. Matrix inversion is a zero-forcing method that cancels cross-talk, regardless of the performance of the system in relation to noise. Consequently, as compared to the single-channel case, noise may be increased and hence a power penalty may be induced to maintain the SNR of the single-channel case. This power penalty depends on the spatial overlap among the intensity profiles of the detected mode groups. The larger the overlap, the higher the power penalty and its sensitivity to changes in the value of the transmission matrix elements $h_{i,j}$. Such changes may be due to misalignments, temperature variations and/or mechanical fluctuations. From a mathematical viewpoint, the lower the condition number of $\mathbf{H}$, the more robust the MGDM system.

The design and implementation of an MGDM system is a non-trivial challenge. An MGDM multi/demultiplexer is required. This can be achieved by N radially offset Gaussian-like beams at the input facet of the GI-MMF and an N-segment detector with annular segments responding to the near-field pattern (NFP) at the output facet of the GI-MMF. The areas of the detector segments and the radial offsets of the input beams must be chosen such, so as to minimize, on average, the optical cross-talk. For standard silica-based GI-MMFs, at least up to 1 km long, the choice of the radial offsets and the detector segments does not depend on the length of the GI-MMF. This is because differential mode delay and attenuation, as well as the very limited mode mixing that occurs do not change the overall NFP, although they do affect the speckle pattern. Further, the dependence of the overall NFP on small deviations of the refractive index profile is very weak. This approach for the design of an MGDM system retains the characteristics of high coupling efficiency, simplicity and robustness with the GI-MMF length. However, it may fail in case the refractive index profile of the GI-MMF exhibits a central dip. Such a defect is not uncommon in legacy GI-MMFs. In this case, central excitation is to be avoided.

MGDM can be also applied to GI-POF systems. PMMA-based GI-POFs are more attractive candidates for MGDM transmission than PF-based GI-POFs due to their large core diameter and NA. However, mode mixing in GI-POFs, both PMMA-based and PF-based ones, is very strong. This makes matrix $\mathbf{H}$ strongly dependent on the fiber length, as opposed to the case of GI-GOFs. The flexibility of the PMMA material, although it facilitates the installation of in-building and in-house networks, renders PMMA-based GI-POFs sensitive to bending-induced macroscopic deformations of the refractive index profile. This can significantly affect the NFP at the output facet of a PMMA-based GI-POF. To observe such changes in the NFP, bending should take place close to the output end of a PMMA-based GI-POF, at a distance in the order of 1 cm. In addition, applying stress on a PMMA-based GI-POF induces mode mixing and changes the overall NFP. The use of connectors and coating around a PMMA-based GI-POF can increase its tolerance with respect to external forces. This sensitivity, due to certain bend-

ing and stress, is not observed in GI-GOFs, and together with the strong mode mixing in PMMA-based GI-POFs can cause practical problems in the application of MGDM over PMMA-based GI-POF connections.

An MGDM system must be adaptive, in order to accommodate changes in the value of $h_{i,j}$. Such changes may be induced due to different factors, such as temperature changes and mechanical vibrations. It is indeed possible to build a system which is fairly stable over time, as was experimentally shown in this thesis. In such a system, adaptivity can be simply realized at the receiving side of the link, by tracking small changes in the value of $h_{i,j}$, for instance by using pilot tones. No feedback is then required from the receiver to the transmitter, which greatly simplifies the implementation of the MGDM technique.

The significance of MSSF

The characterization of an MGDM system with a real-valued $\mathbf{H}$ and the demultiplexing of the channels based on electronic matrix inversion allow for a simple system design and transparency with respect to the signal format. It is rather straightforward to design a system with a non-singular $\mathbf{H}$. However, a very important parameter is the condition number of $\mathbf{H}$. The lower the condition number, the more robust the system. The robustness of the system is related to the tolerance of its performance to changes in the value of $h_{i,j}$. A low condition number means limited optical cross-talk, i.e. limited spatial overlap among the intensity profiles of the detected mode groups. At the same time, when this spatial overlap is limited, the power penalty due to matrix inversion is small. Furthermore, limited optical cross-talk relaxes the requirement of mutual incoherence among the fields of the detected mode groups, since these field distributions interfere only partially.

Mode-selective spatial filtering (MSSF) is a new optical method that can be used to reduce cross-talk among the channels of an MGDM system. A great advantage of MSSF is the ease of implementation. MSSF only requires an imaging system with a lower NA than the central NA of the GI-MMF. Such an imaging system can be a single lens. MSSF makes an MGDM system more robust to changes in the value of $h_{i,j}$, leads to better scalability with respect to the number of channels and relaxes some restrictions on the spectral content of the optical sources of the system. For all these reasons, the aggregate bandwidth of the system can be increased significantly and hence MGDM can be interesting for more bandwidth-demanding applications that also benefit from the signal format transparency. The only drawback of MSSF is that some of the optical power at the output of the GI-MMF is lost. However, the great advantages that MSSF offers in MGDM transmission will often justify this power loss. For standard 62.5/125 μm silica-based GI-MMFs, a robust five-channel MGDM system could be built with MSSF. Without MSSF, this number reduces to three. In addition, it would be possible to build a three-channel MGDM system, in which MSSF fully mitigates cross-talk and therefore the need for electronic demultiplexing is eliminated.

Comparison of MGDM with other multiplexing techniques

Multiplexing can be achieved with different methods in GI-MMF transmission. Subcarrier multiplexing (SCM) and wavelength division multiplexing (WDM) are two methods that are widely used in optical communications. Both SCM and WDM can support signal format transparency and use IM-DD. Therefore a comparison of these techniques with MGDM is of great interest. WDM requires a different wavelength at every channel and optical filters for the demultiplexing of the channels. The number of channels within a certain system wavelength range depends on the channel spacing in the wavelength domain. Narrow spacing allows for a large number of channels, however it requires high wavelength selectivity of the related components, e.g. lasers and filters, as well as wavelength stability over time. Dense WDM is a powerful technique that comes at the expense of relatively high cost. However, when the target number of channels is small, e.g. four, coarse WDM (CWDM) may be a valid option for short-reach applications that require simplicity and relatively low cost. For in-house networks, the cost of the proposed solution should be very low. This is a real challenge for optics, since typically, optical components are more costly than electronic ones. MGDM with MSSF can offer a robust solution for a small number of channels that could meet the low-cost requirement, since a significant part of the signal processing in the system is done in the electrical domain.

SCM with IM-DD requires one laser and one photodiode. The multiplexing and demultiplexing of the channels take place in the electrical domain. Therefore SCM can be more cost-effective than WDM. The 3-dB bandwidth of the GI-MMF should be shared among the channels. This means that each channel must be a narrowband one. To overcome this limitation, higher passband lobes in the transmission spectrum of the GI-MMF could be used as well. Would such a system be stable? As with MGDM, any changes in the distribution of the optical power among the guided modes will affect the frequency response of the GI-MMF. For low frequencies, the change may not be significant, however for high frequencies the same change could be destructive. Therefore transmission in the higher order passband regions can be sensitive and may require adaptivity based on feedback from the receiver to the transmitter. By contrast, MGDM creates broadband parallel channels which do not exceed the 3-dB bandwidth and therefore such a need for feedback can be eliminated.

MGDM requires more complex optical components than SCM. An MGDM system is potentially more cost-effective than a WDM one. MGDM creates broadband channels and the same holds for WDM. For SCM in the baseband region, the bandwidth of each channel is less broad than in MGDM and WDM. MGDM is limited to a small number of channels. The same holds for CWDM compared to dense WDM, but for a relatively large system wavelength range CWDM is more scalable regarding the number of channels than MGDM. In SCM, the number of channels within an available frequency range depends on the bandwidth of each channel. What is the best option for a GI-MMF transmission system? The an-

swer of course depends on the specific application and resources. The following example, although it only represents a single case, gives a nice perspective to the answer of this question.

The needs of the average current residential user can be covered by a single IM-DD channel. The easiest way to introduce more channels would be to apply SCM in the baseband region, as long as the single IM-DD channel does not make use of the whole baseband region. The next step could be to apply MGDM. Solutions based on combination of different techniques should be also considered. A two-channel MGDM system with cross-talk being fully mitigated with MSSF can be very easily realized and it creates two independent IM-DD optical channels where SCM can apply in each one. As a further step, a two-channel WDM system can be introduced, which is a very simple case of WDM transmission. Of course, the combination of several techniques requires suitable components and this is something to be investigated.

8.2 Recommendations for further research

The way of exploiting research results is a very interesting issue. It is not always the case that research bears fruits that can lead to practical applications and drive future activities. In some cases, research may reveal fundamental problems associated with the viability of the investigated methods. Although this does not diminish the importance of the research work, it is not the most fortunate outcome. Happily, this is not the case for the research work presented in this dissertation. It is the hope of the author that based on the presented results, the reader shares the conviction that MGDM is a robust, stable and simple to implement method that can be useful in practical applications.

The investigation presented in this thesis is from the system point of view. However, the results on the definition of the geometric parameters of the MGDM multi/demultiplexer can be used for the design and manufacture of MGDM components, such as a multi-segment photodetector and a multi–mode-group launcher. That would be a necessary step in order to demonstrate systems that fully exploit the potential of the MGDM technique. To this direction, high frequency electronics should be also designed and manufactured. This has not been a part of this thesis. Furthermore, research can be carried out to explore how other transmission scenarios can benefit from the ideas described in this thesis. For example, MIMO schemes that are restricted with respect to the signal format in favor of bandwidth maximization or combination of several multiplexing techniques could be explored. Next to this, adaptivity implementation methods need to be investigated. Throughout this thesis, it has been assumed that the effects of dispersion can be neglected. This may limit the transmission bandwidth and the length of the GI-MMF. It would be interesting to see how to surpass this limitation posed by dispersion. Further, the possibility of a bidirectional MGDM link could be investigated, primarily as regards its practical implementation. In such a link, adaptivity

based on feedback from the receiver to the transmitter can be easily incorporated. This would open new possibilities for the signal processing approach in an MGDM system and would also facilitate the application of MGDM in network architectures, such as point-to-multipoint. Undoubtedly, the spatial modes of a GI-MMF offer extra degrees of freedom that can be exploited in very pragmatic transmission systems.

References

[1] F. W. Kerfoot and W. C. Marra, "Undersea Fiber Optic Networks: Past, Present, and Future," *IEEE J. Sel. Areas Commun.*, vol. 16, pp. 1220–1225, Sept. 1998.

[2] T. Koonen, "Fiber to the Home/Fiber to the Premises: What, Where, and When?," *Proc. IEEE*, vol. 94, pp. 911–934, May 2006.

[3] A. Flatman, *Presentation to IEEE 802.3 High-Speed Study Group*. Montreal, Canada, July 1999.

[4] A. Flatman, *Presentation to IEEE 802.3 10GBE over FDDI-Grade Fiber Study Group*. Orlando, FL, USA, Mar. 2004.

[5] D. A. B. Miller, "Rationale and Challenges for Optical Interconnects to Electronic Chips," *Proc. IEEE*, vol. 88, pp. 728–749, June 2000.

[6] A. F. J. Levi, "Optical Interconnects in Systems," *Proc. IEEE*, vol. 88, pp. 750–757, June 2000.

[7] C. V. Cryan, "Two-dimensional multimode fibre array for optical interconnects," *Electron. Lett.*, vol. 34, pp. 586–587, Mar. 1998.

[8] B. E. Lemoff, M. E. Ali, G. Panotopoulos, G. M. Flower, B. Madhavan, A. F. J. Levi, and D. W. Dolfi, "MAUI: Enabling Fiber-to-the-Processor With Parallel Multiwavelength Optical Interconnects," *IEEE/OSA J. Lightwave Technol.*, vol. 22, pp. 2043–2054, Sept. 2004.

[9] Y. Yadin and M. Orenstein, "Parallel Optical Interconnects Over Multimode Waveguides," *IEEE/OSA J. Lightwave Technol.*, vol. 24, pp. 380–386, Jan. 2006.

[10] J. C. Knight, J. Broeng, T. A. Birks, and P. S. J. Russell, "Photonic Band Gap Guidance in Optical Fibers," *Science*, vol. 282, pp. 1476–1478, Nov. 1998.

[11] P. Russell, "Photonic Crystal Fibers," *Science*, vol. 299, pp. 358–362, Jan. 2003.

[12] D. Hondros and P. Debye, "Elektromagnetische Wellen an dielektrischen Drähten," *Annalen der Physik (Leipzig) Ser. 4*, vol. 32, pp. 465–476, 1910.

[13] A. W. Snyder and J. D. Love, *Optical Waveguide Theory.* Chapman and Hall, London, 1983.

[14] H. A. Haus, *Waves and Fields in Optoelectronics.* Prentice Hall, 1984.

[15] A. H. Cherin and L. Short, *An introduction to optical fibers.* McGraw-Hill, New York, 1983.

[16] J. Gowar, *Optical Communication Systems.* Prentice Hall, London, 2nd ed., 1993.

[17] G. P. Agrawal, *Fiber-Optic Communication Systems.* John Wiley and Sons, Inc., New York, 3rd ed., 2002.

[18] H. P. A. van den Boom, W. Li, P. K. van Bennekom, I. T. Monroy, and G.-D. Khoe, "High-Capacity Transmission Over Polymer Optical Fiber," *IEEE J. Select. Topics in Quantum Electron.*, vol. 7, pp. 461–470, May/June 2001.

[19] B. J.-C. Deboux, E. Lewis, P. J. Scully, and R. Edwards, "A Novel Technique for Optical Fiber pH Sensing Based on Methylene Blue Adsorption," *IEEE/OSA J. Lightwave Technol.*, vol. 13, pp. 1407–1414, July 1995.

[20] S. Savović and A. Djordjevich, "Optical power flow in plastic-clad silica fibers," *OSA Appl. Opt.*, vol. 41, pp. 7588–7591, Dec. 2002.

[21] T. Kibler, S. Poferl, G. Böck, H.-P. Huber, and E. Zeeb, "Optical Data Buses for Automotive Applications," *IEEE/OSA J. Lightwave Technol.*, vol. 22, pp. 2184–2199, Sept. 2004.

[22] T. Koonen, A. Ngoma, P. Smulders, H. van den Boom, I. T. Monroy, and G.-D. Khoe, "In-house networks using multimode polymer optical fibre for broadband wireless services," *Photon. Network Comm.*, vol. 5, pp. 177–187, Mar. 2003.

[23] T. Ishigure, M. Satoh, O. Takanashi, E. Nihei, T. Nyu, S. Yamazaki, and Y. Koike, "Formation of the Refractive Index Profile in the Graded Index Polymer Optical Fiber for Gigabit Data Transmission," *IEEE/OSA J. Lightwave Technol.*, vol. 15, pp. 2095–2100, Nov. 1997.

[24] C. Koeppen, R. F. Shi, W. D. Chen, and A. F. Garito, "Properties of plastic optical fibers," *J. Optic. Soc. Amer. B*, vol. 15, pp. 727–739, Feb. 1998.

[25] B. E. Lemoff, L. B. Aronson, and L. A. Buckman, "Zigzag waveguide demultiplexer for multimode WDM LAN," *Electron. Lett.*, vol. 34, pp. 1014–1016, May 1998.

[26] L. B. Aronson, B. E. Lemoff, L. A. Buckman, and D. W. Dolfi, "Low-Cost Multimode WDM for Local Area Networks Up to 10 Gb/s," *IEEE Photon. Technol. Lett.*, vol. 10, pp. 1489–1491, Oct. 1998.

[27] L. A. Buckman, B. E. Lemoff, A. J. Schmit, R. P. Tella, and W. Gong, "Demonstration of a Small-Form-Factor WWDM Transceiver Module for 10-Gb/s Local Area Networks," *IEEE Photon. Technol. Lett.*, vol. 14, pp. 702–704, May 2002.

[28] P. Koutessis, T. Quinlan, E. Rochat, S. D. Walker, M. Wehster, I. H. White, R. V. Penty, and M. C. Parker, "0.6 Tb/s/km multimode fiber feasibility experiments using 40 channel DWDM over quadrature-subcarrier transmission," *Electron. Lett.*, vol. 38, pp. 813–815, July 2002.

[29] R. A. Panicker, J. P. Wilde, J. M. Kahn, D. F. Welch, and I. Lyubomirsky, "10×10 Gb/s DWDM Transmission Through 2.2-km Multimode Fiber Using Adaptive Optics," *IEEE Photon. Technol. Lett.*, vol. 19, pp. 1154–1156, Aug. 2007.

[30] T. E. Darcie, "Subcarrier Multiplexing for Lightwave Networks and Video Distribution Systems," *IEEE J. Sel. Areas Commun.*, vol. 8, pp. 1240–1248, Sept. 1990.

[31] L. Raddatz and I. H. White, "Overcoming the Modal Bandwidth Limitation of Multimode Fiber by Using Passband Modulation," *IEEE Photon. Technol. Lett.*, vol. 11, pp. 266–268, Feb. 1999.

[32] E. J. Tyler, M. Webster, R. V. Penty, and I. H. White, "Penalty Free Subcarrier Modulated Multimode Fiber Links for Datacomm Applications Beyond the Bandwidth Limit," *IEEE Photon. Technol. Lett.*, vol. 14, pp. 110–112, Jan. 2002.

[33] E. J. Tyler, M. Webster, R. V. Penty, I. H. White, S. Yu, and J. Rorison, "Subcarrier Modulated Transmission of 2.5 Gb/s Over 300 m of 62.5-μm-Core Diameter Multimode Fiber," *IEEE Photon. Technol. Lett.*, vol. 14, pp. 1743–1745, Dec. 2002.

[34] S. Kanprachar and I. Jacobs, "Diversity Coding for Subcarrier Multiplexing on Multimode Fibers," *IEEE Trans. on Comm.*, vol. 51, pp. 1546–1553, Sept. 2003.

[35] J. Zeng, A. Ng'oma, S. C. J. Lee, Y. Wanatabe, H. P. A. van den Boom, and A. M. J. Koonen, "1.25 Gb/s Subcarrier Modulated Transmission over Graded-index Perfluorinated Polymer Fibre," in *Proc. International Plastic Optical Fibers Conference*, pp. 99–101, Seoul, South Korea, 2006.

[36] T. Morioka, H. Takara, S. Kawanishi, O. Kamatani, K. Takiguchi, K. Uchiyama, M. Saruwatari, H. Takahashi, M. Yamada, T. Kanamori, and H. Ono, "1 Tbit/s (100 Gbit/s x 10 channel) OTDM/WDM transmission using a single supercontinuum WDM source," *Electron. Lett.*, vol. 32, pp. 906–907, May 1996.

[37] C. Scheerer, C. Glingener, A. Färbert, J.-P. Elbers, A. Schöpflin, E. Gottwald, and G. Fischer, "3.2Tbit/s (80 x 40Gbit/s) bidirectional WDM/ETDM transmission over 40 km standard singlemode fibre," *Electron. Lett.*, vol. 35, pp. 1752–1753, Sept. 1999.

[38] U. Feiste, R. Ludwig, C. Schubert, J. Berger, C. Schmidt, H. G. Weber, B. Schmauss, A. Munk, B. Buchold, D. Briggmann, F. Kueppers, and F. Rumpf, "16O Gbit/s transmission over 116 km field-installed fibre using 16O Gbit/s OTDM and 40 Gbit/s ETDM," *Electron. Lett.*, vol. 37, pp. 443–445, Mar. 2001.

[39] S. Bhandare, D. Sandel, B. Milivojevic, A. Hidayat, A. A. Fauzi, H. Zhang, S. K. Ibrahim, F. Wüst, and R. Noé, "5.94-Tb/s 1.49-b/s/Hz ($40\times2\times2\times40\times$ Gb/s) RZ-DQPSK Polarization-Division Multiplex *C*-Band Transmission Over 324 km," *IEEE Photon. Technol. Lett.*, vol. 17, pp. 914–916, Apr. 2005.

[40] R. E. Wagner, R. H. Stolen, and W. Pleibel, "Polarisation preservation in multimode fibres," *Electron. Lett.*, vol. 17, pp. 177–178, Mar. 1981.

[41] E. Rochat, S. D. Walker, and M. C. Parker, "C-band polarisation orthogonality preservation in 5Gb/s, 50μm multimode fibre links up to 3km," *OSA Opt. Express*, vol. 11, pp. 508–514, Mar. 2003.

[42] J. Y. Hui, "Pattern Code Modulation and Optical Decoding-A Novel Code-Division Multiplexing Technique for Multifiber Networks," *IEEE J. Sel. Areas Commun.*, vol. SAC-3, pp. 916–927, Nov. 1985.

[43] S. V. Maric, O. Moreno, and C. J. Corrada, "Multimedia Transmission in Fiber-optic LANs Using Optical CDMA," *IEEE/OSA J. Lightwave Technol.*, vol. 14, pp. 2149–2153, Oct. 1996.

[44] A. Stok and E. H. Sargent, "The Role of Optical CDMA in Access Networks," *IEEE Comm. Magazine*, pp. 83–87, Sept. 2002.

[45] B. Huiszoon, L. M. Augustin, R. Hanfoug, L. Bakker, M. J. H. Sander-Jochem, E. R. Fledderus, G.-D. Khoe, J. J. G. M. van der Tol, H. de Waardt, M. K. Smit, and A. M. J. Koonen, "Integrated Parallel Spectral OCDMA En/Decoder," *IEEE Photon. Technol. Lett.*, vol. 19, pp. 528–530, Apr. 2007.

[46] G. J. Foschini, "Layered space-time architecture for wireless communication in fading environments when using multi-element antennas," *Bell Labs Tech. J.*, pp. 41–59, Autumn 1996.

[47] G. J. Foschini and M. J. Gans, "On Limits of Wireless Communications in a Fading Environment when Using Multiple Antennas," *Wireless Personal Commun.: Kluwer Academic Press*, vol. 6, pp. 311–355, Mar. 1998.

[48] A. Goldsmith, S. A. Jafar, N. Jindal, and S. Vishwanath, "Capacity Limits of MIMO Channels," *IEEE J. Sel. Areas Commun.*, vol. 21, pp. 684–702, June 2003.

[49] J. R. Barry, E. A. Lee, and D. G. Messerschmitt, *Digital Communications*. Kluwer Academic Publishers, Dordrecht, 3rd ed., 2004.

[50] M. Saffman and D. Z. Anderson, "Mode multiplexing and holographic demultiplexing communication channels on a multimode fiber," *OSA Opt. Lett.*, vol. 16, pp. 300–302, Mar. 1991.

[51] D. Z. Anderson and M. E. Saffman, "Fiber optic communication method and apparatus providing mode multiplexing and holographic demultiplexing," *United States Patent: 5,136,666*, Aug. 1992.

[52] P. L. Neo and T. D. Wilkinson, "Holographic Implementationof Optical Multiple-Inputs Multiple-Outputs (MIMO) on a Multimode Fiber," in *Proc. Conference on Lasers and Electro-Optics/Quantum Electronics and Laser Science Conference and Photonic Applications Systems Technologies*, paper CMNN2, Long Beach, CA, USA, 2006.

[53] S. Berdagué and P. Facq, "Mode Division Multiplexing in Optical Fibers," *OSA Appl. Opt.*, vol. 21, pp. 1950–1955, June 1982.

[54] U. Levy, H. Kobrinsky, and A. A. Friesem, "Angular Multiplexing for Multichannel Communication in a Single Fiber," *IEEE J. Quantum Electron.*, vol. QE-17, pp. 2215–2224, Nov. 1981.

[55] R. C. Stearns, C. K. Asawa, and S.-K. Yao, "Angular Division Multiplexer for Fiber Communication Using Graded-Index Rod Lenses," *IEEE/OSA J. Lightwave Technol.*, vol. LT-2, pp. 358–362, Aug. 1984.

[56] U. W. Krackhardt, R. Klug, and K.-H. Brenner, "Broadband parallel-fiber optical link for short-distance interconnection with multimode fibers," *OSA Appl. Opt.*, vol. 39, pp. 690–697, Feb. 2000.

[57] H. P. A. van den Boom, A. M. J. Koonen, F. M. Huijskens, and W. van Gils, "Angular Mode Group Diversity Multiplexing for Multi-channel Communication in a Single Step-Index Plastic Optical Fibre," in *Proc. IEEE/LEOS Symposium Benelux Chapter*, pp. 121–124, Mons, Belgium, Dec. 2004.

[58] P. Facq, P. Fournet, and J. Arnaud, "Observation of tubular modes in multimode graded-index fibres," *Electron. Lett.*, vol. 16, pp. 648–649, Aug. 1980.

[59] F. Dubois, P. Emplit, and . Hugon, "Selective mode excitation in graded-index multimode fiber by a computer-generated optical mask," *OSA Opt. Lett.*, vol. 19, pp. 433–435, Apr. 1994.

[60] H. R. Stuart, "Dispersive multiplexing in multimode fiber," in *Proc. Optical Fiber Communication Conference*, vol. 3, pp. 305–307, paper ThV2, Baltimore, MD, USA, Mar. 2000.

[61] H. R. Stuart, "Dispersive Multiplexing in Multimode Optical Fiber," *Science*, vol. 289, pp. 281–283, July 2000.

[62] R. C. J. Hsu, A. Shah, and B. Jalali, "Coherent Optical Multiple-Input Multiple-Output communication," *IEICE Electronics Express*, vol. 1, pp. 392–397, Oct. 2004.

[63] A. R. Shah, R. C. J. Hsu, A. Tarighat, A. H. Sayed, and B. Jalali, "Coherent Optical MIMO (COMIMO)," *IEEE/OSA J. Lightwave Technol.*, vol. 23, pp. 2410–2419, Aug. 2005.

[64] R. C. J. Hsu, A. Tarighat, A. Shah, A. H. Sayed, and B. Jalali, "Capacity Enhancement in Coherent Optical MIMO (COMIMO) Multimode Fiber Links," *IEEE Comm. Lett.*, vol. 10, pp. 195–197, Mar. 2006.

[65] M. Greenberg, M. Nazarathy, and M. Orenstein, "Data Parallelization by Optical MIMO Transmission Over Multimode Fiber With Intermodal Coupling," *IEEE/OSA J. Lightwave Technol.*, vol. 25, pp. 1503–1514, June 2007.

[66] T. Koonen, H. van den Boom, F. Willems, J. Bergmans, and G.-D. Khoe, "Broadband multi-service in-house networks using mode group diversity multiplexing," in *Proc. International Plastic Optical Fibers Conference*, Tokyo, Japan, 2002.

[67] T. Koonen, H. P. A. van den Boom, I. T. Monroy, and G.-D. Khoe, "High Capacity Multi-service In-house Networks Using Mode Group Diversity Multiplexing," in *Proc. Optical Fiber Communication Conference*, vol. 2, paper FG4, Los Angeles, CA, USA, 2004.

[68] S. Schöllmann and W. Rosenkranz, "Experimental Investigations of Mode Coupling as Limiting Effect Using Mode Group Diversity Multiplexing on GI-MMF," in *Proc. European Conference on Optical Communications*, paper We3.P.87, Cannes, France, 2006.

[69] S. Schöllmann and W. Rosenkranz, "Experimental Equalization of Crosstalk in a 2×2 MIMO System Based on Mode Group Diversity Multiplexing in MMF Systems @ 10.7 Gb/s," in *Proc. European Conference on Optical Communications*, paper 7.4.2, Berlin, Germany, 2007.

[70] M. Webster, L. Raddatz, I. H. White, and D. G. Cunningham, "A Statistical Analysis of Conditioned Launch for Gigabit Ethernet Links Using Multimode Fiber," *IEEE/OSA J. Lightwave Technol.*, vol. 17, pp. 1532–1541, Sept. 1999.

[71] P. G. Ciarlet, *Introduction to numerical linear algebra and optimisation.* Cambridge Univeristy Press, Cambridge, 1989.

[72] B. N. Datta, *Numerical Linear Algebra and Applications.* Brooks/Cole, Pacific Grove, 1995.

[73] G. H. Golub and C. F. van Loan, *Matrix Computations.* The Johns Hopkins Univeristy Press, Baltimore and London, 1996.

[74] R. Dändliker, A. Bertholds, and F. Maystre, "How Modal Noise in Multimode Fibers Depends on Source Spectrum and Fiber Dispersion," *IEEE/OSA J. Lightwave Technol.*, vol. LT-3, pp. 7–12, Feb. 1985.

[75] A. M. J. Koonen, "Bit-Error-Rate Degradation in a Multimode Fiber Optic Transmission Link Due to Modal Noise," *IEEE J. Sel. Areas Commun.*, vol. SAC-4, pp. 1515–1522, Dec. 1986.

[76] G. C. Papen and G. M. Murphy, "Modal Noise in Multimode Fibers under Restricted Launch Conditions," *IEEE/OSA J. Lightwave Technol.*, vol. 17, pp. 817–822, May 1999.

[77] L. Raddatz, I. H. White, D. G. Cunningham, and M. C. Nowell, "An Experimental and Theoretical Study of the Offset Launch Technique for the Enhancement of the Bandwidth of Multimode Fiber Links," *IEEE/OSA J. Lightwave Technol.*, vol. 16, pp. 324–331, Mar. 1998.

[78] S. S.-H. Yam and F. Achten, "Single wavelength 40 Gbit/s transmission over 3.4km broad wavelength window multimode fibre," *Electron. Lett.*, vol. 42, pp. 592–593, May 2006.

[79] S. Randel, S. C. J. Lee, B. Spinnler, F. Breyer, H. Rohde, J. Walewski, A. M. J. Koonen, and A. Kirstädter, "1 Gbit/s Transmission with 6.3 bit/s/Hz Spectral Efficiency in a 100 m Standard 1 mm Step-Index Plastic Optical Fibre Link Using Adaptive Multiple Sub-Carrier Modulation," in *Proc. European Conference on Optical Communications*, post-deadline paper Th4.4.1, Cannes, France, 2006.

[80] A. M. J. Koonen, J. Yang, M. S. Alfiad, X. Li, and H. P. A. van den Boom, "High-Capacity Data Transport via Large-Core Plastic Optical Fiber Links using Quadrature Amplitude Modulation," in *Proc. Optical Fiber Communication Conference*, paper OMR6, Anaheim, CA, USA, 2007.

[81] P. S. Szczepanek and J. W. Berthold III, "Side launch excitation of selected modes in graded-index optical fibers," *OSA Appl. Opt.*, vol. 17, pp. 3245–3247, Oct. 1978.

[82] J. Saijonmaa, A. B. Sharma, and S. J. Halme, "Selective excitation of parabolic-index optical fibers by Gaussian beams," *OSA Appl. Opt.*, vol. 19, pp. 2442–2452, July 1980.

[83] H. Roscher, M. B. Sanayeh, S. B. Thapa, and R. Michalzik, "VCSEL Arrays with Redundant Pixel Designs for 10 Gbit/s 2-D Space-Parallel Multimode Fiber Transmission," in *Proc. European Conference on Optical Communications*, vol. 3, pp. 687–688, paper We4.P.093, Glasgow, UK, 2005.

[84] C. K. Asawa, "Intrusion-Alarmed Fiber Optic Communication Link Using a Planar Waveguide Bimodal Launcher," *IEEE/OSA J. Lightwave Technol.*, vol. 20, pp. 10–18, Jan. 2002.

[85] J. B. Schlager, M. J. Hackert, P. Pepeljugoski, and J. Gwinn, "Measurements for Enhanced Bandwidth Performance over 62.5 μm Multimode Fiber in Short-Wavelength Local Area Networks," *IEEE/OSA J. Lightwave Technol.*, vol. 21, pp. 1276–1285, May 2003.

[86] M. Calzavara, R. Caponi, and F. Cisternino, "Selective Excitation of Annular Zones in Graded Index Multimode Fiber," *J. Opt. Commun.*, vol. 5, pp. 82–86, July 1984.

[87] At the time this investigation was carried out, Fiberdyne (`http://www.fiberdyne.com/`) had announced the manufacture of such components.

[88] *Mode Scrambler Requirements for Overfilled Launching Conditions to Multimode Fibers.* FOTP-54, ANSI/TIA/EIA-455-54-2001, Dec. 2001.

[89] M. Wegmuller, S. Golowich, G. Giaretta, and M. Nuss, "Evolution of the Beam Diameter in a Multimode Fiber Link Through Offset Connectors," *IEEE Photon. Technol. Lett.*, vol. 13, pp. 574–576, June 2001.

[90] M. Düser and P. Bayvel, "2.5 Gbit/s transmission over 4.5 km of 62.5 μm multimode fibre using centre launch technique," *Electron. Lett.*, vol. 36, pp. 57–58, Jan. 2000.

[91] Z. Haas and M. A. Santoro, "A Mode-Filtering Scheme for Improvement of the Bandwidth-Distance Product in Multimode Fiber Systems," *IEEE/OSA J. Lightwave Technol.*, vol. 11, pp. 1125–1131, July 1993.

[92] A. M. J. Koonen, H. P. A. van den Boom, L. P. Bakker, J. Zeng, A. Ng'Oma, and G.-D. Khoe, "Integration of services in short-range multimode polymer optical fibre networks by exploiting the higher-order fibre passbands," in

Proc. International Plastic Optical Fibers Conference, Nuremberg, Germany, 2004.

[93] K. M. Patel, A. Polley, K. Balemarthy, and S. E. Ralph, "Spatially Resolved Detection and Equalization of Modal Dispersion Limited Multimode Fiber Links," *IEEE/OSA J. Lightwave Technol.*, vol. 24, pp. 2629–2636, July 2006.

[94] C. K. Asawa and H. F. Taylor, "Propagation of light trapped within a set of lowest-order modes of graded-index multimode fiber undergoing bending," *IEEE/OSA J. Lightwave Technol.*, vol. 39, pp. 2029–2037, May 2000.

[95] D. Gloge and E. A. J. Marcatili, "Multimode Theory of Graded-Core Fibers," *Bell Syst. Tech. J.*, vol. 52, pp. 1563–1578, Nov. 1973.

[96] S. Kawakami and H. Tanji, "Evolution of Power Distribution in Graded-Index Fibres," *Electron. Lett.*, vol. 19, pp. 100–102, Feb. 1983.

[97] G. Yabre, "Comprehensive Theory of Dispersion in Graded-Index Optical Fibers," *IEEE/OSA J. Lightwave Technol.*, vol. 18, pp. 166–177, Feb. 2000.

[98] M. Bingle and B. P. de Hon, "Differential Mode Delay Full-wave Modeling and Various Levels of Approximations," in *Proc. of the General XXVIIth Assembly of the International Union of Radio Science*, no. 2060, Maastricht, The Netherlands, 2002.

[99] J. G. Dil and H. Blok, "Propagation of Electromagnetic Surface Waves in a Radially Inhomogeneous Optical Waveguide," *Opto-electronics*, vol. 5, pp. 415–428, 1973.

[100] Y. Daido, E. Miyauchi, T. Iwama, and T. Otsuka, "Determination of modal power distribution in graded-index optical waveguides from near-field patterns and its application to differential mode attenuation measurement," *OSA Appl. Opt.*, vol. 18, pp. 2207–2213, July 1979.

[101] O. G. Leminger and G. K. Grau, "Near-Field Intensity and Modal Power Distribution in Multimode Graded-index Fibers," *Electron. Lett.*, vol. 16, pp. 678–679, July 1980.

[102] M. Rousseau and L. Jeunhomme, "Optimum index profile in multimode optical fiber with respect to mode coupling," *Opt. Commun.*, vol. 23, pp. 275–278, Nov. 1977.

[103] `http://www.ieee802.org/3/aq/public/tools/`.

[104] G. W. de Jong, J. R. M. Bergervoet, J. H. A. Brekelmans, and J. F. P. van Mil, "A DC-to-250MHz Current Pre-Amplifier with Integrated Photo-Diodes in Standards CBiMOS, for Optical-Storage Systems," in *Proc. of ISSCC*, paper 21.8, San Francisco, CA, USA, Feb. 2002.

[105] G. J. Meslener, "Chromatic Dispersion Induced Distortion of Modulated Monochromatic Light Employing Direct Detection," *IEEE J. Quantum Electron.*, vol. QE-20, pp. 1208–1216, Oct. 1984.

[106] E. E. Bergmann, C. Y. Kuo, and S. Y. Huang, "Dispersion-Induced Composite Second-Order Distortion at 1.5 μm," *IEEE Photon. Technol. Lett.*, vol. 3, pp. 59–61, Jan. 1991.

[107] M. R. Phillips, T. E. Darcie, D. Marcuse, G. E. Bodeep, and N. J. Frigo, "Nonlinear Distortion Generated by Dispersive Transmission of Chirped Intensity-Modulated Signals," *IEEE Photon. Technol. Lett.*, vol. 3, pp. 481–483, May 1991.

[108] C. Buoli, C. Esposito, and G. Mora, "AM/PM Compensation Improves Performances of Microwave Link Using a Multimode Optical Fibre and a Multimode VCSEL," in *Proc. European Microwave Conference*, pp. 499–502, Amsterdam, the Netherlands, 2004.

[109] M. de Boer, *Design and implementation of a Mode Group Diversity Multiplexing optical fibre receiver system.* MSc Thesis, Eindhoven University of Technology, the Netherlands, 2006.

[110] P. N. de la Calle, *Electronic design and implementation of adaptive demultiplexing for mode group diversity multiplexing.* MSc Thesis, Eindhoven University of Technology, the Netherlands, 2007.

[111] T. Ishigure, S. Tanaka, E. Kobayashi, and Y. Koike, "Accurate Refractive Index Profiling in a Graded-Index Plastic Optical Fiber Exceeding Gigabit Transmission Rates," *IEEE/OSA J. Lightwave Technol.*, vol. 20, pp. 1125–1131, Aug. 2002.

[112] A. Kondo, T. Ishigure, and Y. Koike, "Fabrication Process and Optical Properties of Perdeuterated Graded-Index Polymer Optical Fiber," *IEEE/OSA J. Lightwave Technol.*, vol. 23, pp. 2443–2448, Aug. 2005.

[113] T. Ishigure, K. Ohdoko, Y. Ishiyama, and Y. Koike, "Mode-Coupling Control and New Index Profile of GI POF for Restricted-Launch Condition in Very-Short-Reach Networks," *IEEE/OSA J. Lightwave Technol.*, vol. 23, pp. 4155–4168, Dec. 2005.

[114] K. Ohdoko, T. Ishigure, and Y. Koike, "Propagating Mode Analysis and Design of Waveguide Parameters of GI POF for Very Short-Reach Network Use," *IEEE Photon. Technol. Lett.*, vol. 17, pp. 79–81, Jan. 2005.

[115] T. Ishigure, Y. Koike, and J. W. Fleming, "Optimum Index Profile of the Perfluorinated Polymer-Based GI Polymer Optical Fiber and Its Dispersion Properties," *IEEE/OSA J. Lightwave Technol.*, vol. 18, pp. 178–184, Feb. 2000.

[116] G. Giaretta, W. White, M. Wegmuller, and T. Onishi, "High-Speed (11 Gbit/s) Data Transmission Using Perfluorinated Graded-Index Polymer Optical Fibers for Short Interconnects (¡100 m)," *IEEE Photon. Technol. Lett.*, vol. 12, pp. 347–349, Mar. 2000.

[117] S. E. Golowich, W. White, W. A. Reed, and E. Knudsen, "Quantitative Estimates of Mode Coupling and Differential Modal Attenuation in Perfluorinated Graded-Index Plastic Optical Fiber," *IEEE/OSA J. Lightwave Technol.*, vol. 21, pp. 111–121, Jan. 2003.

Appendix A

List of Acronyms

A/D	analog-to-digital
CATV	cable television
CCD	charge-coupled device
CDM	code division multiplexing
CDMA	code division multiple access
CWDM	coarse wavelength division multiplexing
DSL	digital subscriber line
DWDM	dense wavelength division multiplexing
FC	fiber concentrator
FC/PC	fixed-connection/physical-contact
FDM	frequency division multiplexing
FFT	fast Fourier transform
FTTH	fiber to the home
FTTP	fiber to the premises
FWHM	full width at half maximum
GI-GOF	graded-index glass optical fiber
GI-MMF	graded-index multimode fiber
GI-POF	graded-index polymer optical fiber
GOF	glass optical fiber
HOMs	higher order modes
IM-DD	intensity-modulation direct-detection
IP	internet protocol
LAN	local area network
LED	light emitting diode
LOMs	lower order modes
LP	linearly polarized
LPF	low-pass filter
MFD	mode field diameter
MGDM	mode group diversity multiplexing

MIMO	multiple-input multiple-output
MMF	multimode fiber
MSSF	mode-selective spatial filtering
NA	numerical aperture
NAPF	normalized annular power flux
NFP	near-field pattern
OC	optical cross-talk
PCS	plastic-clad silica
PD	photodiode
PDIC	photodiode integrated circuit
PDM	polarization division multiplexing
PF	perfluorinated
PMG	principal mode group
PMMA	polymethylmethacrylate
POF	polymer optical fiber
RHS	right-hand side
RIN	relative intensity noise
SCM	subcarrier multiplexing
SI-MMF	step-index multimode fiber
SI-POF	step-index polymer optical fiber
SISO	single-input single-output
SMF	single-mode fiber
SNR	signal-to-noise ratio
TDM	time division multiplexing
TLS	tunable laser source
VOA	variable optical attenuator
WDM	wavelength division multiplexing

Appendix B

List of Publications

Journal Papers

1. C. P. Tsekrekos and A. M. J. Koonen, "Mode-selective spatial filtering for increased robustness in a mode group diversity multiplexing link," *OSA Opt. Lett.*, vol. 32, pp. 1041–1043, May 2007.

2. C. P. Tsekrekos, R. W. Smink, B. P. de Hon, A. G. Tijhuis, and A. M. J. Koonen, "Near-field intensity pattern at the output of silica-based graded-index multimode fibers under selective excitation with a single-mode fiber," *OSA Opt. Express*, vol. 15, pp. 3656–3664, Apr. 2007.

3. C. P. Tsekrekos, M. de Boer, A. Martinez, F. M. J. Willems, and A. M. J. Koonen, "Temporal Stability of a Transparent Mode Group Diversity Multiplexing Link," *IEEE Photon. Technol. Lett.*, vol. 18, pp. 2484–2486, Dec. 2006.

4. C. P. Tsekrekos, A. Martinez, F. M. Huijskens, and A. M. J. Koonen, "Design Considerations for a Transparent Mode Group Diversity Multiplexing Link," *IEEE Photon. Technol. Lett.*, vol. 18, pp. 2359–2361, Nov. 2006.

5. T. Houbavlis, K. E. Zoiros, G. Kanellos, and C. Tsekrekos, "Performance analysis of ultrafast all-optical Boolean XOR gate using semiconductor optical amplifier-based Mach-Zehnder Interferometer," *Opt. Commun.*, vol. 232, pp. 179–199, 2004.

International Conferences

6. C. P. Tsekrekos and A. M. J. Koonen, "Effectiveness of mode-selective spatial filtering in mode group diversity multiplexing links," in *Proc. OptoElec-*

tronics and Communications Conference/International Conference on Integrated Optics and Optical Fiber Communication, paper 12A3-2, Yokohama, Japan, 2007.

7. C. P. Tsekrekos, M. de Boer, A. Martinez, F. M. J. Willems, and A. M. J. Koonen, "Demonstration of a Transparent 2-Input 2-Output Mode Group Diversity Multiplexing Link," in *Proc. European Conference on Optical Communications*, paper We3.P.145, Cannes, France, 2006.

8. C. P. Tsekrekos, M. de Boer, A. Martinez, F. M. J. Willems, and A. M. J. Koonen, "Experimental Study of the Temporal Behaviour of a Mode Group Diversity Multiplexing Link," in *Proc. Conference on Lasers and Electro-Optics/Quantum Electronics and Laser Science Conference and Photonic Applications Systems Technologies*, paper CMJ6, Long Beach, CA, USA, 2006.

9. C. P. Tsekrekos, A. Martinez, F. M. Huijskens, and A. M. J. Koonen, "Mode Group Diversity Multiplexing Transceiver Design for Graded-Index Multimode Fibres," in *Proc. European Conference on Optical Communications*, paper We4.P.113, Glasgow, UK, 2005.

10. M. de Boer, C. P. Tsekrekos, A. Martinez, H. Kurniawan, J. W. M. Bergmans, A. M. J. Koonen, H. P. A. van den Boom, and F. M. J. Willems, "A first demonstrator for a mode group diversity multiplexing communication system," in *Proc. IEE Seminar on Optical Fibre Communications and Electronic Signal Processing*, London, UK, 2005.

Regional Conferences

11. C. P. Tsekrekos and A. M. J. Koonen, "Mode Group Diversity Multiplexing over Graded-Index Polymer Optical Fiber Links," in *Proc. IEEE/LEOS Symposium Benelux Chapter*, accepted for publication, Brussels, Belgium, 2007.

12. C. P. Tsekrekos and A. M. J. Koonen, "The Effect of Passive Optical Components in Multimode Fibre Links Using Mode Group Diversity Multiplexing," in *Proc. IEEE/LEOS Symposium Benelux Chapter*, pp. 185–188, Eindhoven, The Netherlands, 2006.

13. C. P. Tsekrekos, M. de Boer, A. Martinez, H. Kurniawan, F. M. J. Willems, and A. M. J. Koonen, "An Experimental Investigation of the Mode Group Diversity Multiplexing Technique," in *Proc. IEEE/LEOS Symposium Benelux Chapter*, pp. 161–164, Mons, Belgium, 2004.

14. C. P. Tsekrekos, A. M. J. Koonen, and H. P. A. van den Boom, "Selective Excitation of Graded-Index Multimode Fibres Resulting in Annular Near Field Patterns," in *Proc. IEEE/LEOS Symposium Benelux Chapter*, pp. 211–214, Ghent, Belgium, 2004.

15. R. W. Smink, C. P. Tsekrekos, B. P. de Hon, A. M. J. Koonen, and A. G. Tijhuis, "Near Field Pattern Simulations of Graded-Index Multimode Fibres," in *Proc. IEEE/LEOS Symposium Benelux Chapter*, pp. 257–260, Eindhoven, The Netherlands, 2006.

Samenvatting

Mode groep diversiteit multiplexing in multimode vezel transmissiesystemen

Multimode vezels (multimode fibers, MMFs) met een geleidelijk veranderende brekingsindex in de radiële richting (graded index, GI) worden veelal gebruikt in lokale netwerken op campussen en binnen gebouwen. Ook voor de wat kleinere thuisnetwerken kan de MMF in de toekomst een interessante optie zijn. Naast de op silicium gebaseerde MMF vormt de polymeer optische vezel (polymer optical fiber, POF) ook een interessant alternatief. Dit vanwege zijn grote diameter en de flexibiliteit van het gebruikte materiaal, welke plaatsing in kabelgoten vergemakkelijkt. Verder kan een MMF verbinding een grotere bandbreedte bieden dan een elektronische (draadloze) verbinding. Licht in een MMF propageert in verscheidene spatiële modi. De bandbreedte van MMF verbindingen wordt gelimiteerd door modale dispersie, welke onstaat door de verschillende propagatiesnelheden van de modi. Tegelijkertijd creëren deze spatiële modi extra vrijheidsgraden, die kunnen worden gebruikt om een meer breedbandige overdracht te verkrijgen.

De meeste MMF systemen maken gebruik van licht intensiteit modulatie en directe detectie (IM-DD). IM-DD is de meest eenvoudige manier om een optische communicatie verbinding tot stand te brengen. Voor de velden van de propagerende modi in een MMF bestaat een orthogonaliteitsrelatie. Echter, iets vergelijkbaars bestaat niet voor de intensiteits profielen van de modi. Omdat MMFs veelal worden gebruikt voor korte afstanden waar eenvoud en kosten bepalend zijn, moet iedere poging die wordt ondernomen om gebruik te maken van de spatiële modi ook simpel en pragmatisch zijn. De ontwikkeling van de zogenaamde MIMO technieken in draadloze communicatie systemen, waar tegelijkertijd meerdere antennas als zender en ontvanger worden gebruikt, heeft ook voor MMF verbindingen als inspiratiebron gediend. Tot dusver zijn er al enkele schema's voorgesteld. Een ervan is mode groep diversiteit multiplexing (MGDM). Met behulp van de MGDM techniek kunnen onafhankelijke kanalen worden gecreëerd door gebruik te maken van propagerende modale groepen. MGDM gebruikt IM-DD, maar orthogonaliteit van de verschillende intensiteits profielen van de waargenomen modale groepen is niet vereist omdat overspraak met behulp van elektronische signaalverwerking kan worden onderdrukt.

Naar ons inziens is dit het eerste proefschrift waarin zowel een theoretisch als een experimenteel onderzoek wordt verricht naar de MGDM techniek. De inhoud

van dit proefschrift gaat hoofdzakelijk over de optische aspecten van MGDM signaaloverdracht door GI-MMFs. Hiervoor is een mathematisch model ontwikkeld. De voorwaarden waaronder een breedbandig MGDM systeem kan worden beschreven met een reële transmissiematrix zijn gespecificeerd. Deze matrix relateert ontvangen elektrische signalen aan verzonden elektrische signalen. In het meest algemene geval moeten de velden van de verscheidene modale groepen aan de uitgang van de GI-MMF onderling incoherent zijn, ongeacht de hoeveelheid spatiële overlap tussen de betreffende velden. De reële transmissiematrix drukt de spatiële overlap tussen de intensiteitsprofielen van de ontvangen modale groepen uit en kan niet compenseren voor differentiële vertragingen in het systeem. Daarom is het noodzakelijk dat het MGDM systeem opereert beneden de dispersie limiet. Daarnaast is het effect van ruis onderzocht waarbij matrix inversie als het demultiplexing algoritme wordt beschouwd. Dit is in lijn met de noodzaak om het kanaal transparant te maken met betrekking tot de signaal modulatie.

De mogelijkheid tot het bouwen van een eenvoudig, doch stabiel MGDM systeem dient als een hoofddoel van dit proefschrift. Richtlijnen voor het ontwerp van zo'n systeem worden gegeven en concrete conclusies zijn verkregen, welke gebruikt kunnen worden voor het ontwerpen en realiseren van een MGDM multi/demultiplexer. Uit experimentele waarnemingen volgt dat propagatie in GI-MMFs geen effect heeft op het ontwerp van een multi/demultiplexer voor afstanden tot 1 km. Numerieke simulaties zorgen voor een onderbouwing van deze waarnemingen. Voor GI-POFs geldt dat de modale koppeling sterker is dan bij GI-MMFs. Dit heeft als gevolg dat de bijbehorende transmissiematrix in hoge mate beïnvloed wordt door de lengte van de GI-POF. Daar komt bij dat de GI-POF gevoeliger is voor druk en buigingen. Een stabiele 2×2 MGDM verbinding is gerealiseerd met behulp van een op silicium gebaseerde GI-MMF, gebruikmakend van componenten die normaliter gebruikt worden voor andere toepassingen.

Het voorgestelde ontwerpproces voor een MGDM systeem heeft profijt van de elektronische vermindering van overspraak. Toch ontbreekt er een schaalbaarheid naar het aantal kanalen. Hoewel het mogelijk blijkt een robuust systeem bestaande uit twee of drie kanalen te realiseren, wordt bij toepassing van nog meer kanalen het succes negatief beïnvloed door de hoge gevoeligheid van de transmissiematrix. Het meest ideale geval vormt een systeem zonder overspraak, d.w.z. een systeem dat gekarakteriseerd wordt door de eenheidsmatrix. Om de robuustheid van een MGDM syteem te vergroten en tevens een groot aantal kanalen te realiseren, is modale selectieve spatiële filtering (MSSF) geïntroduceerd.

MSSF is een nieuwe optische techniek, dat werd onderzocht in het kader van het onderzoeksplan voor dit proefschrift. Het maakt enkel gebruik van een afbeeldingssysteem, bijvoorbeeld een lens, om het intensiteitspatroon aan het einde van de MMF op de detectoren te projecteren. De numerieke apertuur (NA) van het afbeeldingssysteem moet kleiner zijn dan de centrale NA van de GI-MMF. MSSF biedt een optische manier om overspraak te reduceren. Voor een systeem bestaande uit maximaal drie kanalen kan MSSF de noodzaak van elektronisch demultiplexen elimineren. Daarnaast kan met behulp van MSSF en partiële elektronische over-

spraak vermindering een robuust vijfkanaals MGDM systeem worden gerealiseerd. De noodzaak voor onderlinge incoherentie tussen de velden van de modale groepen aan de uitgang van de GI-MMF wordt door MMSF sterk gereduceerd. Een combinatie van MGDM met golflengte divisie multiplexing is hierdoor mogelijk.

De getoonde resultaten in dit proefschrift geven inzicht in lichtpropagatie door GI-MMFs en heeft ons een nieuwe invalshoek gegeven voor het gebruik van de propagerende modi van de GI-MMF voor transmissie doeleinden. Een stabiel, robuust en transparant vijfkanaals modaal multiplexing systeem leek aanvankelijk slechts een hersenschim. Toch laat dit proefschrift zien dat deze fantasie realiteit kan worden.

Acknowledgements

On the occasion of the completion of my doctoral thesis, I would like to take the opportunity to thank the people who helped me with their support.

First, I would like to thank my promoter Prof. Ton Koonen for offering me the opportunity to carry out my research in the Electro-optical Communication (ECO) group of the Eindhoven University of Technology (TU/e). His comments and suggestions in the last years helped me develop my personal research approach and present my results in a clear way. Next to this, I would like to thank him for reviewing my PhD thesis.

My research work in the Mode Group Diversity Multiplexing (MGDM) project required the cooperation with the Signal Processing Systems (SPS) group of the TU/e, and more specifically with Alfonso Martinez, Dr. Frans Willems and Prof. Jan Bergmans. I would like to thank Alfonso Martinez for the many discussions on several topics of optical communications and his input as co-author of several publications. His support on my early stage of writing scientific papers was significant. I would like to acknowledge Dr. Frans Willems and Prof. Jan Bergmans for their contribution to the development of the MGDM demonstrator. I would further like to thank Prof. Jan Bergmans for acting as the second promoter of my thesis and for his comments on the manuscript.

During my research, I had the chance to cooperate with Dr. Bas de Hon and Rutger Smink from the Electromagnetics group of the TU/e. I wish to thank them for our cooperation in the study of the near-field pattern of silica-based graded-index multimode fibers and the several interesting discussions we had. Further, I would like to thank Dr. Bas de Hon for acting as the co-promoter of my thesis and for his comments on my work, as well as Rutger Smink for translating the summary of my thesis into Dutch.

In the frame of the MGDM project, I was co-supervisor of three students of the SPS group, namely Marcel de Boer, Helmi Kurniawan and Pablo Núñez de la Calle. I wish to thank them for their contribution to the implementation of the electronic part of the MGDM demonstrator. I would especially like to acknowledge Marcel de Boer for his work on the data acquisition system of the laboratory that was used to measure the temporal stability of the MGDM system.

From the ECO group, I would like to thank Prof. Giok-Djan Khoe for his availability and his comments on several of my published papers, as well as Henrie

van den Boom for his interest in MGDM and his contribution to the MGDM project, as well as for his comments on my work, some of my papers and my thesis. Further, I am indebted to Frans Huijskens for his support and guidance in the laboratory facilities. In addition, I would like to thank Daniel Báez Puche, José Machado, Jorge Caetano Alves and Pedro Filipe da Costa Teixeira for their contribution to the development of the experimental setup for the study of the near-field pattern of multimode fibers under selective excitation. I would also like to thank Susan de Leeuw who together with Els Gerritsen and more recently José Hakkens try to do their best to help the ECO group members in administrative and other matters.

I am grateful to the Freeband Impulse Program of the Ministry of Economic Affairs of the Netherlands for financially supporting my research. In addition, I would like to thank Dr. Piet Matthijsse, Dr. Frank den Hartog, Dr. Jeroen Wellen, Dr. Sel Colak, and Dr. Fred Snijders for their comments and suggestions as members of the users' committee of the MGDM project, as well as Dr. Frank Karelse (Technology Foundation STW) for managing the project. I would also like to thank Dr. Alexander van der Lee (Philips Research Laboratories) for providing the PDIC. I would further wish to thank Dr. Piet Matthijsse (Draka Comteq) for providing the silica-based multimode fiber samples, for his openness and interesting discussions, as well as for reviewing my thesis as a member of the core committee of my PhD promotion. I am equally grateful to Prof. Ian White and Dr. Huug de Waardt for reviewing my thesis as members of my PhD core committee. Further, I wish to thank Dr. Takaaki Ishigure from Keio University, for providing the polymer optical fiber sample.

There are certainly many people who, although not directly related to my work, have one way or another contributed so as to make my work and academic life more enjoyable and often easier. I wish therefore to thank very much Dr. Jarek Turkiewicz, Dr. Juan José Vegas Olmos, Dr. Shaoxian Zhang, Dr. Yong Liu, Dr. Hyun-Do Jung, Dr. Zhonggui Li, Dr. Oded Raz, Dr. Nicola Calabretta, Dr. Eduward Tangdiongga, Prof. Harm Dorren, Jianming Zeng, as well as Ni Yan, Jia Yang, Maria García Larrodé, Jeffrey Lee, Archi Delphinanto, Bas Huiszoon, Patryk Urban, Kun Wang, Hejie Yang, Youbin Zheng, René Kramer, Dr. Erwin Verdurmen, Dr. Anthony Ng´oma, Arvind Mishra, Dr. Xuelin Yang, Dr. Francisco Soares, Georgi Petkov, Dr. Javier Molina Vázquez, Dr. Kevin Williams, Prof. Anton Tijhuis, Dr. Idelfonso Tafur Monroy, Johan van Zantvoort, Dr. Heongkyu Ju, Peter van Bennekom, Dr. Javier Herrera Llorrente, Poh Ling Neo, and Hans Christian Hansen Mulvad.

The completion of my PhD work would not have been possible without the constant support of my family and friends, who throughout the years have offered me their help and have always encouraged me to take new steps. It is because of their love and support that I still feel like taking risks to further explore myself and the world.

Curriculum Vitæ

Christos P. Tsekrekos was born in Athens, Greece, in 1980. He is a graduate engineer of the Faculty of Electrical and Computer Engineering of the National Technical University of Athens (2003). His graduation thesis concerned the simulation of an all-optical XOR gate using an SOA-MZI structure. In 2001, he spent an academic semester at the Technical University of Denmark, supported by a scholarship from the European exchange program Erasmus/Socrates. In 2003, he carried out a six-week internship at the Institute of Applied Optics, in Warsaw, Poland. This internship was organized by the International Association for the Exchange of Students for Technical Experience. Since February 2004, he has been with the Electro-optical Communication group of the Eindhoven University of Technology, the Netherlands, working towards his PhD degree. His research has been focused on multimode fiber communications. In particular, it involves the study of mode group diversity multiplexing, a novel optical multiple-input multiple-output technique. Christos P. Tsekrekos is the first author of four international journal papers and his research has been presented in several international and regional conferences. His work has been cited in at least 14 international journal/conference papers by other authors. He serves as a reviewer for the IEEE/OSA Journal of Lightwave Technology.